MOLECULAR STRUCTURE OF α,β,δ,γ-TETRA-PHENYLPORPHINATOINDIUM(III) CHLORIDE, AND PERTURBED ANGULAR CORRELATION STUDY ON RECONSTITUTED MYOGLOBIN

by

KAI MON, LEE
B. Tech. (Hons.), University of Bradford, England, 1977, Grad RIC

A THESIS SUBMITTED IN PARTIAL FULFILLMENT OF
THE REQUIREMENTS FOR THE DEGREE OF
MASTER OF SCIENCE

in

CHEMISTRY
THE FACULTY OF GRADUATE STUDIES
(Department of Chemistry)

We accept this thesis as conforming
to the required standard

THE UNIVERSITY OF BRITISH COLUMBIA

June, 1979

In presenting this thesis in partial fulfilment of the requirements for an advanced degree at the University of British Columbia, I agree that the Library shall make it freely available for reference and study. I further agree that permission for extensive copying of this thesis for scholarly purposes may be granted by the Head of my Department or by his representatives. It is understood that copying or publication of this thesis for financial gain shall not be allowed without my written permission.

Department of CHEMISTRY

The University of British Columbia
2075 Wesbrook Place
Vancouver, Canada
V6T 1W5

Date AUGUST 23, 1979

ABSTRACT

The first crystal and molecular structure of an indium porphyrin, α,β,δ,γ-tetraphenylporphinatoindium(III) chloride (InTPP:Cl) has been determined by X-ray diffraction. The indium is five-coordinate in a square-pyramidal complex with chloride as the axial ligand. The average In-N bond is 2.156(6)Å, with an In-Cl distance of 2.369(2)Å. The porphinato core is somewhat expanded with an average radius of 2.067(3)Å, and the macrocycle is non-planar with a net doming (0.1Å) toward the indium. The indium atom is located 0.61Å above the mean plane of the four pyrrole nitrogen atoms.

Based on the high degree of analogy between the principal structural features of InTPP:Cl, Fe(III) porphyrins, and Fe(II) deoxyhemoglobin (e.g., displacement of metal atom above the mean porphyrin plane, distance from the metal to pyrrole nitrogen, porphyrin core expansion, doming of porphyrin skeletal core atoms), the present study suggests that reconstitution of an indium porphyrin into apohemoglobin and apomyoglobin should produce the quaternary "tense" conformation. This provides an unique opportunity to study the porphyrin-apoprotein interactions in the "T" state of hemoglobin and myoglobin.

The present reconstitution of indium-111 meso-protoporphyrin IX (^{111}InMPP IX) into myoglobin represents the first location of a motional probe at the central metal of the active site of the protein. The rotational correlation time (τ_c) of the reconstituted myoglobin has been determined by the Perturbed Angular Correlations (P.A.C.) technique. Since ^{111}InMPP IX is structurally similar to ferro-protoporphyrin IX (heme), there should be very little internal rotation

of the ^{111}InMPP IX at the active site of the reconstituted myoglobin. Furthermore, the indium-labelled myoglobin is very likely to retain its native conformation, in contrast to other labelling techniques in which there is always uncertainty as how much the label distorts the structure of the protein being studied. Finally, since no additional flexibility is introduced at the labelled site of the protein, the present determination of τ_c(P.A.C.) for myoglobin is more direct than fluorescence depolarization or ESR determinations.

TABLE OF CONTENTS

LIST OF FIGURES

LIST OF TABLES

ACKNOWLEDGEMENTS

In 1977, I joined Prof. A. G. Marshall's biophysical group in U.B.C. where I was first introduced to the Perturbed Angular Correlation (P.A.C.) of gamma radiation technique, and porphyrin chemistry. I should like to express my sincere appreciation to Prof. Marshall for his continuing guidance and encouragement throughout my stay at U.B.C.

I am particularly indebted to Prof. P.W. Martin of the Physics Department, U.B.C. who carried out the P.A.C. measurements, and also to Dr. R. G. Ball who did the X-ray analysis of the indium porphyrin complex. A special thanks to Miss Mandy of the Pathology Department, U.B.C. who carried out the viscosity measurements.

I wish to acknowledge with gratitude the helpful and critical suggestions from Drs. D. C. Roe, Lewis Choi, Mr. G. A. Louma and J. L. Smith who read this thesis.

A measure of acknowledgement must be extended to Mr. T. Dekleva, R. Snoek, Ms. Roxanne LeBlanc Lemieux, and Mrs. J. Carruthers for their support and encouragement.

I would like to thank Dr. A. W. Addison of Drexel University, and Drs. D. Dolphin, B. R. James, A. Storr and J. Trotter of U.B.C. for their helpful comments and discussions.

Although space limitations prohibit a listing of all those who have make my stay an enjoyable and fruitful one in Vancouver, I wish to record my gratitute to them. Finally, I would like to express my appreciation to Mrs. Anna Wong for typing this thesis.

CHAPTER I

GENERAL INTRODUCTION

The last decade has witnessed a number of major publications in metalloporphyrin research. A high level of continuing activity in this field stems from interest in biological systems to which these compounds are related. Metalloporphyrins are also studied for developing superconductors (1), anti-cancer drugs (2), and catalysts (3). The biologically important metalloporphyrins are principally iron porphyrins, and these are the porphyrins that serve as the prosthetic group in several classes of the hemoproteins (4) such as hemoglobins, myoglobins, catalases, erythrocruorins, some peroxidases, and cytochromes. For the present case, only myoglobins and hemoglobins will be considered.

This thesis is divided into two parts. Part one deals with the stereochemistry of indium(III) meso-tetraphenylporphyrin chloride (InTPP:Cl) and metalloporphyrins in general. Part two describes the determination of the rotational correlation time of reconstituted myoglobin by means of the directional gamma-gamma angular correlation technique.

Structural studies of metalloporphyrins contribute significantly to the understanding of the chemical and physical properties of porphyrins, and elucidation of the structure of iron porphyrins in particular carries many biologically significant implications; this aspect is dealt with in details in Chapter I.

According to the most recent published compilation (5), the crystal and molecular structures of more than 120 porphyrins and metalloporphyrins had been determined by X-ray diffraction by 1976. A major reason for the

high and continuing interest in such details as the bond lengths, metal disposition, and distortions in the porphyrin core structure of metalloporphyrins is that pronounced variations in these structural parameters occur on oxygen-binding, and these variations are proposed to relate directly to the co-operative oxygen-binding function of hemoglobin (6). Although at least 20 metalloporphyrin complexes exhibit structures with the metal atom displaced by varying distances above the mean plane of the 4 pyrrole nitrogens of the porphyrin skeleton, virtually none fulfills the useful requirements that the metal displacement be similar to that in hemoglobin, and that the metal be stable to oxidation. Since indium(III) is oxidation-stable in aqueous solution, and has an ionic radius similiar to that of iron(II), it was decided to determine the crystal and molecular structure of an indium porphyrin complex. The present results suggest that reconstitution of myoglobin or hemoglobin with indium porphyrins should provide information of direct relevance to the proposed models for hemoglobin function.

The potential of perturbed angular correlation (P.A.C.) measurements to yield motional and structural information about biological macromolecules has been discussed in several publications (7-12). The simplicity of experimental measurements, in combination with concentration sensitivity approaching 10^{-12}M enhance the appeal of the P.A.C. technique. Another attractive feature of the P.A.C. technique is the ability to study both the liquid and solid states, which opens the possibility for "in vivo" experimentation. Despite the obvious potential of such applications, relatively few studies of this type have been performed. The reason for this paucity of publications is probably the lack of versatility in selective attachment of radioactive "rotational labels" to specific sites on macromolecules. This thesis shows that indium-111

labelled porphyrins can be selectively incorporated into myoglobin.

Indium has an isotope (^{111}In) that is radioactive with an initial state half-life of 2.8 days, and the decay process produces two gamma rays in succession, each with a convenient energy for detection. Marshall et al., (13,14) were the first to show how gamma-gamma coincidence measurements for this sort of energy cascade can give direct information about the chemical bonding and motional flexibility at an indium-labelled site on a macromolecule. The present results (Part two) confirm the applicability of this measurement technique to indium-labelled myoglobin.

The present reconstitution of indium-III meso-tetraphenylporphyrin into myoglobin represents the first motional probe located at the central metal at the center of the active site of protein.

Justification for the content of this thesis is two-fold. Firstly, this thesis proposes that reconstitution of hemoglobin with indium porphyrins could provide an insight into the mechanism of co-operative oxygen-binding function of hemoglobin. Secondly, the present work demonstrates that the P.A.C. technique could provide an alternative means of obtaining rotational correlation times of biological macromolecules.

Hemoglobin is postulated by Perutz (6) to exist in two conformational forms. The form in which the central five-coordinate Fe(II) atom is displaced above the heme plane is known as the "T" ("tense") form. The other "R" ("relaxed") form is one in which the central six-coordinate Fe(II) atom lies nearly coplanar with the heme plane. The heme iron is five-coordinate in deoxy-hemoglobin (deoxy-Hb) which is responsible for the "T" form. On binding molecular oxygen, the heme iron becomes six-coordinate and moves into the heme plane, and the oxy-Hb is said to be in the "R" form.

According to Perutz, the transition from "T" to "R" forms causes protein conformational changes that are necessary for the observed co-operative oxygenation effect in hemoglobin. A critical test for this proposal would be to "freeze" one or more subunits into the "T" form, and then monitor changes in the kinetic, electronic, and motional properties of the remaining native subunits upon oxygenation. In oxy-Hb, native subunits in the "T" forms are very difficult to obtain since Fe(II) binds oxygen to give the "R" form.

Since the "T" form cannot be stably maintained in oxy-Hb using native iron heme, other means such as reconstitution or "metal replacement" must be sought. Hemoglobins have been reconstituted with various metalloporphyrins containing Mn, Co, Zn, and Mg in an oxidation state similar to Fe(II). However, Co binds oxygen, and Mn(II) autoxidizes to Mn(III). Both Mg and Zn may be stable to oxidation but they exhibit relatively small out-of-plane displacements of the metal atoms above the porphyrin plane relative to that of the Fe atom in native Hb.

A comparison of the structural data on various metalloporphyrins (Table 4.7) shows that the out-of-plane displacement of indium in InTPP:Cl is by far the most similar to that of Fe in horse deoxy-Hb and human deoxy-Hb. Other attractive features of indium are that In(III) is oxidation stable, and does not bind oxygen. The combination of near-ideal In...Pμ* distance, stability to oxidation, and inability to bind oxygen suggest that an indium porphyrin may be an ideal candidate for inducing the "T" conformation. If the current theory of co-operativity by Perutz (6) is correct, indium porphyrin

---

* Indium out-of-plane displacement from the mean plane of the entire macrocycle.

complexes reconstituted in place of heme groups in hemoglobin should "freeze" the indium-labelled subunits into the desired "T" conformation.

The second justification is that P.A.C. technique can be used to obtain motional and structural information about biological macromolecules. Indium has an advantage that it has an isotope (^{111}In) that is suitable for gamma-gamma coincidence measurements. These measurements require the incorporation of a gamma-ray emitter into the molecule under study. Several isotopes can be used: ^{111m}Cd($t_{1/2}$=49 min), ^{62}Zn($t_{1/2}$=9h), ^{119m}Hg($t_{1/2}$=43 min), ^{204m}Pb($t_{1/2}$=68 min), and ^{111}In($t_{1/2}$=2.8 days). It is obvious that ^{111}In is the most convenient isotope from the practical viewpoint.

The present results effectively demonstrate that motional properties such as the rotational correlation time of myoglobin can be determined by means of the P.A.C. technique. This work can be extended to other biological macromolecules such hemoglobins, and cytochromes.

It is interesting to note that for the past decades, many investigators have utilized various marker substances ranging from porphyrin complexes, tetracycline derivatives, radioactive isotopes, and other substances to identify and delineate malignant tissues. Schwartz and coworkers have observed a high concentration of certain porphyrins in tumors. It is conceivable that ^{111}In-labelled porphyrins could be used for tumor-localisation. Indium-111 has ideal physical characteristics (a convenient 2.8 days half-life and gamma rays in the desired energy range) for tumor scanning.

PART ONE

CRYSTAL AND MOLECULAR STRUCTURE OF α,β,γ,δ-TETRAPHENYLPORPHINATOINDIUM(III) CHLORIDE

CHAPTER II

2.1 Metalloporphyrin Stereochemistry

The porphyrins are compounds formed by adding substituents to the nucleus of porphine (Figure 2.1). The naturally occurring porphyrins are generally formed by adding substituents to positions 1-8 and are named according to the number and type of substituents. Table 2.1 lists several porphyrins, both natural and synthetic with their trivial names that most frequently employed for structural studies.

TABLE 2.1

Common Porphyrins and Abbreviations

Porphyrin	Position on ring[a]								
	1	2	3	4	5	6	7	8	α,β,δ,γ
Protoporphyrin[b]	M	V	M	V	M	P	P	M	H
2,4-Diacetyldeutero-porphyrin[c]	M	Ac	M	Ac	M	P	P	M	H
Mesoporphyrin[d]	M	E	M	E	M	P	P	M	H
Etioporphyrin I[e]	M	E	M	E	M	E	M	E	H
Etioporphyrin II[f]	M	E	E	M	M	E	E	M	H
Octaethylporphyring	E	E	E	E	E	E	E	E	H
Tetraphenylporphyrin[h]	H	H	H	H	H	H	H	H	C_6H_5
Tetra(4-pyridyl)-porphyrin[i]	H	H	H	H	H	H	H	H	C_5H_4N

[a] Ac,$COCH_3$;E,CH_2CH_3;M,CH_3;P,CH_2CH_2COOH;V,$CHCH_2$

[b] H_2Proto. [c] H_2Deut. [d] H_2MesoP. [e] H_2Etio I. [f] H_2Etio II.

[g] H_2OEP. [h] H_2TPP. [i] H_2TPyP.

The notation that will be used throughout this chapter is illustrated

in Figure 2.1. C_α and C_β for a- and b-carbon atoms of a pyrrole ring, N for pyrrole nitrogen, and Cm for methine carbon. Ct denotes the center of the porphyrin, M a coordinated metal ion, and Nε the coordinated axial nitrogeneous base. M-N is used to represent a metal-pyrrole nitrogen bond distance, and M-Nε the metal-axial nitrogen bond distance. A non-bonded separation between two atoms is denoted by three centered dots(...); a bonded distance is designated by a dash(-).

The chief impediment to the elucidation of metalloporphyrin structure is the difficulty (especially for derivatives of biologically important protoporphyrin IX) of obtaining the single crystals suitable for X-ray diffraction analysis. The crystals are often too small or when large enough, are often subject to crystal defect due to internal packing disorder. The nature of the crystal disorder may vary markedly both in kind and degree. It is often found that crystalline disorder can be so extensive so as to preclude meaningful structural investigation. Structural analysis can often be misleading if the nature of the crystalline defect is not identified and its importance assessed. For example, the present crystallographic analysis of InTPP:Cl indicates non-equivalence of the phenyl tilt angles which can be explained from internal packing.

Derivatives of the symmetric porphyrins (H_2EtiO,H_2OEP, H_2TPP, and H_2TPyP) are most frequently employed for structural determination because of their availability and ease in obtaining the necessary single crystals. Within the accuracy of the experimental data, there are only small differences between the naturally occurring porphyrins and synthetic derivatives, in cases where structures of both have been determined.

Removal of the two pyrrole protons yields a porphyrin dianion that

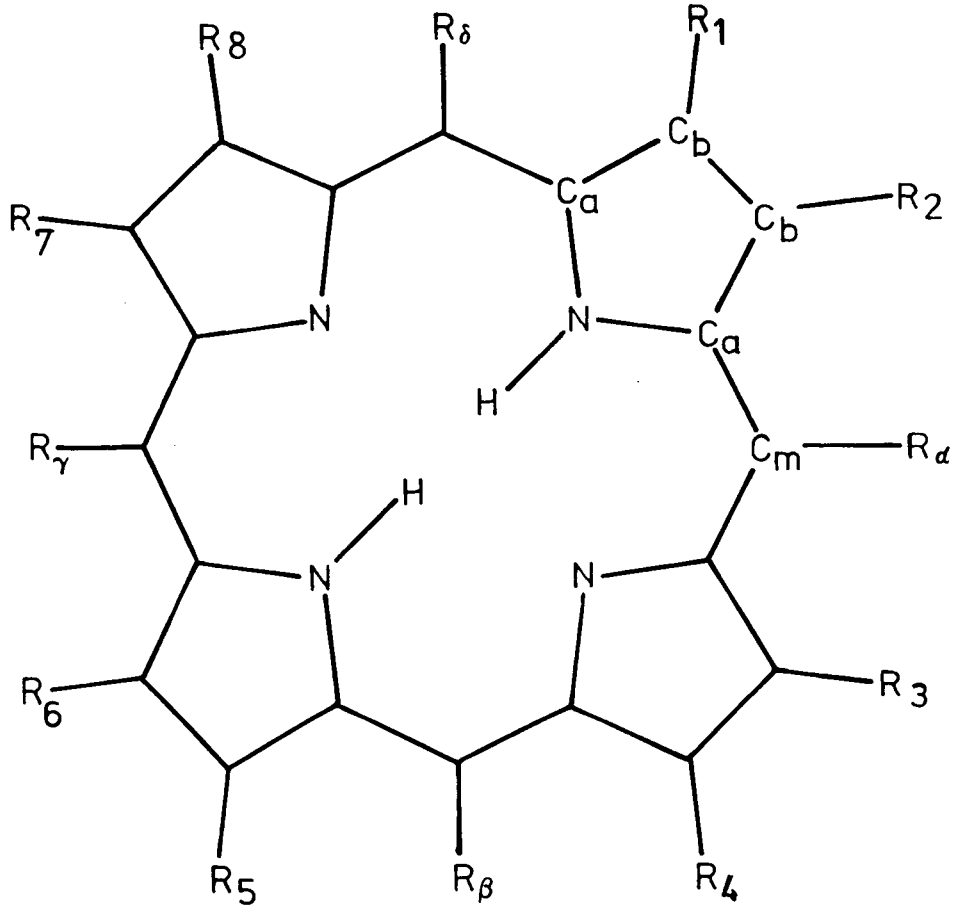

Figure 2.1. The nucleus of porphine, illustrating the positions of possible substituents and the notation used for the unique atoms of the core.

behaves as a tetradentate ligand which readily complexes any of a variety of metal ions. As expected, the minimum coordination number is four. Addition of axial ligands, either neutral or anionic, gives metalloporphyrin derivatives wherein the metal ion has a coordination of five, six or eight. Only the five-coordinate metalloporphyrins are of interest in the present case. Figure 2.2 gives the "periodic-table of metalloporphyrins".

Porphyrins, in common with other macrocyclic ligands, have a central hole of essentially fixed dimensions. The porphinato core resists undue radial expansion and contraction in equatorial plane. In certain metal complexes, the metal is unable to fit into this hole and, as has been shown by Hoard (15). Thus, the perpendicular displacement of the metal atom is related to the effective radius, since the size of the central hole in the porphyrin is relatively constant. An inspection of Table 4.7 shows no simple correlation between ionic radii and metal ion displacements. The porphyrins are not rigid but rather remarkably flexible macrocycle molecules (16,17,18).

In 1961 R.J.P. Williams (19) pointed out that the transition from high to low spin should be accompanied by a marked reduction in the ionic radius of the iron. He further suggested that change in the structure of hemoglobin on oxygenation "is related to the change in the imidazole-iron distance or possibly to the concomitant change in the steric arrangement of the imidazole (of the heme-linked histidine) relative to the porphyrin plane".

From the crystallographic studies of metalloporphyrins (especially ferric porphyrin complexes), J. L. Hoard and associates demonstrated

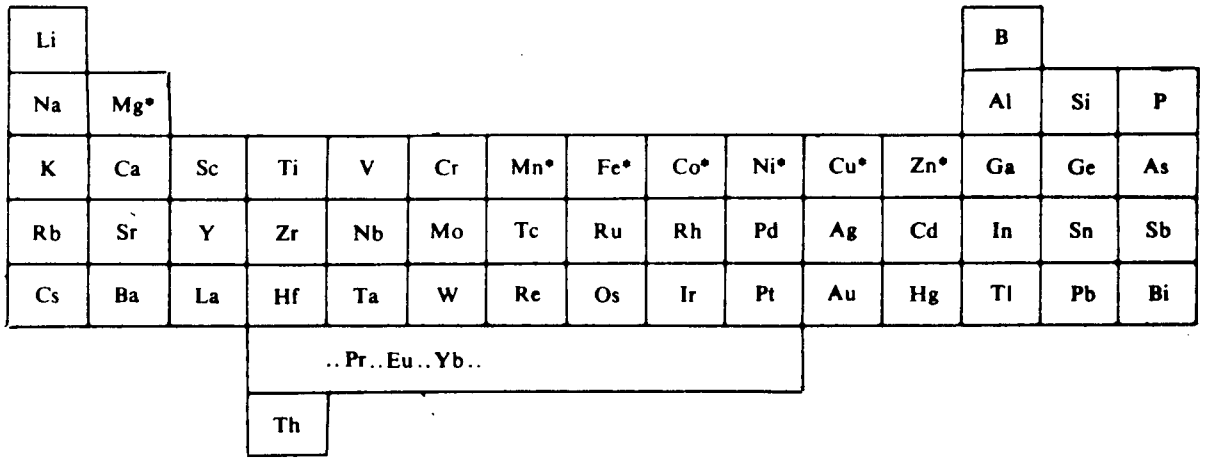

Figure 2.2. The periodic table of metalloporphyrins.(Metals which are inserted by nature are marked with an asterisk.)

experimentally that the high to low spin transition is accompanied by a marked reduction in radius of the iron (15,20,21,22,23). He predicted that the same should hold true for ferrous complexes. Hoard then proposed that the high-spin ferrous ion in deoxy-Hb and deoxy-Mb is five-coordinated and is displaced from the porphyrin plane toward the proximal histidine by 0.5-0.8Å. Upon binding an oxygen molecule, the iron atom becomes six-coordinate and low-spin, and moves back toward the plane of porphyrin. This planarity has been verified in cyanomethemoglobin by Hendrickson and Love (24), and CO-erythrocuorin by Huber et al., (25), and very recently for oxy-myoglobin by S.Phillips (26).

Williams (19), and Hoard (27) suggested that the movement of the iron atom causes a change in the position of the imidazole group of the proximal histidine. This movement is in turn responsible for the conformational changes in hemoglobin and myoglobin upon oxygenation.

Based on his structural studies of oxy(met)- and deoxy-Hb, Perutz (28,29) has proposed the stereochemical mechanism for the co-operative phenomenon (See Appendix A). At the heart of this proposal is the assumption, based on earlier ideas of Hoard (27), and Williams (19) that in hemoglobin the high-spin to low-spin transition should be associated with a movement of the iron toward the porphyrin plane (22,23,27,28,30, 31). The resulting motion of the proximal histidine (>0.5Å) causes the necessary conformational changes in the protein that are responsible for the co-operativity.

Obviously, the principal metalloporphyrin structural parameters of greatest interest are thus the displacement of the metal atom from the mean plane, Ct...M, and the M-N bond distances.

The bond distances within the porphine skeleton itself are quite invariant with respect to the porphyrin compounds studied. As expected the small distance variations are due to substituent effects. The M-N bond distance, however, does vary appreciably depending on the nature of the metal atoms coordinated to the porphyrin. M-N can range from 2.32Å in bismuth porphyrins to 1.95Å in nickel porphyrins. A long M-N bond can be expected if the metal is positioned out of the mean plane of the pyrrole nitrogen atoms. Table 2.2 shows that there is no simple correlation between ionic radii and M-N distances.

TABLE 2.2

Variations of M-N distances with ionic radii

Metal	Ionic radius	M-N distance
	Å	Å
Fe(III)	0.64	2.07
Ni(II)	0.68	1.96
Cu(II)	0.72	1.98
Zn(II)	0.74	2.05
In(III)	0.81	2.16
Pd(II)	0.86	2.00
Tl(III)	0.95	2.21
Bi(III)	0.96	2.32

The porphinato core is often not planar but rather easily subjected to deformation normal to the mean plane into a ruffled or domed configuration.

This observation has been confirmed by structural determination of tetraphenylporphine (32) and its copper and palladium derivatives (33). The InTPP:Cl also exhibits marked deviations from planarity of the porphinato core (See Chapter IV, Section 4.3). Planar conformations are necessary to ensure maximum π-interaction between the substituents and the extensive conjugated porphyrin systems. Nonplanar conformations, however, predominate in crystalline metalloporphyrins. The likely explanation is that nonplanar conformations result from packing constraints in the crystal or intramolecular repulsions of axial ligands with atoms of the core.

Hoard (34) examined the correlation between M-N distances and geometry of the macrocycle in metalloporphyrins. He concludes that deformations are more likely for contracted core which has short M-N distances. Recent studies (35,36) confirm Hoard's observations. Cullen and co-workers (35) compared two crystalline forms of NiOEP so as to eliminate the effects of different substituents on the ring on the geometry. The tetragonal form has the average Ni-N distance (1.93Å), the shortest M-N distance yet reported for a metalloporphyrin, and the macrocycle is highly distorted (37). In contrast, the triclinic NiOEP is essentially planar and the M-N distance is 1.96Å. The M-N distance of 2.01Å appears to be a nearly optimal value of minimal strain and undistorted accomodation of the metal atom within the central porphinato core (21). Structural studies also show that for a highly expanded core, the most efficient nonplanar conformation is doming of the core (18,34). The present study of InTPP:Cl also confirms this observation. InTPP:Cl has a highly expanded porphinato core with $(M-N)_{av}$ distance of 2.16Å. As expected the plane of the four pyrrole nitrogens is

displaced i.e. domed upward by 0.1Å from the mean plane of the porphinato core.

The five-coordinate geometry is a very common one in metalloporphyrins, especially prominent for zinc, magnesium, cobalt(II), and high-spin iron porphyrins. Figure 2.3 represents the schematic diagram of the square-pyramidal coordination group for five-coordinate metalloporphyrins. A brief consideration of the Pythagorean theorem demonstrates that the out-of-plane displacement, Ct...M of the metal atom from the mean porphinato core can be calculated if Ct...N and M-N distances are known. A modest doming of the core is a nearly invariable feature among five-coordinate metalloporphyrins especially those with large central metal atoms. Consequently, the doming of the core toward the metal atom leads to the inequality of $M...P_N < M...P_C$. Generally $P_N...P_C$ (doming) is small <0.05Å. For this class of metalloporphyrins, typical Ct...N values are found in the range of 1.98-2.05Å, and the M-N distances are usually <2.01Å (Table 2.3 and 4.7). The displacement of the metal atom from the mean plane is a measurable property of all metalloporphyrins of this class. The magnitude varies from 0.10Å to >0.50Å. The length of the axial ligand-metal bond is dependent on the nature of the axial ligand.

Due to the doming effect, steric interaction between the axial ligand and the porphinato core is reduced and less important in five-coordinate than six-coordinate metalloporphyrins; its importance is obviously diminished with an increasing displacement of the metal atom out-of-plane.

A short discussion of the stereochemistry of iron porphyrins is

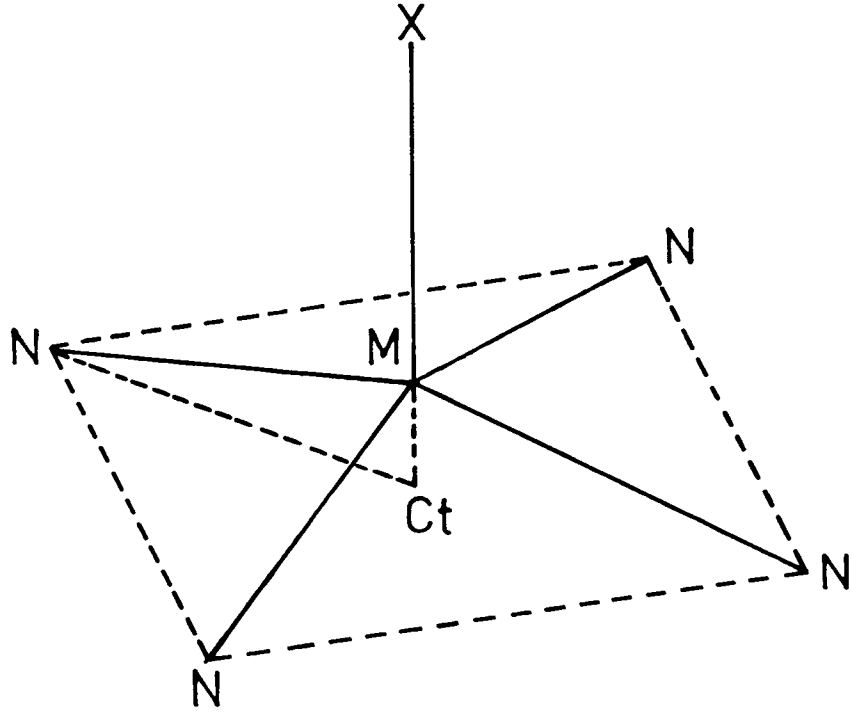

Figure 2.3. A diagram of the square-pyramidal coordination group for five-coordinate metalloporphyrins

warranted in view of their relationships to biologically important molecules such as hemoglobin and myoglobin. Cobalt porphyrins will also be included because of the relation of cobalt porphyrin stereochemistry to the cobalt-substituted hemoproteins.

A number of interesting features emerge from the stereochemical data in Table 2.3. The metal atom lies in plane with the four pyrrole nitrogen atoms only if M-N < 2.01Å. The normal radius of the central "hole" in an undistorted metalloporphyrin has been estimated to be 2.01Å (21). It is interesting to note that the value of 2.01Å corresponds nearly to the mean of the smallest (1.93Å for tetragonal NiOEP) and the largest (2.21Å for Tl(OEP)Cl) M-N values (See Table 4.7) so far reported for metalloporphyrins. The Table 2.3 also shows that the metal ion displacement is substantial in each of the iron porphyrins; all of these (including ferrimyoglobin) are high-spin Fe^{+++} derivatives with the exception of 2-MeImFe(II)TPP in which iron atom is in oxidation state two.

TABLE 2.3

Stereochemical parameters for porphyrins and metalloporphyrins (distances in Angstroms)

	M-N[a]	Ct-N[b]	Δ[c]	Axial Ligands	Ref
NiEtio	1.957	1.957	-	None	38
NiDeut	1.960	1.960	-	None	39
CuTPP	1.981	1.981	-	None	33
PdTPP	2.009	2.009	-	None	33
H_2OZnTPP	$\geq$2.05	2.042	$\geq$0.19	H_2O at $\leq$ 2.21 Å	20
ClFeTPP	2.049	2.012	0.383	Cl at 2.19 Å	40
Chlorohemin	2.062	2.008	0.475	Cl at 2.218 Å	41
MeOFeMeso	2.073	2.022	0.455	OMe at 1.842 Å	23
Porphine	-	2.051	-	None	42
tet-TPP	-	2.054	-	None	17
tr-TPP	-	2.065	-	None	43
Fe(III)Mb	~1.9	~1.9	~0.30	N at ~1.9 Å H_2O ~2.1 Å	44

[a] Metal-nitrogen distance
[b] Radius of central hole: see text
[c] Out-of-plane displacement of the metal atom

From J. L. Hoard (Ref. 22)

2.1a Iron Porphyrins

Iron porphyrins provide the typical examples of the influence of the spin-states and oxidation states of the central metal ions on the stereochemistry of metalloporphyrin. The effective radius of high-spin iron(III) ion is too large to allow the iron to fit into the central hole. A typical displacement of the iron of about 0.48Å out-of-plane is as expected. A small amount of doming of the porphinato core toward the iron(II) ion is frequently observed with $P_c...P_N$ < 0.05Å. A qualitative picture for this observation is gained by considering a square-pyramidal model for a high-spin iron porphyrin.

In the simple model, the Z-direction is defined as normal to the porphinato core (Figure 2.4). The $d_{x^2-y^2}$ orbital of a coordinated metal ion is then in a plane parallel to the mean porphinato core. A metal ion where the $d_{x^2-y^2}$ orbital is populated will be relatively large and have commensurately long M-N bonds. In any high-spin Fe(II) or Fe(III) metalloporphyrin, there is one unpaired electron in each of the $3d_{x^2-y^2}$ and $3d_{z^2}$ orbitals in the metal atom. The presence of the unpaired electron in $3d_{x^2-y^2}$ orbital is responsible for the substantial displacement of the iron from the plane of the pyrrole nitrogen atoms. In a low-spin Fe(II) or Fe(III), the pairing of electron spins in the d_{xy}, d_{yz}, and d_{xz} valence-shell orbitals of the metal atom allows full utilization of the unoccupied $3d_{x^2-y^2}$ and $3d_{z^2}$ orbitals for complexing two axial ligands.

The high-spin complex of 2-methylimidazoleiron(II) (45) is a five-coordinate, square-pyramidal, and the iron(II) is displaced 0.42Å from the mean plane of the four pyrrole nitrogens and 0.55Å from the mean porphinato core. The doming i.e. $P_N...P_c$ separation is 0.13Å.

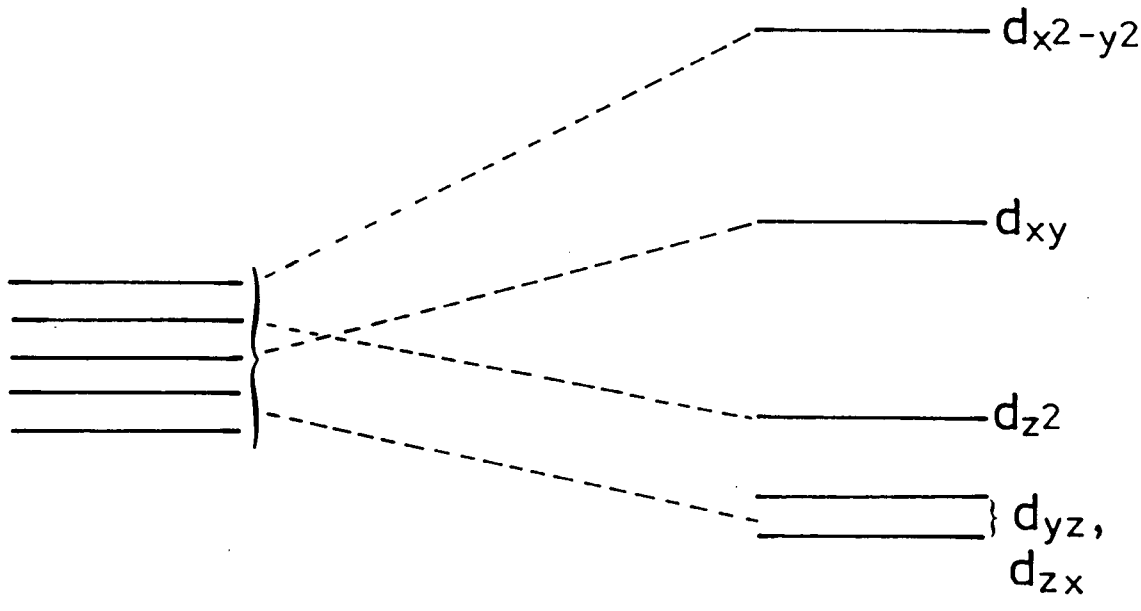

Figure 2.4. Energy-level diagram for square-pyramidal coordination.

Both the Fe(II) and Fe(III) can form low-spin complexes when coordinated to two appropriate type of axial ligands. According to Hoard's observation (15,20,21,23) in the low-spin six-coordinate complexes, the iron is coplanar or nearly coplanar with the porphinato core. A substantially shorter Fe-N bond distance relative to the high-spin can also be anticipated.

The structure of a low-spin six-coordinate $(Im_2FeTPP)^+Cl^-$ has shown that the position of the iron(III) is only 0.009Å (30) from the mean porphinato nitrogens. The $(Fe-N)_{av}$ distance of 1.989Å is significantly shorter than those of the high-spin complexes with $(Fe-N)_{av}$ > 2.04Å (See Table 2.4).

TABLE 2.4

Parameters of the Square-Pyramidal Coordination Group in Several High-Spin Iron(III) Porphyrins

Derivative	$(Fe..N)_{av}$	Distance (A)			Ref
		Ct...N	Ct...Fe	Fe-X	
ClFeProtoDME[a]	2.062(10)	2.008	0.475	2.218(6)	41
CH_3OFeMesoPDME[b]	2.073(6)	2.022	0.455	1.842(4)	23
ClFeTPP	2.049(9)	2.012	0.38	2.192(12)	40
$O(FeTPP)_2$	2.087(5)	2.027	0.50	1.763(1)	48
(SCN)FeTPP	2.065(5)	2.007	0.485	1.957(5)	49
N_3FeTPP	2.055	2.027	0.34	1.909	50
$O(FeProtoDME)_2$[a]	2.08	-	-	1.73	51
$O(FeODM)_2$[c]	2.065(8)	2.002	0.53	1.752(1)	52

[a] Dimethyl ester of protoporphyrin
[b] Dimethyl ester of mesoporphyrin
[c] α,γ-Dimethyloctaethylporphyrin

From Scheidt (Ref. 47).

The stereochemical pattern is maintained for an Fe(III) porphyrin derivative in which two non-equivalent axial ligands are coordinated. In N_3(Py)FeTPP (46), the Fe(III) ion is centered to within 0.03Å and has a shortened $(Fe-N)_{av}$ distance of 1.990Å.

The low-spin Fe(II) porphyrins exhibit stereochemical behavior similar to Fe(III) derivatives. The Fe(II) ion in the centrosymmetric Pip_2FeTPP (31) is exactly centered. The equatorial $(Fe-N)_{av}$ bond distance is 2.004Å which is slightly larger than the characteristic low-spin Fe(III) derivatives.

2.1b Cobalt Porphyrins

All cobalt porphyrins, either cobalt(III), d^6, or cobalt(II), d^7, are low-spin complexes. Unlike iron porphyrins, cobalt complexes do not exhibit spin-state transitions. The stereochemistry of cobalt porphyrins is greatly influenced by the oxidation states and the number of axial ligands.

Table 2.5 gives the stereochemical parameters of five-coordinate low-spin cobalt(II) porphyrin derivatives. Table 2.3 shows that displacement of the metal atom from the mean porphinato nitrogen plane occurs only if the complexing M-N > 2.01Å. An inspection of Table 2.5, however, indicates that cobalt porphyrins do not obey the above observation; the cobalt atom is displaced from the mean plane of the pyrrole nitrogens by the same distances irrespective whether the M-N bond distance is greater or less than 2.01Å. With an unoccupied $d_{x^2-y^2}$ orbital, the cobalt(II) is appropriately found to have a smaller out-of-plane displacement than high-spin iron porphyrins.

TABLE 2.5

Stereochemical Parameters of the Square-Pyramidal Coordination Group for Low-Spin Cobalt(II) Porphyrins

Derivative	Distance (Å)					Ref.
	$(Co-N)_{av}$	$Co-N_{ax}$ [a]	$Co...P_N$	$Co...P_c$	$N_{ax}...P_c$	
NMeImCoTPP	1.977(3)	2.157(3)	0.13	0.14	2.30	54
NMeImCoOEP	1.96(1)	2.15(1)	0.13	0.16	2.33	55
(3,5-Lut)CoTPP	2.000(5)	2.161(5)	0.14	0.17	2.33	56
DiMeImCoTPP[b]	1.985(2)	2.216(2)	0.15	0.18	2.37	57

[a] N_{ax} is the nitrogen atom of the axial ligand

[b] DiMeIm is 1,2-dimethylimidazole

From Scheidt (Ref. 47)

The $Pip_2Co(III)TPP^+$ (Co,d^4) cation (53) and low-spin $Pip_2Fe(II)TPP$ (Fe,d^4) are both isoelectronic and isostructural. Both porphinato cores are essentially planar. The $(Co-N)_{av}$ bond distance is 1.978Å compared to the $(Fe-N)_{av}$ of 2.004Å. The difference between the two M-N distances is the direct consequence of the differing nuclear charge on the two ions.

The porphinato core of $O_2N(3,5-Lut)CoTPP$ (36) is extremely ruffled with the corresponding short $(Co-N)_{av}$ distance of 1.954Å which probably represents the minimum Co(III)-N distance. The axial $Co-N_{NO2}$ distance is 1.948Å as opposed to the axial $Co-N_{(3,5-Lut)}$ distance of 2.036A. The difference

in the two bond lengths primarily reflects the differing steric requirements of the two axial ligands.

2.2 Application of Metalloporphyrin Stereochemistry to Heme Stereochemistry in Hemoproteins (Myoglobin and Hemoglobin)

This section concerns the application of metalloporphyrin stereochemistry discussed in Section 2.1 to heme stereochemistry in myoglobin and hemoglobin. The objective is to show how structural determination of metalloporphyrins can provide an insight into the mechanism of reversible oxygenation in hemoglobin and myoglobin. It must be pointed out that there is still a lot of controversy and continuing debate concerning the allosteric model proposed by Perutz on the oxygen-binding co-operativity phenomenon in hemoglobin (28,58).

In hemoglobin the ferrous heme is directly anchored to the globin (protein) framework through the axial complexing bond formed by the iron(II) atom with an imidazole nitrogen atom of the proximal histidine residue (F8). In the low-spin, oxy-Hb, molecular oxygen occupies the vacant sixth position in the coordination group of the iron atom. There is no sixth ligand in the high-spin, deoxy-Hb.

When the structure of hemoglobin was finally solved, the hemes (59-63) were found to lie in isolated pockets with entrances on the surface of the subunits. The minimum spacing between any two heme iron atoms in deoxy-Hb or oxy-Hb is >25Å (28,6). Direct heme-heme interactions hence are an implausible source of co-operative phenomenon. As Perutz (6) posed the question "without contact between them (hemes) how could one of them sense whether the others had combined with oxygen?". Yet communication between the hemes in each subunit is prerequisite because all the co-operative effects disappear if the hemoglobin molecule is merely split in half.

It was noted by Hoard in 1966 (27) that the probable starting point for a stereochemical mechanism of co-operative interaction was the movement >0.5Å of the iron atom relative to the porphinato core upon oxygenation accompanied by the concomitant high-spin to low-spin transition. In Perutz's subsequently developed mechanism (28,29) for the co-operative oxygenation of hemoglobin, the primary trigger is the shrinkage of about 0.90Å in the Pμ...Nε[a] distance that accompanies the transition from high-spin five-coordination in deoxy-Hb to low-spin six-coordination in oxy-Hb. It is important to note that only the mean plane, Pμ, of the entire macrocycle in deoxy-Hb that can be identified; the protoporphyrin is viewed "edge-on as a rather thick band of unresolved electron density in which a substantial doming of the porphyrin core toward the iron atom may be wholly obscured". M-N distance in both (non-equivalent) α- and β-subunits of deoxy-Hb are estimated to be ∿0.6Å. According to Perutz's proposal, there must be a "tension" in the axial connection between the ferroheme and the globin (protein). A comparison of the Pμ...Nε distance in deoxy-Hb with an externally unconstrained five-coordinate 2-MeImFe(II)TPP (64,65) provides direct evidence for Perutz's proposal. It is interesting to note that sterically hindered 2-Methyl imidazole rather than unsubstituted imidazole is used as the axial ligand in the high-spin five-coordinate species. The reason is to preclude the formation of the low-spin six-coordinate species.

---

[a] Pμ...Pε is the perpendicular distance separating the axial nitrogen atom (Nε) of the heme-linked histidine (F8) from the mean plane (Pμ) of the ferroheme.

The Pμ...Nε distance is 2.90Å in deoxy-Hb as opposed to 2.60Å in the unconstrained high-spin, five-coordinate 2-MeImFe(II)TPP[a] (64). This corresponds to a shortening of the Pμ...Nε by 0.30Å in 2-MeImFe(II)TPP relative to the Pμ...Nε in deoxy-Hb. In other words, the axial connection between the ferroheme and the globin is in tension. Another piece of evidence comes from the high-spin (1-MeIm)Mn(TPP) complex (66). The Mn...Pc distance is 0.515Å and the doming parameter is still only 0.04Å (66) as compared to Fe...Pμ=0.75Å in horse deoxy-Hb. Unless the Fe...Pμ distance in deoxy-Hb is overestimated by at least 0.25Å, it appears that the axial connection must be in tension. Hopfield (67) has quoted an error of ±0.1Å in connection with the out-of-plane displacement of the Fe(II) atoms in deoxy-Hb.

Some further evidence in support of the tension model come from n.m.r. studies of normal and abnormal hemoglobin's (68-73). Little and Ibers (55) have discussed the pros and cons of the n.m.r. and resonance Raman studies.

Perutz (6,62) estimated that the Fe atom is displaced by 0.75Å from the mean plane of the 24-atoms porphyrin skeleton in horse deoxy-Hb. It has been estimated that as much as ∿0.20Å is due to doming of the core toward the Fe atom leaving 0.55Å to the out-of-plane displacement of the

---

[a] The Pμ...Nε in deoxy-Hb is the summation of Fe...Pμ=0.75Å and Fe...Nε=∿2.15Å. The Pμ...Nε in 2-MeImFe(II)TPP is obtained by the summation of Fe...P_N=0.42Å, P_N...P_C=0.05Å and Fe...Nε=2.16(Cos 10.3)A where 10.3 is the angle of tilt of this bond from the normal.

iron (64). The magnitude of the doming of 0.20Å can be calculated as follows:

Figure 2.5

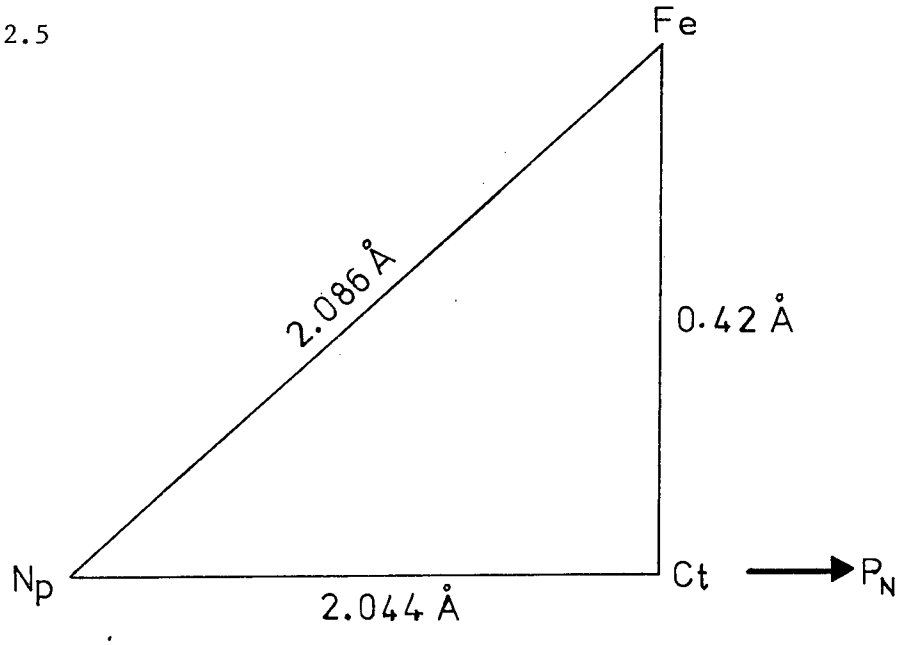

The stereochemical parameters for 2-MeImFe(II)TPP are: Fe-Np=2.086Å, Fe...P_N=0.42, and Ct...Np=2.044Å. If however, the Ct...Np distance is decreased to 2.01Å (minimum equatorial strain to the macrocyle ring; in human deoxy-Hb, it is 2.0-Å (74)) while maintaining the Fe-Np distance at 2.086Å, from the Pythagorean theorem, the Fe...P_N displacement can be calculated to be 0.55Å. In other words, 0.20Å is to be assigned to doming of the core.

As can be seen from Figure 2.6, transition from deoxy-Hb to oxy-Hb involves a shrinkage of ∿0.9Å in the Pμ...Nε which is the sum of three

components: (a) a decrease in Fe-Nε axial bond, (b) a movement of the iron atom toward the Pμ plane, and (c) the movement required to bring Pμ and P_N planes into coplanar or near coplanar. It is important to point out the calculation involves bond distances and displacements of the metal atoms taken from appropriate metalloporphyrins (55). The structure of oxy-Hb is still awaiting; Fe(II) autoxidises readily to Fe(III) giving met-Hb.

The replacement of the natural prosthetic group i.e. iron protoporphyrin IX with different metalloporphyrins in myoglobin and hemoglobin has proved to be a useful approach (75). Metalloporphyrins containing zinc (75,76), manganese (77-81), copper (77), and nickel (82) have been reconstituted into hemoglobins. Their properties have been studied and compared with the native hemoglobin. These reconstituted proteins are incapable of reversible oxygenation. Hoffman and associates (83-86) have shown that cobalt substituted myoglobin (CoMb) and hemoglobin (CoHb) can combine reversibly and cooperatively with molecular oxygen. The oxygen affinity is reduced by 10-100 times for CoMb and CoHb compared to native Mb and Hb (86).

Since low-spin Co(II) exhibits a smaller ionic radius than does high-spin Fe(II), Hoffman (83-85) predicted the displacement of the Co(II) atom in CoHb would be relatively small compared with that of the Fe(II) in deoxy-Hb. The structure of the low-spin, five-coordinate 1-MeImCo(II)TPP was subsequently determined by Scheidt (54). As predicted by Hoffman, Scheidt found that the cobalt atom is displaced 0.13Å from the mean plane of the porphinato nitrogens and the doming ($P\mu...P_N$) is only ∿0.01Å; consequently, the cobalt atom is displaced by ∿0.14Å from the mean plane

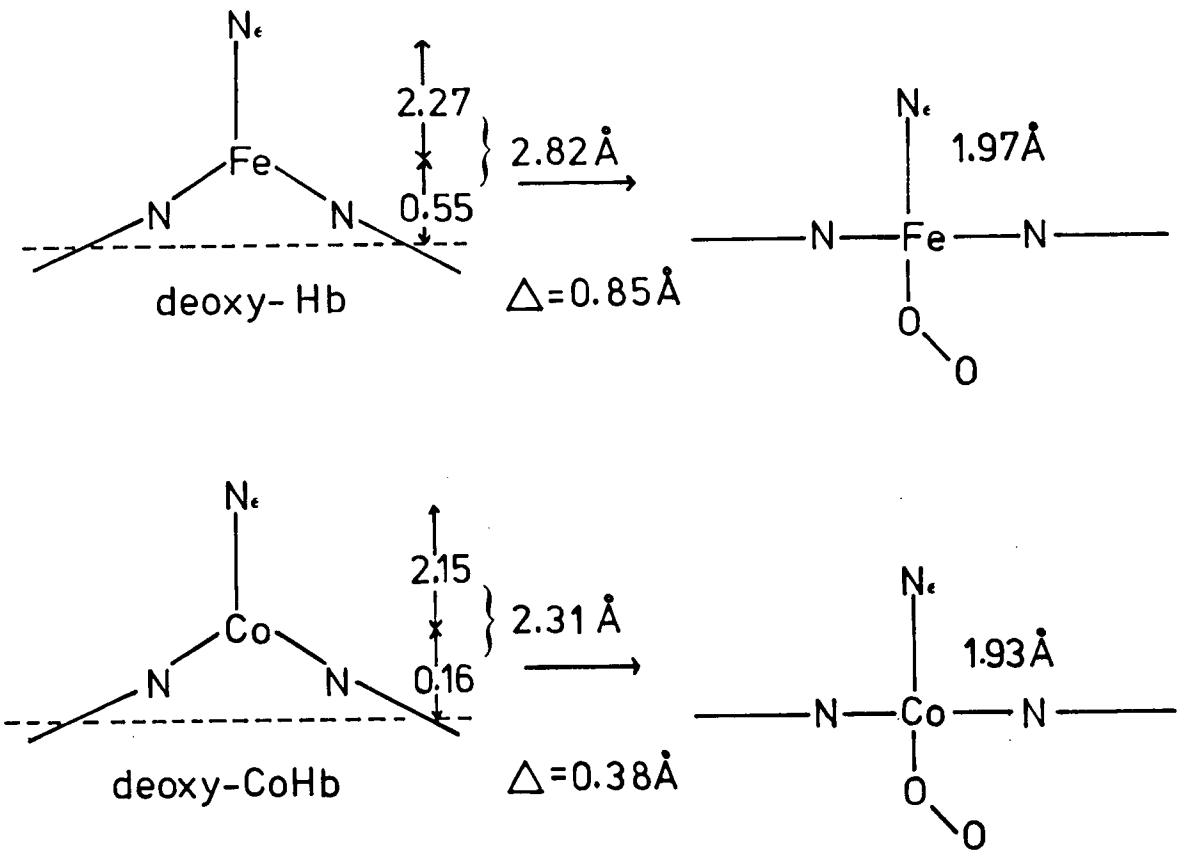

Figure 2.6. Illustration of calculation of the total movement of the proximal histidine in Hb(top) and CoHb(bottom). The displacements are taken relative to the 24-atom porphyrin core. From Little & Ibers (Ref. 55)

of the porphyrin. Similarly, in the low-spin, five-coordinate 1-MeImCo(II)OEP, Little and Ibers (55) found the Co atom is displaced by 0.13Å from the mean plane of the pyrrole nitrogen atoms and 0.16Å from the mean plane of the porphyrin core. It appears that the out-of-plane displacement of the Co atom in CoHb is unlikely to exceed 0.2Å. On this basis, Hoffman et al., (83), and Little et al., (55) questioned whether the relatively small out-of-plane displacement of the Co atom would be consistent with the trigger mechanism for cooperative oxygenation proposed by Pertuz (28,29).

The unpaired electron in the $3d_{x^2-y^2}$ orbital of the high-spin Fe(II) atom accounts for the substantial Fe...P_N displacement of 0.42Å in 2-MeImFe(II)TPP, whereas the absence of such an electron in the low-spin Co(II) atom allows the Co...P_N displacement to be 0.13Å in the 1-MeImCo(II)TPP (54) and 1-MeImCo(II)OEP (55). In other words, in deoxy-CoHb, the Co atom is already closer to the mean porphyrin plane than Fe atom in deoxy-Hb and is likely to have created a real strain in the Co-Nε connection. This is demonstrated by the lengthening of the Co-Nε bond in DiMeImCoTPP (Co...P_N=0.15Å) relative to 1-MeImCoTPP (Co...P_N=0.13Å) as shown in Table 2.5. More stretch and enhanced tension in the axial connection will require greater strain in the globin in deoxy-CoHb than in deoxy-Hb and consequently a reduction in the Pμ...Nε separation realtive to that in deoxy-Hb. The above argument assumes that the globin can support increased tension in Co-Nε bond so that quaternary structure of deoxy-Hb is retained.

Figure 2.6 also illustrates the calculation of the total movement of the proximal histidine in Hb and CoHb by Little and Ibers (55). However, it is important to point out that no doming of the cobalt porphinato core is assumed. The total movement of the proximal histidine

is estimated to be 0.38Å which is approximately half that for Hb. On this basis, Little and Ibers conclude that "it is unlikely that such a small movement (0.38Å) could trigger the conformation changes observed in Co-Hb".

A counterproposal has been advanced by Hoard and Scheidt (64) that moderate doming of the porphinato core in combination with modest stretch in the Co-Nε bond can readily lead to an Pμ...Nε separation approaching 2.90Å in deoxy-Hb (Figure 2.7). In 1974, Hoard (65) proposed the doming to be 0.3Å instead of 0.5Å. The essence of the Hoard and Scheidt argument is that tension within the protein in deoxy-CoHb not only causes the porphyrin to undergo substantial doming but also increases the Co-Nε(histidine) bond. The doming raises the Co atom out-of-plane displacement to ∿0.70Å compatible to the Fe atom (0.75Å) is horse deoxy-Hb.

Results from several studies (87,88) are against the tension model in Co-Hb proposed by Hoard et al., (64). Resonance Raman studies of CoHb and Hb by Woodruff et al., (87) indicate that the Co(II) atom out-of-plane displacement in deoxy-CoHb cannot exceed 0.2Å. Besides, the resonance Raman spectrum of deoxy-CoHb is essentially the same as for 1-MeImCo(II)OEP. EPR experiments with CoHb and model systems (88) also gives no convincing indications of tension within the globin that would increase the out-of-plane displacement of the Co atom or stretch the Co-Nε(histidine) bond in CoHb.

However, the structure of spermwhale oxymyoglobin recently determined by Phillips (26) provides further evidence for Perutz's allosteric model. The X-ray data was collected at -12°C to prevent autoxidation of Fe(II) to Fe(III) giving met-Mb. Phillips found that the iron atom is displaced

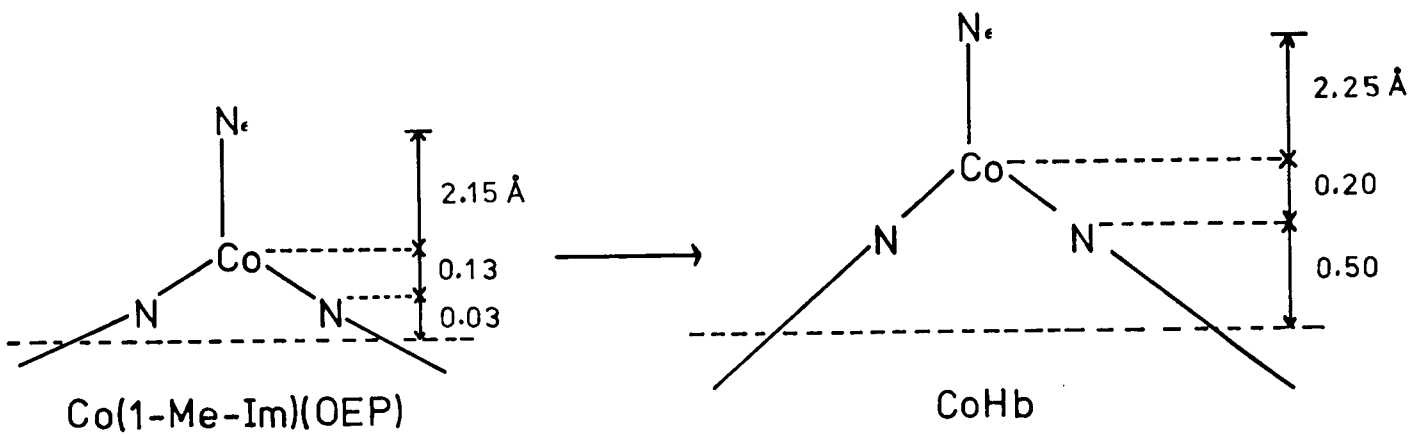

Figure 2.7. Illustration of possible points of distortion of the Co(II) porphyrin prosthetic group as proposed by Hoard & Scheidt (64).
From Little & Ibers (Ref. 55)

from the mean porphyrin plane by 0.26Å towards the proximal histidine (F8), and the bound oxygen has the bent-geometry. So far there is no measure of the corresponding Fe displacement in oxy-Hb because under the normal conditions of X-ray crystallography, oxy-Hb is readily oxidised to met-Hb. It is a common notion that the Fe atom is coplanar with the heme plane in oxy-Hb, however, the structure of oxy-Mb indicates this is not the case.

An interesting feature of oxy-Mb is that the heme-linked imidazole of histidine (F8) and Fe-O-O are approximately coplanar and elcipsed with the Fe-N bond of the pyrrole II ring. It seems probable the steric arrangement of the histidine (F8) and Fe-O-O plane that prevent the Fe atom from being coplanar with the porphyrin plane.

Table 2.6 shows that the transition from deoxy-Mb to oxy-Mb involves the movement of the Fe atom towards the heme plane and a shrinkage of 0.59Å in the Pμ...Nε as opposed to ∿0.90Å in the transition from deoxy-Hb to met-Hb. The difference in shortening of the Pμ...Nε is conceivably attributed to the fact that myoglobin is a single polypeptide which hence does not exhibit oxygen-binding co-operativity. Phillips (26) clearly demonstrates that the Fe atom does move towards the porphyrin on oxygenation as expected according to Perutz's allosteric model (6,62).

TABLE 2.6 Heme geometry in Mb and Hb derivatives

	Deoxy-Mb	Oxy-Mb	Met-Mb	CO-Mb	Deoxy-Hb	Met-Hb
Fe-(heme plane)	0.55	0.26*	0.40	0.24	0.60(α-heme) 0.63(β-heme)	0.07(α-heme) 0.21(β-heme)
Fe(Nε)-(heme-plane)	2.6	2.3	2.5	2.4	2.6(α-heme) 2.8(β-heme)	2.2(α-heme) 2.4(β-heme)

Values are given in Å
*Value from refined model (Phillips, private communication)
Adapted from Phillips (Ref.26)

2.3 Myoglobin and Hemoglobin - The Heme Group/Globin Structure

The details of the structure of myoglobin are mostly derived from the impressive X-ray crystallographic studies of J. C. Kendrew et al., (44, 89,90), and the structure of hemoglobin from M. F. Perutz et al., (61,62).

Myoglobin of 17,000 molecular weight represents the simplest hemoprotein capable of reversible oxygenation. This protein contains only one polypeptide chain of 153 residues and one heme group per molecule. In contrast, mammalian hemoglobins have a molecular weight of near 65,000 and are made up of four polypeptide chains, identical in pairs (α and β chains). The α-chains have 141 amino acid residues each while the β-chains have 146 residues each. Each chain harbors one heme (ferro-protoporphyrin IX, Figure 2.8) which when oxygenated, gives blood its red color. A single polypeptide chain combined with a single heme is called a subunit of hemoglobin. It is evident, however, that the hemoglobin subunits and myoglobin have a similar overall structure, and that, more specifically, the basic linkages between the heme and protein are essentially the same (92-94). It is hence felt that hemoglobin is appropriately included in this section.

The prosthetic group of myoglobin and hemoglobins is a protoheme (Figure 2.8) in which the iron is strongly coordinated to the four pyrrole nitrogens of the protoporphyrin IX. Ferro-protoporphyrin IX is known as heme; Ferri-protoporphyrin IX as hemin. The fifth site of the heme is linked to the imidazole nitrogen of a histidine residue, number 93 of the myoglobin chain, number 87 of the hemoglobin α-chain, and number 92 of the hemoglobin β-chain (44,89,90). The sixth, and last, of the iron coordination sites in heme is available for oxygen or ligand binding (Figure 2.9). Directly

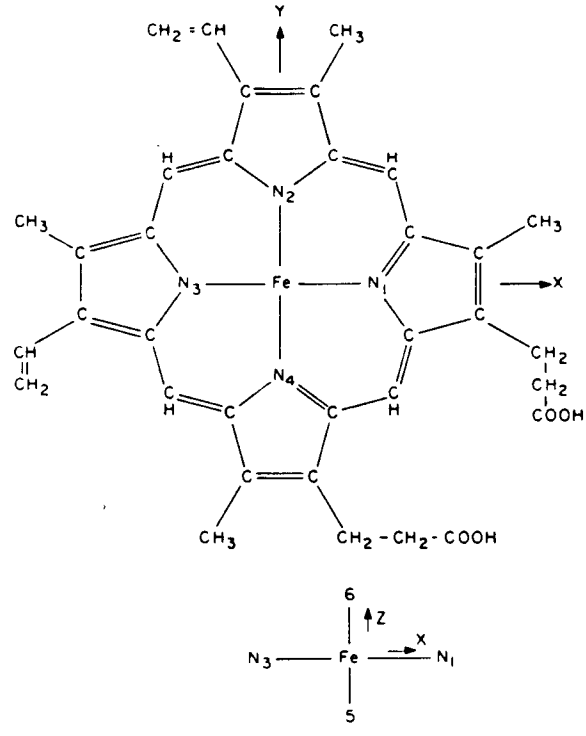

Figure 2.8. Ferro-protoporphyrin IX (heme) and its coordinate system.

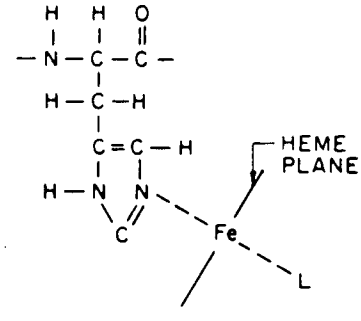

Figure 2.9. Attachment of heme iron to N_ϵ of histidine F8. L represents a ligand in the sixth position.

opposite to the iron-linked imidazole is the "distal histidine", number 64 in myoglobin, number 58 in the hemoglobin α-chain, and number 63 in the β-chain of hemoglobin. It has been suggested that the distal histidine may play an important role in the reversible oxygenation process.

Recent crystallographic refinement of spermwhale metmyoglobin to 2.0Å shows that the iron atom is displaced by 0.40Å from the mean plane of the heme, Pμ, and the Fe-Nε (proximal histidine) is 2.13Å (95). The doming of the porphinato core is 0.13Å which is in agreement with that found in 2-MeImFe(II)TPP (64). Takano (95) reported that the displacement of the iron atom from the mean plane of the heme increases from 0.40Å to 0.55Å on going from met-to deoxy.

The structure of oxy-Mb was recently solved by Phillips in 1978 (26). The Fe atom out-of-plane displacement from the mean plane of the porphyrin is 0.26Å towards the proximal histidine (F8). Table 2.6 gives the heme geometry in Mb and Hb derivatives.

Recently G. Fermi (74) obtained a refined structure of human deoxy-Hb at 2.5Å resolution using the electron-density map obtained by Ten Eyck and Arnone (96). The displacement of the iron atom from Pμ is less than that previously reported for horse deoxy-Hb (62), but the discrepancy probably lies within the measurement errors. The Fe...Pμ is 0.60Å in the α-heme and 0.63Å in the β-heme. The estimated error is ±0.1Å. With the available 2.5Å data, Fermi could not assess the doming magnitude accurately. Fermi, however, pointed out that the doming of the porphinate core is unlikely to exceed the value of 0.17 to 0.22Å. The Pμ...Nε (proximal histidine) is 2.6Å which is compatible with the value of 2.68Å quoted by Hoard and Scheidt (64) for high-spin ferrous five-corrdinate 2-MeImFe(II)TPP.

In horse met-Hb, Bolton and Perutz (62) found the iron atom to be displaced from the mean plane of the porphyrin skeletal towards the heme-linked histidine by 0.3Å. In both the α- and β-chains of horse deoxy-Hb this displacement is increased to 0.75Å. This observation formed part of the experimental basis for Perutz's trigger mechanism of oxygen-binding co-operative phenomenon (6,29).

The overall shape of myoglobin is a flattened sphere. The heme group is near the surface of the molecule in a non-polar, hydrophobic pocket formed by the amino acids, Ala, Ilu, Phe, Leu, and Val. Figure 2.10 gives the stereo drawing of myoglobin. The presence of several nearly aromatic rings such as Phe parallel to the heme, introduces the possibility of π-bonding interactions. The plane of the heme group is approximately normal to the surface of the myoglobin. The heme is in van der Waals contact with 83 atoms of the globin (excluding hydrogens). The hydrophilic chains are directed towards the surface to interact with the solvent.

The structure of the native protein appears to be held together especially by non-polar interactions between sidechains, and between sidechains and the heme group, with polar interactions contributing to a lesser extent. About 70 to 80 per cent of the polypeptide chain is arranged as an α-helix. In the α-helical regions, the non-polar residues repeat at very regular intervals, every 3.6 residues, so that the side of the helix which faces the interior of the molecule is composed of a row of non-polar residues.

The X-ray studies have revealed that each of the four subunits in hemoglobin has a structure similar to that of myoglobin, especially in regard to the folding of the polypeptide chain, the number and distribution

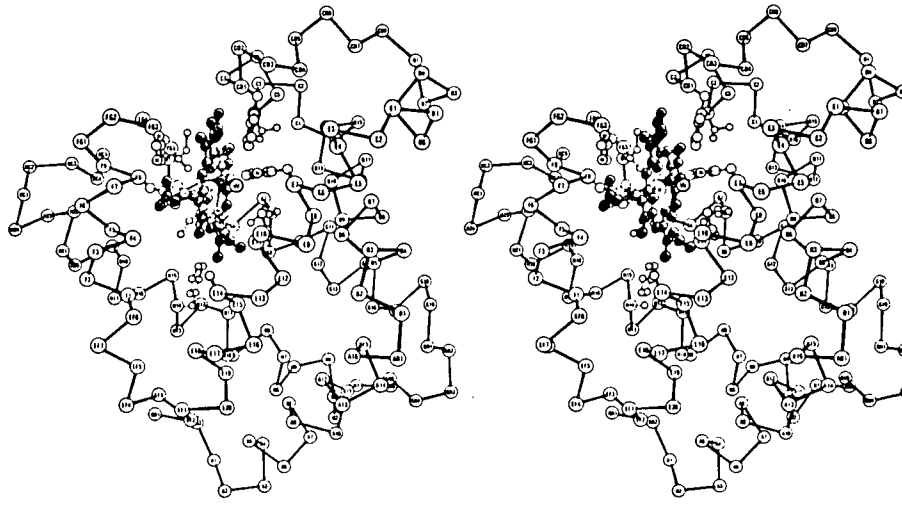

Figure 2.10. A three-dimensional stereo-pair drawing myoglobin.

From Dickerson and Geis (Ref.97) .

of the helical and non-helical segments, and the position and orientation of the heme group.

The four hemoglobin subunits are arranged to form a nearly regular tetrahedron to give the whole molecule a spherical appearance (Figure 2.11). Again the heme groups are near the surface. The α- and β-chains are complementary, and these chains are in close contact, in contrast to the much looser association between the identical chains.

A major difference between myoglobin and hemoglobin is that myoglobin exhibits no co-operative interaction with molecular oxygen.

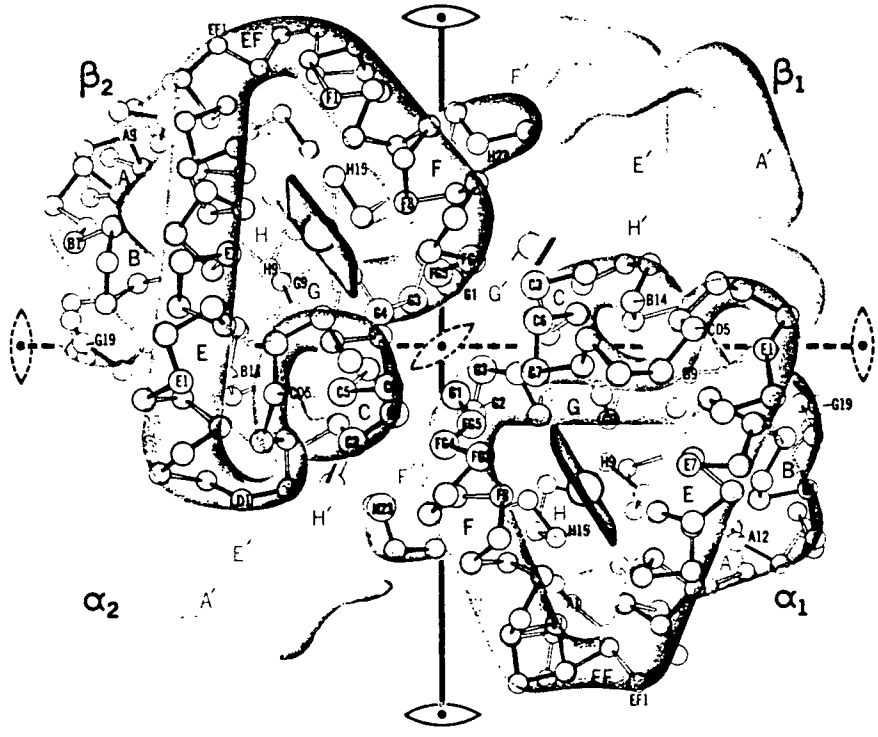

Figure 2.11. The folding and packing of chains in hemoglobin.

From Dickerson and Geis (Ref.97).

2.4 Models for Myoglobin and Hemoglobin

Several groups of investigators have developed models that mimic the active-site (i.e. heme of myoglobin and hemoglobin. The synthetic complexes are capable of reversible oxygen-binding but in non-aqueous media and often at very low temperatures, typically -40°C. A good review article on synthetic oxygen-carriers is by B. R. James (98) in the treatise consisting of seven volumes on porphyrins edited by D. Dolphin (99). Studies on such model systems would give information about the nature of the metal-dioxygen bond and the associated kinetic and thermodynamic factors.

Isolated heme is rapidly oxidised to Fe(III) with the sixth site of the iron coordination sites occupied by a hydroxyl ion or certain other ligands so that it cannot bind oxygen. The irreversible oxidation to Fe(III) is believed to proceed through an intermediate in which two iron porphyrins are covalently linked known as μ-oxo-bis(porphyrin(III)) as shown in Figure 2.12. This creates a major obstacle in designing a suitable high-spin five-coordinate Fe(II) complex as a protein-free model for myoglobin. Several models have been synthesized in the recent years (100-102). An important point to note is that all the model compounds so far reported are monomers; hence, they are more correctly considered to be models of myoglobin rather hemoglobin. In all of the model systems, oxygen-binding can be accomplished only when the fifth site of the coordination of the metal atom is covalently bound to a base, generally, an imidazole. This leaves only the sixth coordination site of the metal atom available for oxygen-binding.

Figure 2.12 A schematic drawing of μ-oxo-bis(porphyrin-iron (III))

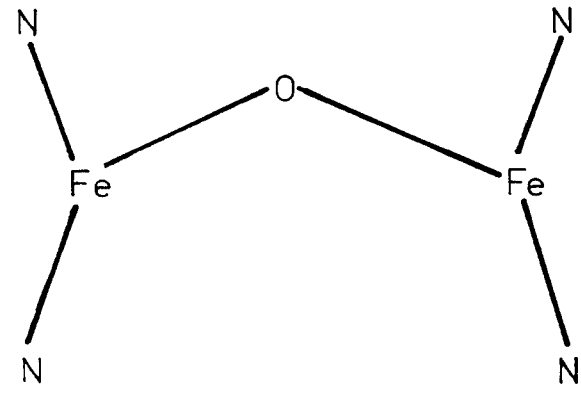

In hemoglobin and myoglobin, the hemes are embedded in non-polar, hydrophobic pockets as discussed in Section 2.3. X-ray crystallographic studies (6,28) show the distance between any two iron atoms in deoxy-Hb or oxy-Hb is >25Å; that probably explains why the oxygen molecule binds to Fe(II) atom in hemoproteins without oxidizing the iron to Fe(III). On this basis, Collman's group at Stanford synthesized a porphyrin ring with four bulky o-pivalamidephenyl groups projecting from one side of the ring like stakes in a picket fence, hence, known as "picket fence" porphyrin (100,103,104,105). Figure 2.13 illustrates the "picket fence" porphyrin. The purpose of the bulky substituents is to prevent the intimate contact by the Fe atoms necessary for oxidation. Instead of a five co-ordinate species, a hexa-coordinate Fe(II) complex with two nitrogenous bases as the axial ligands is produced. In benzene at 20°C, the imidiazole complexes undergo reversible oxygenation (98), although irreversible oxidation occurs slowly.

Traylor's group (101) and Baldwin's group (102) have also constructed severally sterically hindered porphyrins designed to prevent dimerization. These complexes are capable of reversible oxygenation.

Baldwin and associates (102) reported the synthesis of "capped" porphyrins (Figure 2.14). The "cap" prevents the formation of hexa-coordinate species, and molecular oxygen enters the cavity on the protected site. The complexes are capable of reversible oxygen-binding in pyridine at 25°C.

Chang and Traylor (106) synthesized an *in situ* ferrous complex such as shown in Figure 2.15 in which an imidazole is covalently bound to a porphyrin ring. It is interesting to note that the geometry of the complex is similar to that of myoglobin. Reversible oxygen-binding occurs only at -45°C in dichloromethane.

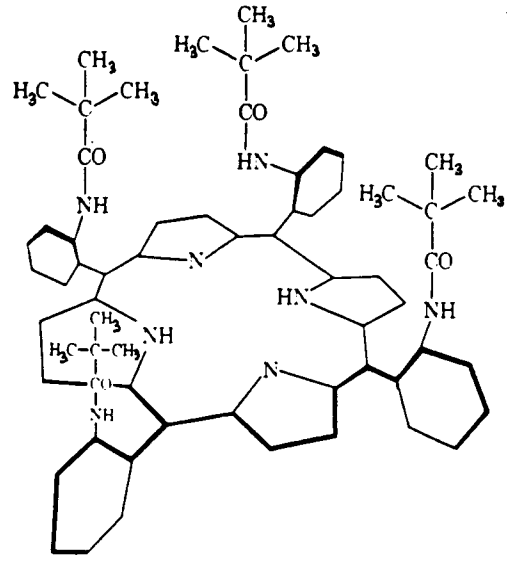

Figure 2.13. "Picket-fence" porphyrin
Collman et al., (100,103-105)

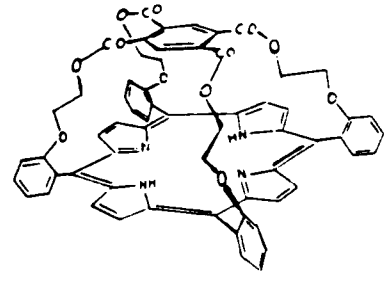

Figure 2.14. "Capped" porphyrins
Baldwin et al., (102)

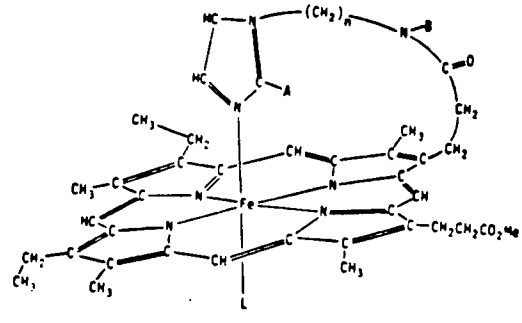

Figure 2.15. Chelated hemes having varying degrees of steric hindrance toward base chelation.
Traylor et at., (106).

CHAPTER III

EXPERIMENTAL WORK

3.1 Preparation of α,β,γ,δ-Tetraphenylphinatoindium(III) chloride

Materials:

Indium chloride, $InCl_3$ (anhydrous, ultra-pure) was obtained from Alfa; meso-tetraphenylporphine was obtained from Strem Chemicals, Inc., and reagent glacial acetic acid from Allied Chemical Canada, Ltd. Silica gel (70-140 mesh) for column chromatography was obtained from Macherey, Nagel & Co., Germany.

Procedure:

The procedure used to synthesize the indium meso-tetraphenylporphyrin chloride (InTPP:Cl) was essentially that of Bhatti et al., (107). In a one-litre one-necked round-bottom flask fitted with a reflux condenser, indium chloride (0.002M) and meso-tetraphenylporphine (0.001M) were heated to boiling in glacial acetic acid (500 ml) containing 2.2 gm of sodium acetate. The reaction was protected from light by aluminium foil. Refluxing was continued for about 4 hr. Completion of the metalation process was determined spectrophotometrically by the disappearance of the 515 nm peak characteristic of the pure porphine and the appearance of a peak in the 560 nm region characteristic of the indium porphine. Upon cooling to room temperature, lustrous, purple crystals of InTPP:Cl were obtained. The product was collected by vacuum filtration, washed with methanol and air-dried.

The reaction took place according to equation 3.1

$$H_2(TPP) + InCl_3 + 2Na(OAc) \rightleftharpoons InTPP:Cl + 2H(OAc) + 2NaCl \qquad (3.1)$$

The overall stoichiometry in Eq. 3.1, looks rather simple. In fact there must be at least five separate processes taking place in Eq. 3.1. They are as follows:

(a) Protonation/Deprotonation Equilibria

$$H_4(TPP)^{2+} \underset{}{\overset{+2H^+}{\rightleftharpoons}} H_2(TPP) \underset{}{\overset{-2H^+}{\rightleftharpoons}} (TPP)^{2-} \qquad (3.2)$$

Deprotonation of $H_2(TPP)$ will give a dianion, $(TPP)^{2-}$, which will readily complex with a positively charged metal ion. When meso-tetraphenylporphine was first dissolved in glacial acetic acid, a greenish solution was obtained. The greenish color was attributed to the formation of a diacid species, $H_4(TPP)^{2+}$ (See Appendix B). As the reaction progressed, a deep purple solution was obtained indicating the formation of InTPP:Cl. From Eq. 3.2, it is clear that strong acids will impede or reverse metallation by shifting the equilibrium to the left. A weak acid such as glacial acetic acid was used.

At first glance, Eq. 3.2 suggests that basic solvents should be the more appropriate solvents than acids because they will drive the deprotonation equilibrium to the right. However, the basic solvent molecules behave as Lewis bases which may more or less strongly bind as neutral donors to the metal ions. This will shift the equilibria in Eq. 3.3 to the left, thus impeding the formation of "naked" In^{3+} metal ions.

Sodium acetate was added to buffer the solution and to enhance deprotonation of the porphyrins by shifting the equilibrium (Eq. 3.2) to the right.

(b) Deconvolution of the metal ion from the metal carrier

$$InCl_3 + 3Na(OAc) \rightleftharpoons In(OAc)_3 + 3NaCl \qquad (3.3a)$$

$$In(OAc)_3 \rightleftharpoons In^{3+} + 3(OAc)^- \qquad (3.3b)$$

The formation of $In(TPP)^+$ depends on the availability of "naked" In^{3+} ions that will complex with "bare" $(TPP)^{2-}$. This implies that indium acetate has to dissociate readily to give In^{3+} ions. This may be a very decisive step in the metalation reaction.

(c) Formation of the equatorial MN_4 species

$$In^{3+} + (TPP)^{2-} \rightleftharpoons In(TPP)^+ \qquad (3.4)$$

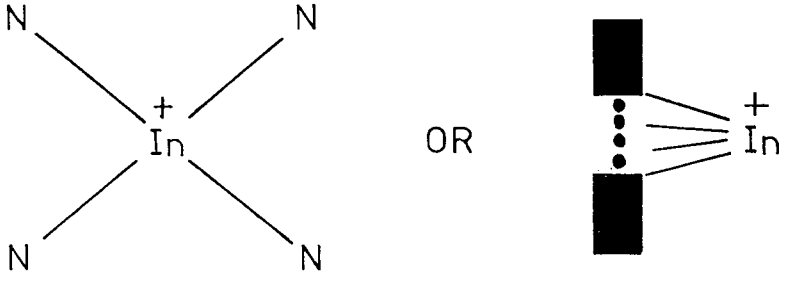

Complexation between a "bare" In^{3+} ion and the dianion $(TPP)^{2-}$ is a straightforward reaction.

(d) Neutralization of the charge

$$In(TPP)^+ + Cl^- \rightleftharpoons InTPP{:}Cl \qquad (3.5)$$

To maintain electroneutrality, an anion is bound to the metal ion. It is astonishing that in spite of the large excess of acetate present, acetate complex was not formed.

(e) Completion of the co-ordination sphere

The In^{3+} is coordinately saturated, thus only five-coordinate square-pyramidal InTPP:Cl is formed. In some metal complexes, six-, and eight-coordinate species are possible.

3.2a Purification of InTPP:Cl

The purification procedure for InTPP:Cl was different from that of Bhatti et al.; (107). The crude complex (100 mg) was dissolved in minimal amount of chloroform and chromatographed on a 62 cm x 1.6 cm column of silica gel packed in toluene. The column was eluted with a 1:1 toluene/chloroform/chloroform mixture, the unreacted TPP was eluted first, followed by InTPP:Cl. All fractions were checked spectroscopically and by tlc. The solvent was evaporated on a vacuum rotary evaporator to recover InTPP:Cl.

3.2b Thin-layer Chromatography

Thin-layer chromatography was used to check the purity of the purified InTPP:Cl. Analytical thin plates of silica gel (Eastman) were spotted with 5 µl samples. A mixture of toluene/chloroform (1:1) was used to develop the chromatogram. The chromatograms were run in the dark. TLC showed the absence of the starting material, meso-TPP in the purified InTPP:Cl.

3.2c Visible Absorption Spectroscopy

The visible absorption spectra of InTPP:Cl and meso-TPP in chloroform were recorded on a Cary 14 spectrometer (Figure 3.1 and Figure 3.2). The meso-TPP shows four absorption bands (excluding the Soret band) in the visible region, labelled I-IV (Figure 3.2). The very intense Soret band ($\varepsilon > 10^5$) could only be determined at a concentration of $\sim 10^{-6}$M.

On formation of InTPP:Cl, the four-banded spectrum collapsed into an essentially two-banded one (α and β bands) in the visible region, whereas the Soret band remained. These bands are bathochromically shifted, the α-band occurring at 600 nm, the β-band at 560 nm, and the Soret band at 419 nm; the intensity sequence is Soret $>> \beta > \alpha$.

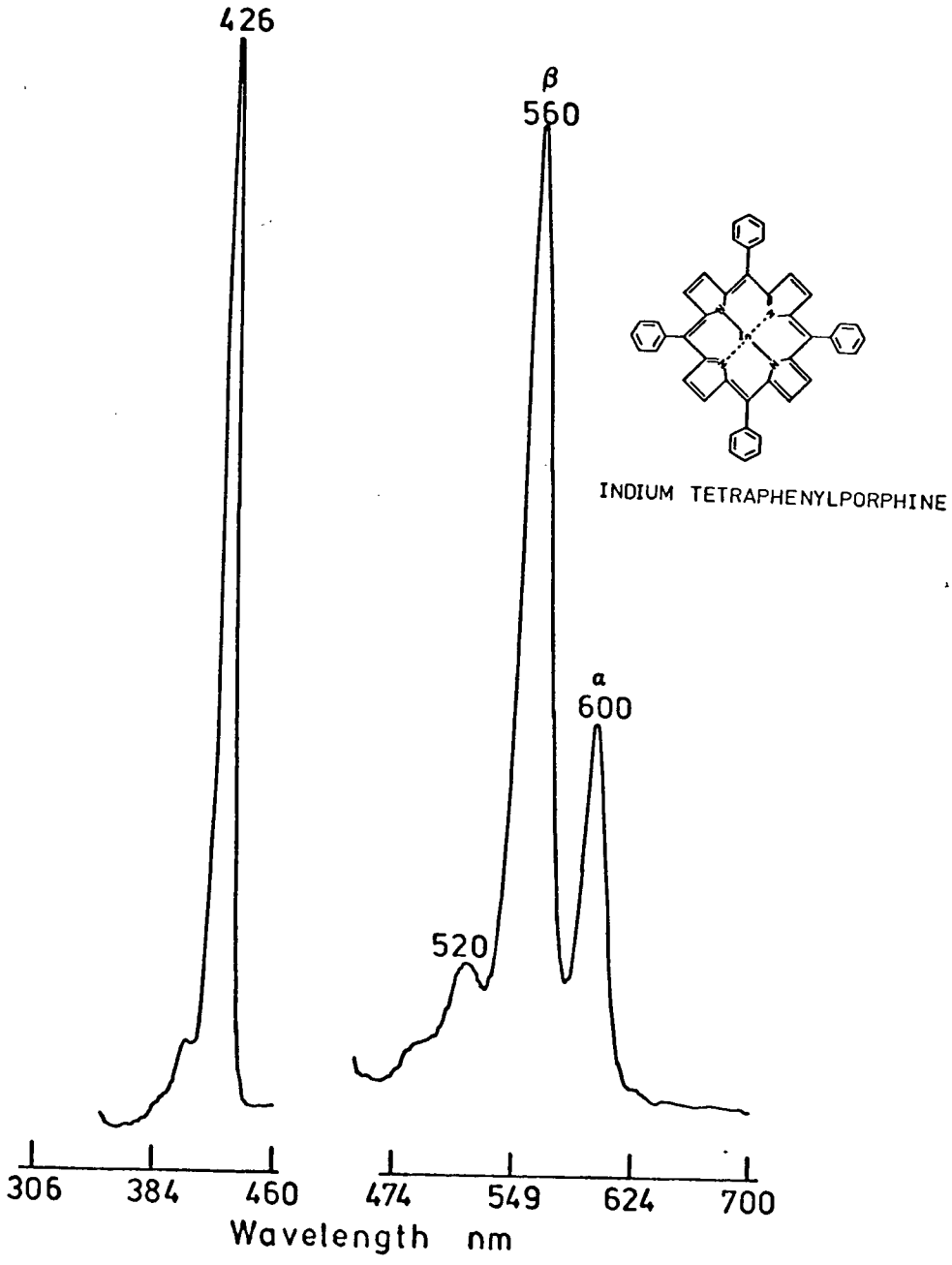

Figure 3.1. Visible absorption spectrum of InTPP:Cl in chloroform.

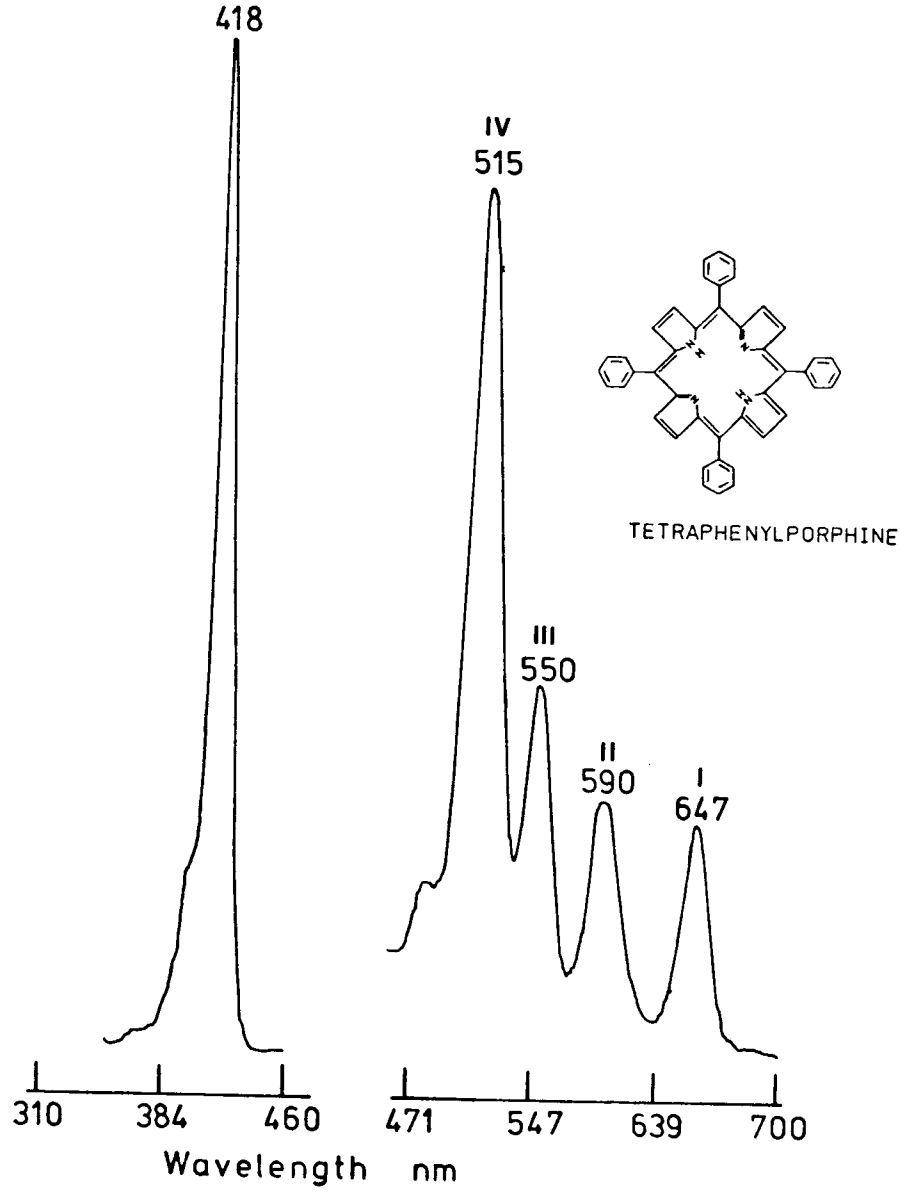

Figure 3.2. Visible absorption spectrum of meso-TPP in chloroform.

3.2d Nuclear Magnetic Resonance Spectroscopy

The n.m.r. spectrum of InTPP:Cl in deuterochloroform was recorded on a Varian XL-100 FT-NMR spectrometer, with ^{2}D-Lock on $CDCl_3$.

3.3 Recrystallisation of InTPP:Cl

Spectroquality chloroform was obtained from MCB, and spectro-methanol was obtained from Eastman.

Recrystallization was carried out by dissolving the metalloporphyrin in a minimal volume of chloroform, and adding methanol dropwise to the boiling solution. With continued boiling, chloroform distilled away, and the methanol concentration increased; the process was allowed to continue until some small crystals formed. Purple single crystals were obtained by letting the mixture stand for several days at room temperature.

CHAPTER IV

RESULTS AND DISCUSSION

4.1 Metal displacement above mean pyrrole nitrogen plane

The crystals are shown to be monoclinic with a space group of $P2_1/n$. The numbering scheme used for the carbon and nitrogen atoms in the asymmetric unit of crystalline InTPP:Cl is shown in Figure 4.1. The contents of the unit cell are shown in Figure 4.2.

The stereo-drawing of InTPP:Cl in Figure 4.3 clearly shows the displacement of the indium atom above the mean plane of the four pyrrole nitrogen atoms, and also significant doming of the porphinato core. The indium atom out-of-plane displacement is 0.71Å from the mean plane of the porphyrin with 0.1Å attributed to the "doming". InTPP:Cl is not planar but exhibits a "ruffling" of the porphyrin skeleton.

A number of interesting features emerge from the stereochemical data of various metalloporphyrins listed in order of decreasing metal displacements (Table 4.7): (a) there is so simple correlation between the ionic radius and metal ion displacement; (b) the displacements for the same metal coordinated to different porphyrins are similar as evident from Co-atom displacement of 0.13Å both in 1-MeImCo(II)TPP (54) and 1-MeImCo(II)OEP (55), and the various high-spin ferric porphyrin complexes also have similar Fe...Pμ distances; and (c) indium(III) atom is displaced essentially the same distance as in high-spin Fe(II) in deoxy-Hb (horse or human). It is often inferred that high-spin states imply five-coordination, which so far is valid for ferrous porphyrins and hemoproteins. In 1978, Mashiko et al., (111) reported the first structural characterisation of six-coordinate high-spin ferric porphyrin derivatives of TPP in which the Fe(III) atom is

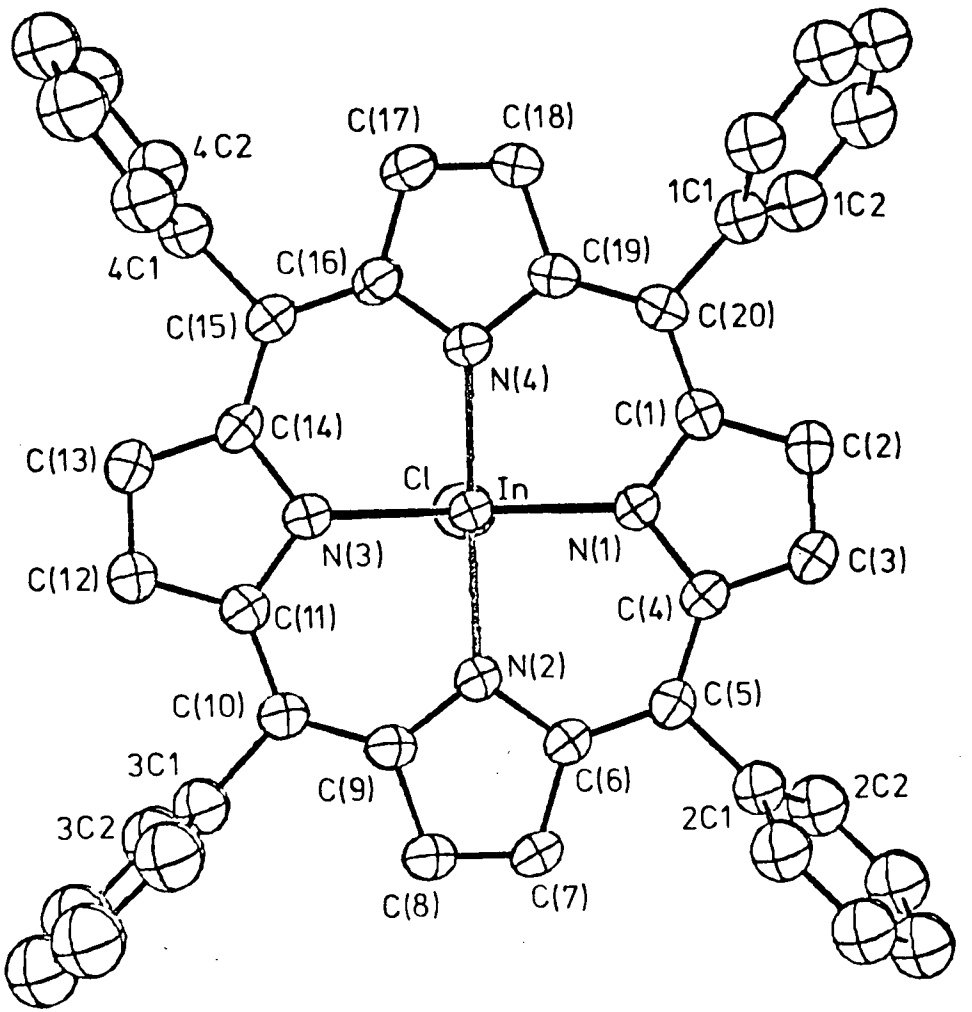

Figure 4.1. Atomic numbering system for crystalline InTPP:Cl. The atoms are drawn as 50% probability thermal ellipsoids. The H atoms have been omitted for clarity. The phenyl rings are numbered as nC_m, where n is the group number (n=1,4) and m is the ring carbon (m=1,6).

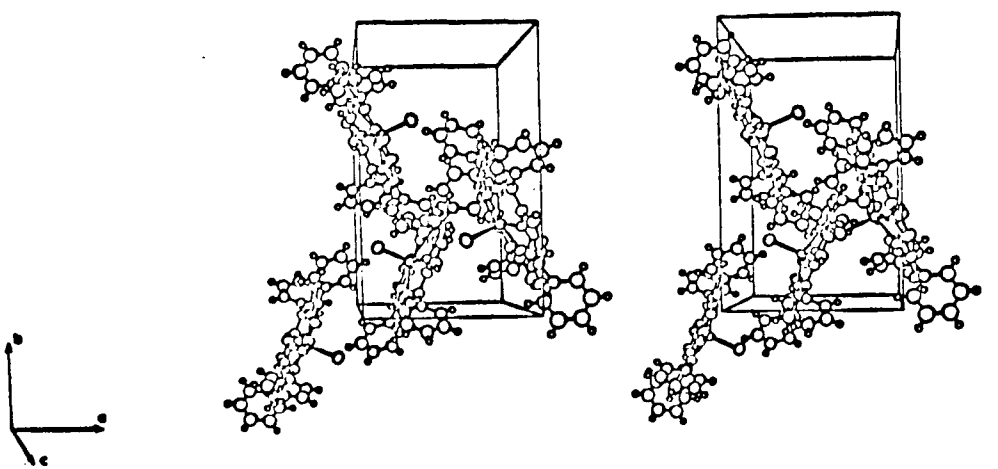

Figure 4.2. Stereoscopic view of the contents of one unit cell of crystalline InTPP:Cl.

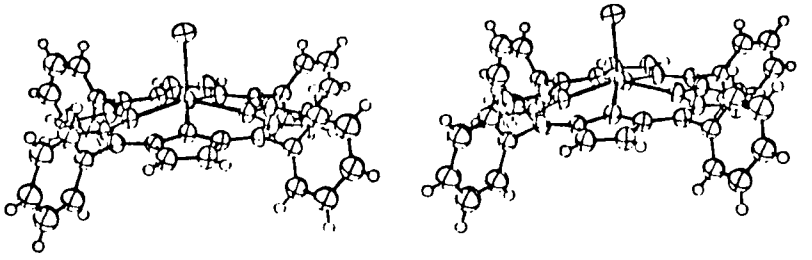

Figure 4.3. Stereo diagram of InTPP:Cl, illustrating the In displacement from the macrocyclic plane, and the "doming" of the porphyrin skeleton. The H atoms have been arbitrarily reduced for clarity.

precisely in the mean porphyrin plane. Six-coordination is also known in high-spin ferric hemoproteins as illustrated by aquo- and fluoro-methemoglobin. In contrast, the Fe(III) atoms are six-coordinate and low-spin in CN-MetHb and CO-MetHb.

The observation (b) emphasises the fact that the metal displacement behavior is similar in all metalloporphyrin complexes of a single metal type. It is logical to assume with confidence that subsequent five-coordinate indium porphyrin complexes will exhibit similar displacement of indium atoms above the mean porphyrin plane.

Perutz (28,29) proposed a stereochemical mechanism to explain the co-operative nature of oxygen-binding. The allosteric model was based on the differences in the tertiary and quaternary structures of horse deoxy- and met-Hb, rather than deoxy- and oxy-Hb. Oxy-Hb is readily oxidised to met-Hb under the normal conditions of X-ray crystallography. Perutz justified his argument on the ground that oxy-Hb and met-Hb are isomorphous i.e. the crystals have the same space group. Huestic and Raftery (112) showed that the ^{19}F-labelled cysteine 93β in met-Hb gives a n.m.r. chemical shift similar to deoxy-Hb but was different from oxy- and CO-Hb. This implies that met-Hb is not a good analog for oxy-Hb. Besides the Fe(III) is six-coordinate and predominantly high-spin in met-Hb as opposed to Fe(II) which is low-spin and six-coordinate in oxy-Hb. Perutz in 1976 (113) proposed that CO-Hb "may be regarded as the closest relative of oxy-hemoglobin" on the ground that CO-Hb is stable and isomorphous with both oxy- and met-Hb. Furthermore, the Fe(II) atoms in oxy- and CO-Hb are low-spin. However, the 2.8Å X-ray data on CO-Hb is not sufficient to determine the exact displacement of the iron atoms from the heme plane. The structure of spermwhale oxymyoglobin has been determined by Phillips in

1978 (26). Phillips clearly demonstrates that the Fe atom does move towards the porphyrin on transition from deoxy-to oxy-Mb (See Section 2.2 and Table 2.6). This finding reinforces Perutz's allosteric model although the total movement of the proximal histidine in Mb is smaller than that expected for Hb.

Perutz (28,29) proposed that the quaternary structure of hemoglobin is in equilibrium between two stable subunit configurations termed as "T" for deoxy-Hb and "R" for oxy-Hb. In the deoxy-Hb, the low-spin, five-coordinate heme iron atom is $\sim$0.75Å (horse hemoglobin) out of the heme plane towards the proximal histidine. When a molecule of oxygen binds to deoxy-Hb, the iron moves into the plane of the porphyrin. According to Perutz's stereochemical mechanism, the transition from "T" state (deoxy-Hb) to "R" state (oxy-Hb) involves a shrinkage of $\sim$0.90Å in the $P_{\mu}...N_{\varepsilon}$ distance. This movement triggers a series of small changes in the quaternary and tertiary structures of the protein that responsible for the oxygen-binding co-operativity. At the present there is still a considerable debate and controversy surrounding the question of the stereochemical mechanism. There are two schools of thought: Perutz advocates that the changes in the stereochemistry at the core of the heme are the key to the trigger mechanism while the other school (Edelstein and Gibson (81(b)), and Little and Ibers (55)) emphasises the importance of the interaction between the distal histidine and the sixth-ligand. A critical test for the trigger mechanism would be to "freeze" one or more subunits into the "T" state and then monitor changes in the oxygenation kinetics, electronic, and motional properties of the remaining intact native subunit or subunits. Native subunits in the "T" state are very

difficult to achieve since heme Fe(II) binds oxygen to become hexa-coordinate and low-spin to give the "R" state.

Since the "T" form cannot be stably generated using native iron heme (readily autoxidises to Fe(III)), other means must be sought. Various metalloporphyrins containing Mn, Co, Zn, and Mg in place of native heme have been reconstituted into hemoglobin. However, Mn(II) is readily oxidised to Mn(III), and Co(II) binds oxygen. Both Mg and Zn may be oxidation stable but they exhibit relatively small metal displacements above the porphyrin plane relative to the Fe atom in native hemoglobin (See Table 4.7). The present X-ray data on InTPP:Cl suggest indium porphyrins are ideal candidates for inducing the "T" conformation (vive infra). Incorporation of indium porphyrins into hemoglobin provide an opportunity to probe the prophyrin-apoprotein interaction in the "T" state hemoglobin and myoglobin.

Hoffman and associates (83-86) have shown that cobalt-substituted myoglobin and hemoglobin can combine reversibly and co-operatively with molecular oxygen, although, to a much lesser extent than the native proteins. It is interesting to note in Table 4.7 that although Co(II) has a larger ionic radium (0.72Å) than Fe(III), the out-of-plane displacement of Co atom from the mean plane of the pyrrole nitrogens is only 0.13Å. In contrast, the smaller Fe(III) (ionic radius = 0.64Å) has a larger metal displacement ranging from 0.38Å to 0.52Å. Resonance Raman studies on CoHb and Hb by Woodruff et al., (87) indicate that the Co(II) atom out-of-plane displacement in Co-Hb cannot exceed 0.2Å. The allosteric model by Perutz on the mechanism of reversible oxygen-binding co-operativity in hemoglobin depends directly on the large change on the $P_\mu...N_\varepsilon$ distance upon oxygenation (See Section 2.2). It is thus logical to wonder whether

the Perutz's "trigger" mechanism is consistent with the much smaller out-of-plane displacement of Co(II) in model metalloporphyrins and CoHb. The most reasonable rationalisation of this dilemma is that of Hoard and Scheidt (64) who propose that the tension within the protein in deoxy-CoHb causes the porphinato core to undergo a substantial doming of $\sim$0.5Å towards the Co atom. The doming raises the Co atom out-of-plane displacement to $\sim$0.70Å compatible to Fe atom (0.75Å) in horse deoxy-Hb and 0.6Å in human deoxy-Hb. A support for the Hoard and Scheidt proposal (64) comes from the fact that the prophyrin skeleton is readily deformed normal to the mean plane. As one example, Ni(OEP) crystallises in both a trinclincic form and a tetragonal form (35). Both crystals are virtually isomorphous, but yet the tetragonal form exhibits marked non-planarity of the porphinato core while the triclinic form is essentia-ly planar. CoHb is therefore thought to achieve the "tense" quaternary structure, not so much by the separation between the Co(II) atom and the mean porphyrin plane, but rather by marked "doming" of the porphyrin skeleton itself to move the cobalt nearer to the heme-linked histidine (F8).

The "R" state quarternary structures of CoHb and FeHb (i.e., after oxygen-binding, so that the metal atom lies in the porphyrin plane) are expected to be similar, while the overall functional properties are very different. For example the oxygen-affir ity of Co-Hb is reduced by 10-100 times relative to native Hb and Mb (86). Furthermore, Collman and associates (124) have shown that the free energy difference between the intrinsic binding of the first and fourth oxygen to CoHb is one-third that of Hb. Therefore, it seems reasonable to conclude that the "T" state quarternary structures of CoHb and Hb must be appreciably di-ferent, most probably because of the much smaller displacement of Co atom above the porphyrin

plane. In seeking a metalloporphyrin which, when reconstituted into apo-hemoglobin, will produce a "tense" conformation more similar to that for the native iron-containing protein, one therefore seeks a case for which the metal displacement above the porphyrin plane is more similar to that for the corresponding high-spin Fe(II) complex.

From Table 4.7, it is clear that there are relatively few attractive candidates. Mn-Hb has been prepared (80), and Moffat et al., (79) concluded from their crystallographic studies on Mn-Hb that deoxy-Mn(II)Hb will adopt the normal "T" quaternary structure. However, Mn(II)-Hb is irreversibly oxidised to Mn(III)-Hb which has been shown to be a close structural analog of met-Hb (79). Mg and Zn (76), while presumably stable toward oxidation, exhibit relatively small metal displacements above the porphyrin plane, and may thus not be appreciably better than Co in this respect. The large ions, Tl, Hf, Zr, and Bi, give displacements which may be too large (compared to Fe), and in the cases of Hf and Zr give unsuitable coordination number. However, the present results suggest that an indium porphyrin may be an ideal candidate for inducing the "tense" conformation in hemoglobin, without the complication of autoxidation, oxygen-binding to the indium-labelled subunits, and with the near-ideal displacement of the metal atom from the mean porphyrin plane.

Indium has a further advantage that it has an isotope (^{111}In) which is suitable for gamma-gamma coincidence measurements. Part two of this thesis describes the reconstitution of ^{111}InMPP IX into apomyoglobin, and how gamma-gamma angular correlation measurements can give motional properties of the protein.

4.2 Bond Lengths and Angles

The bond lengths and angles of Table 4.5 show that the square pyramidal InTPP:Cl molecule has very close to C_{4v} symmetry, as far as the In, Cl, and porphyrin skeleton atoms are concerned. (The phenyl tilts are discussed in Section 4.4). The average In-N distance is 2.156(6)Å, which is substantially larger than for the corresponding high-spin Fe(III) complexes (Ca. 2.06-2.09Å). This increase is due partly to expansion of the porphyrin core (radius of 2.067Å for InTPPCl, compared to approximately 2.00 to 2.04 for iron(III)), and partly to an intrinsically longer In-N bond compared to Fe-N bond. However, the Fe-N bond length for iron in hemoglobin is expected to increase to approximately the present In-N value, due to tension produced by the proximal histidine ligand of Hb (64,65,55); thus the indium porphyrin may still be a close structural analog for Fe(II) in deoxyhemoglobin, even though the isolated porphyrin structures appear rather different with respect to metal-nitrogen bond lengths.

4.3 Doming of the Porphyrin Skeleton

The M-Np distance of 2.01Å appears to be a nearly optimum value for minimal strain and undistorted accomodation of the metal atom within the central "hole" of the porphyrin. Structural studies (21) have shown that for a highly expanded porphinato core, the most efficient non-planar conformation is doming of the core (18,36). Hoard and coworkers (15) also have demonstrated experimentally the high degree of flexibility of the porphyrin skeleton in metalloporphyrin structures. The long $(In-Np)_{av}$ distance, 2.156Å which is undoubtedly responsible for the significant "doming" of the porphinato core is clearly illustrated in the stereo-drawing in Figure 4.3. It is evident from Figure 4.3 that InTPP:Cl is non-planar, and exhibits a marked deviations from planarity of the porphyrin atoms. Atomic displacements from the mean porphyrin plane of InTPP:Cl are illustrated in Figure 4.4. The perpendicular displacements (positive and negative sign correspond to displacement above (i.e., toward the indium) or below the plane) from the mean plane of all 28 core porphyrin atoms in Figure 4.4 show that the porphyrin skeleton is appreciably "domed" upward toward the indium. The plane of the four pyrrole nitrogen atoms is in fact displaced an average of 0.1Å above the mean plane of the core of the porphyrin atoms. The outermost pyrrole ring carbons are depressed by up to 0.214Å below the plane.

It is interesting to note that the doming in 2-MeImFe(II)TPP is 0.13Å while it is 0.1Å for InTPP:Cl. This suggests that the porphyrin skeleton is not significantly distorted by the presence of indium atom. Fermi (74) pointed out that the doming of the porphinato core in human deoxy-Hb is unlikely to exceed the value of 0.17 to 0.22Å. The degree of doming in InTPP:Cl is well within the range observed for high-spin ferric porphyrins

(Table 4.7). It is expected the influence by the protein environment may increase the doming of indium porphinato core compatible to that in native hemoglobin.

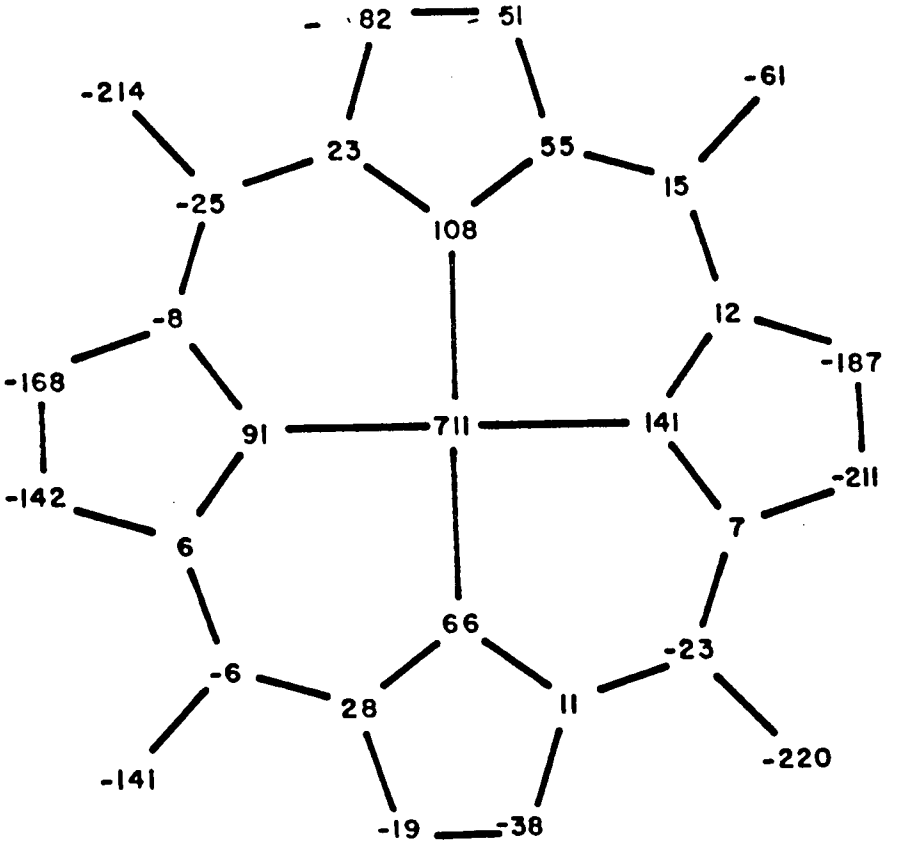

Figure 4.4. Atomic displacements ($\mathring{A} \times 10^3$) from the mean porphyrin plane (plane #2 of Table 4.6) of InTPP:Cl. Positive numbers correspond to displacements toward the indium atom.

4.4 Phenyl Rings: Crystal Packing

A stereo view of a unit cell is shown in Figure 4.2, and illustrates the moelcular packing. The closest nonbonded intermolecular contact is 2.48Å between H4C4 and H3C3 at (1-x, 1-y, $\bar{z}$), indicating that there is no strong hydrogen bonding network and only the normal van der Waals forces between molecules.

It is of interest to note that phenyl ring #1 is close to an inversion center, and as a result it is twisted by only 66.17° with respect to the mean plane of the porphyrin skeleton, in order to minmize the nonbonded contacts to its centrosymmetrically related image. The other three rings have dihedral angles with respect to the porphyrin mean plane which are closer to perpendicular (107.59°, 93.67°, and 98.33° for phenyl rings #2-#4, respectively).

That the four phenyl rings are equivalent in solution is shown by the proton NMR spectrum of InTPPCl in Figure 4.5. When this spectrum was first observed (107), the magnetically inequivalent ortho protons of the phenyl rings were incorrectly ascribed to "non-equivalence of phenyls in pairs", presumably due to two chemically different sets of two phenyls each. The present crystal structure indicate that the inequivalence arises from the displacement of the indium above the porphyrin ring, making the upper (four) and lower (four) ortho protons inequivalent. The coalescence of these two ortho proton peaks on increase in temperature (125,126) must thus arise from internal rotation of the chemically equivalent phenyl groups about the bonds which connect the phenyl rings to the porphyrin.

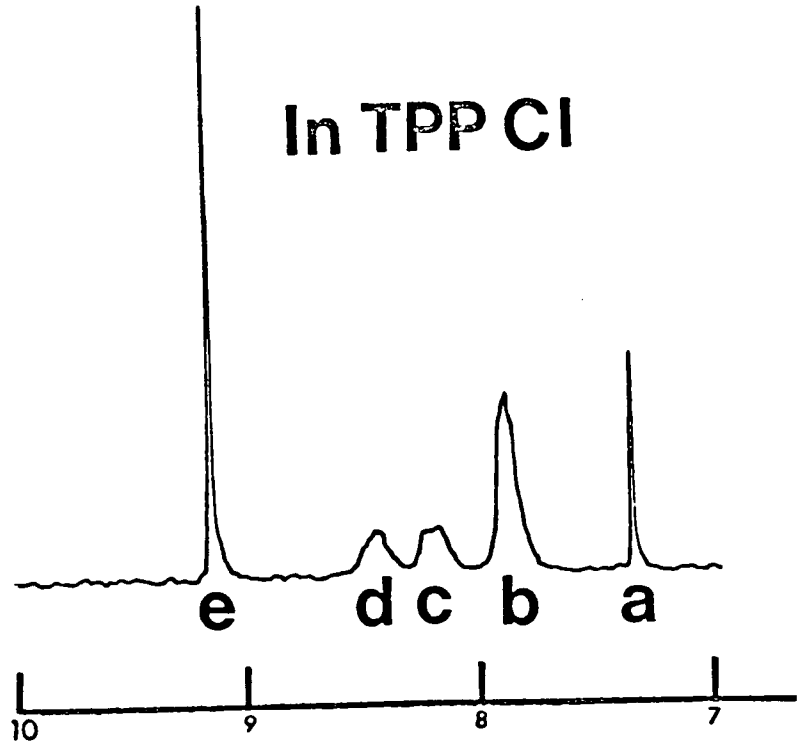

Figure 4.5. ^{1}H 100 MHz FT-NMR spectrum of InTPP:Cl in $CDCl_3$ solvent. Peak assignments are: (a), residual $CHCl_3$ (δ = 7.33); (b), m- and p-phenyl protons (7.87); (c) and (d), o-phenyl protons (8.20 and 8.43); and (e), pyrrole β-protons (9.15). Spectrum was obtained using a Varian XL-100 FT-NMR spectrometer, with $CDCl_3$ used for ^{2}D lock, 10 transients, 6.0 sec pulse delay, and sensitivity enhancement time constant of -1.0 sec.

Table 4.1. Crystal data and conditions for data collection.

$C_{44}H_{28}ClInN_4$	Fw = 763.015
Space Group: $P2_1/n$	Vol = 3432.5 Å^3
a = 10.099(1) Å	Z = 4
b = 16.117(2)	D_c = 1.476 g cm^{-3}
c = 21.090(2)	D_o[a] = 1.48(1) g cm^{-3}
β = 90.70(1)°	μ = 7.22 cm^{-1}

Radiation:	Mo Kα, graphite monochromator
Scan type:	ω - 2θ
Scan range:	(0.47 + 0.35 tanθ)° in ω, extended 25% for each background measurement
Scan speed:	0.75 to 10.1 deg min^{-1}, to give $I/\sigma(I) \geq 20$
Aperture:	1.33 x 4 mm, 173 mm from crystal
Standards:	190, 641, 05$\bar{1}\bar{2}$, 604; measured every hour of exposure time
Data collected:	$\pm$ hkℓ for $2\theta \leq 55°$; 7859 reflections
σ(I):	$\{Int + 4(BG) + (0.04I)^2\}^{1/2}$; Int is integrated peak count, BG is the sum of the background counts and I is the intensity

[a] by neutral buoyancy in CCl_4 and CH_2Cl_2

Table 4.2. Final atomic positional and thermal parameters

Atom	x	y	z	U11[b]	U22	U33	U12	U13	U23
In	3493.1(3)	1797.0(2)	1516.3(1)	4.23(2)	3.38(2)	2.64(2)	-0.39(2)	-0.33(1)	0.20(1)
Cl	1387(1)	2388(1)	1706(1)	5.2(1)	6.1(1)	5.5(1)	0.8(1)	-0.1(1)	-0.5(1)
N(1)	3284(4)	499(3)	1749(2)	5.6(2)	3.4(2)	3.0(2)	-0.4(2)	-0.3(2)	0.2(2)
N(4)	3522(4)	1389(3)	588(2)	5.5(3)	3.5(2)	2.8(2)	-0.3(2)	-0.3(2)	0.0(2)
N(3)	4761(4)	2789(3)	1202(2)	5.1(2)	4.0(2)	3.1(2)	-0.7(2)	-0.3(2)	0.2(2)
N(2)	4579(4)	1891(3)	2401(2)	4.6(2)	3.8(2)	3.1(2)	-0.8(2)	-0.6(2)	0.5(2)
C(1)	2844(5)	-119(3)	1341(2)	4.8(3)	3.4(3)	4.1(3)	-0.5(2)	-0.3(2)	-0.0(2)
C(2)	2665(6)	-863(3)	1703(3)	6.9(4)	3.7(3)	4.6(3)	-1.0(3)	-0.8(3)	0.6(2)
C(3)	3018(6)	-703(3)	2310(3)	7.0(4)	4.1(3)	4.0(3)	-0.8(3)	-0.8(3)	1.0(2)
C(4)	3395(5)	150(3)	2346(2)	5.2(3)	3.7(3)	3.2(2)	-0.2(2)	-0.4(2)	0.5(2)
C(5)	3909(5)	500(3)	2886(2)	4.5(3)	3.9(3)	3.6(2)	-0.6(2)	-0.2(2)	0.7(2)
C(6)	4445(5)	1361(3)	2909(2)	5.0(3)	4.1(3)	3.1(2)	-0.6(2)	-0.4(2)	0.6(2)
C(7)	4976(6)	1760(4)	3462(2)	6.7(3)	5.1(3)	3.1(2)	-0.9(3)	-1.0(2)	0.9(2)
C(8)	5423(5)	2510(4)	3286(2)	5.8(3)	5.5(3)	3.5(3)	-1.4(3)	-0.9(2)	0.4(2)
C(9)	5199(5)	2601(3)	2619(2)	4.3(3)	4.6(3)	3.2(2)	-0.6(2)	-0.7(2)	0.2(2)
C(10)	5581(5)	3277(3)	2247(2)	4.7(3)	4.5(3)	3.5(2)	-0.7(2)	-0.7(2)	0.4(2)
C(11)	5392(5)	3358(3)	1590(2)	4.9(3)	4.4(3)	3.7(2)	-1.2(2)	-0.5(2)	0.4(2)
C(12)	5890(6)	4024(4)	1207(2)	6.5(4)	5.1(3)	4.1(3)	-2.2(3)	-0.7(2)	0.6(3)
C(13)	5575(6)	3846(4)	597(2)	6.1(3)	5.2(3)	3.9(3)	-2.0(3)	-0.1(2)	0.9(2)
C(14)	4856(5)	3077(3)	589(2)	4.7(3)	4.0(3)	3.1(2)	-0.4(2)	0.0(2)	0.9(2)
C(15)	4393(5)	2667(3)	48(2)	4.7(3)	4.3(3)	3.1(2)	-0.3(2)	0.1(2)	0.4(2)
C(16)	3783(5)	1885(3)	33(2)	4.9(3)	4.0(3)	3.1(2)	0.1(2)	0.0(2)	0.4(2)
C(17)	3390(6)	1450(4)	-538(2)	6.9(4)	4.9(3)	2.9(2)	-0.1(3)	-0.1(2)	0.3(2)
C(18)	2896(6)	711(3)	-358(2)	6.4(3)	4.1(3)	3.1(2)	-0.7(2)	-0.5(2)	-0.4(2)
C(19)	2986(5)	663(3)	321(2)	5.0(3)	3.9(3)	3.1(2)	-0.2(2)	-0.3(2)	-0.4(2)
C(20)	2665(5)	-40(3)	688(2)	4.7(3)	3.9(3)	3.6(2)	-0.4(2)	-0.3(2)	-0.7(2)

[a] Estimated standard deviations in this and other tables are given in parentheses and correspond to the least significant digits. The positional parameters have been multiplied by 10^4 and the thermal parameters by 10^2.

[b] $U_{ij} = \beta_{ij}/(2\pi^2 a_i^* a_j^*)$ Å^2. The thermal ellipsoid is given by $\exp[-(\beta_{11}h^2 + \beta_{22}k^2 + \beta_{33}\ell^2 + 2\beta_{12}hk + 2\beta_{13}h\ell + 2\beta_{23}k\ell)]$.

Table 4.3. Rigid group parameters.

Group	x_c[a]	y_c	z_c	δ	ϵ	η
1C1 - 1C6	0.1566(2)	-0.1402(2)	-0.0041(1)	1.430(3)	-2.662(2)	0.666(3)
2C1 - 2C6	0.4074(3)	-0.0409(2)	0.4037(1)	-1.642(3)	3.017(2)	-2.137(3)
3C1 - 3C6	0.7040(3)	0.4590(2)	0.2875(1)	-2.114(3)	2.997(3)	-0.457(3)
4C1 - 4C6	0.4835(3)	0.3297(2)	-0.1213(1)	-1.899(3)	-3.100(2)	1.245(3)

Group	B_1[b]	B_2	B_3	B_4	B_5	B_6
1C1 - 1C6	3.38(9)	4.5(1)	5.3(1)	4.8(1)	4.7(1)	4.1(1)
2C1 - 2C6	3.38(9)	4.6(1)	5.1(1)	5.1(1)	5.0(1)	4.3(1)
3C1 - 3C6	3.37(9)	4.3(1)	4.9(1)	5.2(1)	5.6(1)	4.7(1)
4C1 - 4C6	3.7(1)	5.2(1)	6.3(2)	6.2(2)	6.3(2)	5.5(1)

[a] See S. J. LaPlace and J. A. Ibers, Acta Crystallogr. 18, 511 (1965) for definition of group parameters.

[b] B_n is the temperature factor of atom C_n in the phenyl ring in $\AA^2$.

Table 4.4. Derived Hydrogen atom positional and thermal parameters[a]

Atom	x	y	z	U (Å²)
HC(18)	255	30	-63	5.9
HC(17)	346	165	-96	6.2
HC(13)	579	417	24	6.3
HC(12)	635	450	136	6.5
HC(8)	582	291	356	6.2
HC(7)	501	154	388	6.2
HC(3)	302	-109	265	6.3
HC(2)	235	-138	154	6.3
H1C2	28	-70	70	7.0
H1C3	-64	-179	11	6.3
H1C4	64	-249	-64	7.3
H1C5	285	-210	-79	7.2
H1C6	377	-101	-19	6.5
H4C2	276	349	-75	6.8
H4C3	312	392	-180	7.5
H4C4	519	373	-226	7.8
H4C5	691	311	-167	8.3
H4C6	655	268	-63	7.3
H3C2	475	471	270	7.9
H3C3	590	576	323	7.4
H3C4	819	565	340	9.1
H3C5	933	448	305	9.2
H3C6	818	342	252	8.3
H2C2	200	6	369	7.1
H2C3	219	-70	463	7.8
H2C4	427	-118	497	7.7
H2C5	615	-88	438	7.6
H2C6	596	-11	344	6.7

[a] The positional parameters have been multiplied by 10^4 and the thermal parameters by 10^2.

Table 4.5. Selected interatomic distances (Å) and angles (deg).

Distances

In - N(1)	2.160(4)	C(5) - C(6)	1.400(7)
In - N(2)	2.158(4)	C(6) - C(7)	1.430(7)
In - N(3)	2.158(4)	C(7) - C(8)	1.344(7)
In - N(4)	2.146(4)	C(8) - C(9)	1.431(6)
In - Cℓ	2.369(2)	C(9) - C(10)	1.399(7)
N(1) - N(3)	4.150(6)	C(10) - C(11)	1.403(7)
N(2) - N(4)	4.118(5)	C(11) - C(12)	1.438(7)
N(1) - C(1)	1.386(6)	C(12) - C(13)	1.354(7)
N(1) - C(4)	1.383(6)	C(13) - C(14)	1.436(7)
N(2) - C(6)	1.378(6)	C(14) - C(15)	1.394(7)
N(2) - C(9)	1.380(6)	C(15) - C(16)	1.403(7)
N(3) - C(11)	1.380(6)	C(16) - C(17)	1.437(7)
N(3) - C(14)	1.378(6)	C(17) - C(18)	1.344(7)
N(4) - C(16)	1.377(6)	C(18) - C(19)	1.437(6)
N(4) - C(19)	1.372(6)	C(19) - C(20)	1.412(7)
C(1) - C(2)	1.434(7)	C(20) - C(1)	1.393(7)
C(2) - C(3)	1.349(7)	C(20) - 1C1	1.506(6)
C(3) - C(4)	1.428(7)	C(5) - 2C1	1.495(6)
C(4) - C(5)	1.411(7)	C(10) - 3C1	1.502(7)
		C(15) - 4C1	1.507(6)

Angles

N(1)	- In -	N(2)	85.5(2)	1C1	- C(20) -	C(19)	115.5(2)
N(2)	- In -	N(3)	85.2(1)	1C1	- C(20) -	C(1)	118.4(2)
N(3)	- In -	N(4)	85.4(2)	2C1	- C(5) -	C(4)	116.1(2)
N(4)	- In -	N(1)	85.5(2)	2C1	- C(5) -	C(6)	117.0(2)
N(1)	- In -	N(3)	147.9(2)	3C1	- C(10) -	C(9)	116.3(2)
N(2)	- In -	N(4)	146.3(2)	3C1	- C(10) -	C(11)	117.4(3)
Cℓ	- In -	N(1)	105.1(1)	4C1	- C(15) -	C(14)	118.8(2)
Cℓ	- In -	N(2)	105.9(1)	4C1	- C(15) -	C(16)	115.0(2)
Cℓ	- In -	N(3)	106.9(1)	C(1)	- C(2) -	C(3)	108.1(5)
Cℓ	- In -	N(4)	107.8(1)	C(2)	- C(3) -	C(4)	107.6(4)
In	- N(1) -	C(1)	125.9(3)	C(3)	- C(4) -	C(5)	126.2(4)
In	- N(1) -	C(4)	126.4(3)	C(4)	- C(5) -	C(6)	126.7(4)
In	- N(2) -	C(6)	125.1(3)	C(5)	- C(6) -	C(7)	125.6(4)
In	- N(2) -	C(9)	124.7(3)	C(6)	- C(7) -	C(8)	107.7(4)
In	- N(3) -	C(11)	125.6(3)	C(7)	- C(8) -	C(9)	108.2(5)
In	- N(3) -	C(14)	125.9(3)	C(8)	- C(9) -	C(10)	126.1(5)
In	- N(4) -	C(16)	125.4(3)	C(9)	- C(10) -	C(11)	126.2(5)
In	- N(4) -	C(19)	125.6(3)	C(10)	- C(11) -	C(12)	125.4(5)
N(1)	- C(1) -	C(20)	125.7(4)	C(11)	- C(12) -	C(13)	107.2(5)
N(1)	- C(4) -	C(5)	124.7(5)	C(12)	- C(13) -	C(14)	107.8(4)
N(2)	- C(6) -	C(5)	125.9(4)	C(13)	- C(14) -	C(15)	125.6(4)
N(2)	- C(9) -	C(10)	125.9(4)	C(14)	- C(15) -	C(16)	126.0(4)
N(3)	- C(11) -	C(10)	125.5(4)	C(15)	- C(16) -	C(17)	125.1(4)
N(3)	- C(14) -	C(15)	125.5(4)	C(16)	- C(17) -	C(18)	107.6(4)
N(4)	- C(16) -	C(15)	126.2(4)	C(17)	- C(18) -	C(19)	107.6(4)
N(4)	- C(19) -	C(20)	125.8(4)	C(18)	- C(19) -	C(20)	125.2(4)
N(1)	- C(1) -	C(2)	108.2(4)	C(19)	- C(20) -	C(1)	126.0(4)
N(1)	- C(4) -	C(3)	108.9(4)	C(20)	- C(1) -	C(2)	126.0(5)
N(2)	- C(6) -	C(7)	108.4(4)				
N(2)	- C(9) -	C(8)	108.0(4)				
N(3)	- C(11) -	C(12)	109.0(4)				
N(3)	- C(14) -	C(13)	108.8(4)				
N(4)	- C(16) -	C(17)	108.6(4)				
N(4)	- C(19) -	C(18)	108.8(4)				

Table 4.5, continued.

	Pyrrole 1	Pyrrole 2	Pyrrole 3	Pyrrole 4	Average
N - a	1.386(6)	1.377(6)	1.380(6)	1.378(6)	1.380(4)
N - d	1.383(6)	1.378(6)	1.378(6)	1.380(6)	1.380(2)
a - b	1.434(7)	1.437(6)	1.438(7)	1.430(7)	1.435(4)
b - c	1.349(6)	1.344(7)	1.354(7)	1.344(7)	1.348(5)
c - d	1.428(6)	1.437(7)	1.436(7)	1.431(6)	1.433(4)
a - m	1.393(7)	1.403(7)	1.403(7)	1.400(7)	1.402(7)
d - m	1.411(7)	1.412(7)	1.394(7)	1.399(7)	
a - N - d	107.1(4)	107.3(1)	107.2(4)	107.7(4)	107.3(3)
N - a - b	108.2(4)	108.6(4)	109.0(4)	108.4(4)	108.5(3)
N - d - c	108.9(4)	108.8(4)	108.8(4)	108.0(4)	108.6(4)
a - b - c	108.1(5)	107.6(4)	107.2(5)	107.7(4)	107.6(4)
b - c - d	107.6(4)	107.6(4)	107.8(4)	108.2(5)	107.8(3)

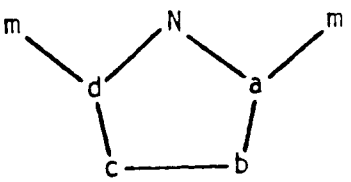

Table 4.6. Selected planes of the porphyrin macrocyclic skeleton

Plane #1: $-0.8983x + 0.4132y + 0.1491z + 2.0711 = 0$[a]

Plane #2: $-0.9052x + 0.4003y + 0.1426z + 2.2543 = 0$

Perpendicular displacements (Å)

Plane #1				Plane #2			
In	0.6104(3)	C(10)	-0.052(5)	In	0.7115(3)	C(10)*	-0.006 (5)
Cl	2.978 (2)	C(11)	-0.049(5)	Cl	3.079 (2)	C(11)*	0.006 (5)
N(1)*	0.014 (4)	C(12)	-0.185(6)	N(1)*	0.141 (4)	C(12)*	-0.142 (6)
N(2)*	-0.014 (4)	C(13)	-0.224(6)	N(2)*	0.066 (4)	C(13)*	-0.168 (6)
N(3)*	0.015 (4)	C(14)	-0.086(5)	N(3)*	0.091 (4)	C(14)*	-0.008 (5)
N(4)*	-0.014 (4)	C(15)	-0.122(5)	N(4)*	0.108 (4)	C(15)*	-0.025 (5)
C(1)	-0.136 (5)	C(16)	-0.095(5)	C(1)*	0.012 (5)	C(16)*	0.023 (5)
C(2)	-0.347 (6)	C(17)	-0.219(6)	C(2)*	-0.187 (6)	C(17)*	-0.082 (6)
C(3)	-0.356 (6)	C(18)	-0.204(5)	C(3)*	-0.211 (6)	C(18)*	-0.051 (6)
C(4)	-0.117 (5)	C(19)	-0.089(5)	C(4)*	0.007 (5)	C(19)*	0.055 (5)
C(5)	-0.128 (5)	C(20)	-0.141(5)	C(5)*	-0.023 (3)	C(20)*	0.015 (5)
C(6)	-0.074 (5)	1Cl	-0.241(3)	C(6)*	0.011 (5)	1Cl	-0.061 (3)
C(7)	-0.103 (6)	2Cl	-0.327(3)	C(7)*	-0.038 (6)	2Cl	-0.220 (4)
C(8)	-0.068 (6)	3Cl	-0.163(3)	C(8)*	-0.019 (6)	3Cl	-0.141 (4)
C(9)	-0.029 (5)	4Cl	-0.310(3)	C(9)*	0.028 (5)	4Cl	-0.214 (4)

[a] The plane equations are in terms of orthogonal coordinates in Å.

* Indicates the atoms included in the calculation of the mean plane.

Table 4.7. Representative metalloporphyrins with significant out-of-plane displacement of the metal ion.[a]

Metal	Oxidation State	Ionic Radius[b]	Metalloporphyrin	Coordination Number	Metal Ion Displacement[c]	$(M-N)_{ave}$	Core Radius[d]	Doming[e]	Reference
Bi	III	0.96 Å	$Bi(OEP)^+$	5	1.09 Å	2.32 Å	2.047 Å	0.13 Å	114
Zr	IV	0.79	$(OAc)_2Zr(OEP)$	8	1.02	2.268,2.259	2.024,2.014	0.17,0.21	115
Hf	IV	0.78	$(OAc)_2Hf(OEP)$	8	1.01	2.257	2.016	0.13	115
Fe	II	0.74	deoxyhemoglobin (horse)	(6)	0.75[f]	----	----	----	62
Tl	III	0.95	ClTl(OEP)	5	0.69	2.212	2.10	0.06	116
In	III	0.81	ClIn(TPP)	5	0.61	2.156	2.067	0.10	This work
Fe	II	0.74	deoxyhemoglobin (human)	(6)	0.60(α);0.63(β)[f]	2.1(αorβ)	2.00[g]	≤0.22(α);0.17(β)	74
(VO)	(II)	----	OV(OEP)	4	0.54	2.101	2.030	0.06	117
Mn	III	0.66	(1-MeIm)Mn(TPP)	5	0.52	2.128	2.065	0.04	66
Fe	III	0.64	$O[Fe(TPP)]_2$	5	0.50	2.087	2.027	0.04	48
Fe	III	0.64	ClFe(proto-IX)	5	0.48	2.062	2.007	0.06	41
Fe	II	0.74	(2-MeIm)Fe(TPP)	5	0.42	2.086	2.044	0.13	64,65
Fe	III	0.64	(2-MeIm)Fe(TpivPP)	5	0.40	2.072	2.033	0.03	118
Fe	III	0.64	ClFe(TPP)	5	0.38	2.049	----	----	40
Zn	II	0.74	$(ClO_4)Zn(TPP)$	5	0.35	2.076	2.046	0.09	119
Zn	II	0.74	(py)Zn(TPyP)	5	0.33	2.073	2.047	0.04	21
Zn	II	0.74	(py)Zn(OEP)	5	0.31	2.067	2.043	0.09	120
Fe	III	0.64	methemoglobin (horse)	(6)	≈0.3[f]	----	----	----	28
Fe	II	0.74	deoxy-erythrocruorin	(6)	≈0.3[f]	----	----	----	25
Fe	III	0.64	metmyoglobin (whale)	(6)	0.27	2.04	2.00[h]	0.13	95
Mn	III	0.66	ClMn(TPP)	5	0.27	2.008	1.989	0.0	121
Mg	II	0.66	$(H_2O)Mg(TPP)$	5	0.27	2.072	2.055	----	122
Mn	III	0.66	$N_3Mn(TPP)$	5	0.23	2.005	1.992	----	123
Co	II	0.72	(1-MeIm)Co(OEP)	5	0.13	1.955	1.950	0.03	55
Co	II	0.72	(1-MeIm)Co(TPP)	5	0.13	1.977	1.973	0.01	54

[a] Abbreviations: OAc, acetate; Me, methyl; py, pyridine; OEP, octaethylporphyrin dianion; TPP, tetraphenylporphyrin dianion; proto-IX, protoporphyrin IX dianion; TpyP, tetra(4-pyridyl)porphyrin dianion.

[b] from reference 8.

[c] perpendicular displacement of the metal ion from the mean plane of the four pyrrole nitrogens.

[d] average distance from the center of the plane of the four pyrrole nitrogens to a pyrrole nitrogen.

[e] difference between the displacement of the metal from the mean plane of the four pyrrole nitrogens and the mean plane of the 24-atom porphyrin skeleton.

[f] displacement in this case is measured from the mean plane of the 24-atom porphyrin skeleton.

[g] this distance was contrained to this value in refining the atomic positions.

PART TWO

PERTURBED ANGULAR CORRELATION STUDY ON MYOGLOBIN

(Radioactive ^{111}In-labelled porphyrin/Reconstitution/ τ_c determination)

CHAPTER V

PERTURBED ANGULAR CORRELATIONS

General Introduction

During the past decade, several labelling techniques have been developed to determine the rotational correlation times, internal motions, and conformational changes in biological macromolecules. As one example, fluorescence depolarization measurements can provide a measure of the rotational correlation time of a small chromophore bound to a macromolecule (127). Rotational correlation times can also be obtained from magnetic relaxation times (128), and from ESR line-shape analysis (129). It is only in very recent years that the method of perturbed angular correlations (P.A.C.) has been utilized as a labelling technique in the study of biological macromolecules. Several publications have discussed how P.A.C. measurements can give motional and structural information about biological macromolecules (7-12).

The information gained from P.A.C. measurements is often similar to that obtained in nuclear and paramagnetic studies but, in some cases not obtainable in any other way. NMR is a relatively an insensitive technique, especially in the case of very dilute samples, which is often the case for biological macromolecules (10^{-4}-10^{-5}M). This difficulty arises from the weakness of an n.m.r. signal compared with the background noise of the instruments used. For proton-n.m.r. of biological macromolecules in which aqueous solvents are required, it is necessary to prepare the sample in D_2O rather than in water. This is to eliminate the strong H_2O-proton resonance that obscures most of the resonances of protons of interest.

Moreover, interpretation of n.m.r. spectra for large macromolecules is rarely simple. The fluorescence depolarization technique requires optical transparency for operation which thus greatly limits its potential use. Both n.m.r. and esr techniques demand expensive equipment for operation. The P.A.C. method has the advantage of being applicable to solutions and solids which opens the possibility for in vivo experimentation. The simplicity of experimental measurements, with concentration sensitivity approaching 10^{-12}M, together with the fact that the theoretical understanding of the effects of molecular motion on angular correlations has now become more complete, make P.A.C. a potentially useful labelling technique. Despite its obvious potential, relatively few P.A.C. studies have been reported. The paucity of data is probably attributable to the lack of versatility in selective attachment of radioactive rotational labels to specific sites on macromolecules. This thesis demonstrates that ^{111}In-labelled porphyrins can be very selectively incorporated into myoglobin.

P.A.C. experiments require the incorporation of a gamma emitter into the molecules under study. Several isotopes (gamma emitters) can be used: ^{111m}Cd($t_{1/2}$=49 min), ^{62}Zn($t_{1/2}$=9h), ^{119m}Hg($t_{1/2}$=43 min), ^{204}Pb($t_{1/2}$=68 min), and ^{111}In($t_{1/2}$=2.8 days). It is obvious that ^{111}In with its convenient half-life, 2.8 days is the useful isotope from the practical viewpoint. Furthermore, indium-111 produces two gamma rays in succession, each with a convenient energy for detection. Marshall et al., (13,14) were the first to show how gamma-gamma coincidence measurements for this type of energy cascade can give direct information about chemical bonding and motional flexibility at an indium-labelled site on a macromolecule.

The radioactive labels can be made specific by binding the radioactive

nuclei first to some chemical complexes. For instance, the Cd isotope can be bound to a chemical complexing agent such as EDTA which is covalently attached to an active group such as a sulfydryl reagent. This part of the thesis describes the preparation of indium-111 labelled meso-protoporphyrin IX, and how P.A.C. measurements can give rotational correlation time of myoglobin. The present reconstitution of indium-111 meso-protoporphyrin IX into apomyoglobin (myoglobin with its native heme removed) represents the first motional probe located at the metal center of the active site on a protein. The rotational correlation time of myoglobin obtained by P.A.C. method is 16 nsec at 12°C. The discrepancy between the experimental τ_c* and the τ_c calculated from Debye's model is probably due to the non-spherical conformation of myoglobin.

---

*τ_c is used to denote the rotational correlation time.

CHAPTER VI

THEORY OF PERTURBED ANGULAR CORRELATIONS OF NUCLEAR RADIATION

6.1 Introduction

For decades physicists have employed the P.A.C. technique for the determination of properties of excited nuclear states and multipolarities of radiations emitted, and of interactions responsible for the emission. It is only within this decade that chemists began to use P.A.C. measurements to obtain motional and structural information on biological macromolecules.

The probability $W(\theta)$ for emission of a nuclear radiation depends on the angle θ between the emitted radiation and some fixed direction. The total radiation from a radioactive sample is isotropic if the nuclear spins are randomly oriented in space since there is no preferred direction for the emission of the radiation. An anisotropic pattern of emission can be observed only from an ensemble of nuclei that are not randomly oriented.

One method of obtaining oriented nuclei is by cooling the nuclear spin system to a very low temperature. At thermal equilibrium, a net orientation of the spin-system occurs with the distribution of spin orientations according to the Boltzman function. Application of a very strong magnetic field or an electric field gradient will also align the spins. Another method is the selection of nuclei with aligned spins as in the case of P.A.C. If the nuclei such as indium-111, decay through successive emission of two radiations, choosing only those nuclei which emit the first radiation in a given direction is equivalent to selecting nuclei whose spins are essentially aligned in that direction. The

succeeding second radiation then shows a definite angular dependence with respect to the direction of the first radiation.

There is a strong angular correlation between the directions of propagation of the gamma rays in cascade. It is this property that enables the P.A.C. method to monitor molecular motion. Following the emission of the first gamma ray, the angular correlation, $W(\theta)$ will be strongly perturbed if the orientation of the spin of the nucleus in the intermediate state changes by interaction with its surroundings. In the semi-classical picture, these interactions produce a precession of the nuclei around the symmetry axis. The change in nuclear orientation produces an altered angular correlation. Several workers (7,8,9) have observed that the angular correlation of the gamma ray cascade following the decay of ^{111}In is strongly perturbed when the radioactive ion is bound to a macromolecule in aqueous solution. In order to observe an anisotropic correlation in the absence of an applied field, the intermediate state much have nuclear spin ≥ 1, so that the nucleus may possess a quadrupole moment. The quadrupolar interaction of the nuclear quadrupole moment with external electric field gradient is the basis of the angular correlation. This interaction turns out to be an advantage for the study of molecular rotational motion, because the nuclear spin orientation rate due to a quadrupolar interaction is affected by molecular rotational motion, but not by relative translational motion.

By the study of the perturbed angular correlation of gamma radiation from a rapidly reorienting radioactive nucleus, the nuclear relaxation time can be measured. Since the nuclear relaxation time depends strongly on the rate of rotation of the molecule to which the radioactive nucleus is bound, it may be used to estimate the rotational correlation time, τ_c

which is a measure of the time it takes for the molecule to change its orientation by the order of one radian.

6.2 Theoretical consideration

The theory of angular correlation is probably one of the best and most comprehensive theories on nuclear phenomena. For the present case, only the theory of extranuclear perturbations on angular correlations will be considered. An excellent review of the theory of perturbed angular correlations is available in the article by Frauenfelder and Steffen (130).

It is felt that a brief discussion of fluorescence depolarization will provide a better understanding to P.A.C. because conceptually and instrumentally it is analogous to P.A.C.

In fluorescence depolarization, if the exciting radiation (usually in the ultra-violet region) is polarized, the probability of absorption will depend on the orientation of the molecule, being maximum if the direction of the dipole moment change is parallel to the direction of propagation. If, within the lifetime of the excited electronic state ($\sim 10^{-9}$ sec), the molecules do not rotate appreciably, then the fluorescent radiation will also be highly polarized. In a solution of molecules, however, rotational movement occurs. Since this is a random process, it leads to randomization of the orientation of the dipole moments in the time between absorption and emission, which results in depolarization of the fluorescent radiation. This means that fluorescence depolarization can be used to measure the rate of rotational motion of the molecule carrying the chromophore. It must be noted that the use of fluorescence depolarization to measure τ_c can never be unambiguous because of the difficulty of separating internal rotation of the chromophore from the rotation of the molecule as a whole. In the case of P.A.C., both the

"polarizing" or aligning of the nuclear spins and emitting radiation come from the radioactive sample whereas an initial external polarizing source is required for the fluorescence measurements. Gamma-rays arise from decay of excited nuclear states rather than excited electronic states in the case of fluorescence (visible region).

Consider an assembly of randomly oriented nuclei in which state A decays by successive emission of two gamma radiations, γ_1 and γ_2, to the levels B and C, as shown in Figure 6.1. The total radiation will be isotropic. The arrangement for the directional correlation experiment is illustrated in Figure 6.2. In the simplest case, the detector 1 is designed to accept only radiation γ_1 which is equivalent to choosing nuclei whose magnetic dipoles (spins) are aligned according to that direction. Detectors 2 and 3 are sensitive only to radiation γ_2. The detectors may count all photons that fall in their solid angles; however the coincidence analyzer selects principally only pairs of radiations γ_1 and γ_2 which are genetically related to each other. This is accomplished by accepting a signal from detector 1 only if a signal from detector 2 arrives at the same time. In other words, only those radiations which are emitted within the resolving time, τ_R of the coincidence circuit are accepted. Typical values of τ_R are 10^{-6} to 10^{-9} second. By proper selection of resolving time and source strength, the possibility of chance coincidence between unrelated radiation may be reduced to a tolerable level. The angular distribution of the second radiation γ_2 with respect to the first radiation γ_1 is expressed as an angular correlation function, $\underline{W(\theta,t)}$ which is a measure of the number of coincidences

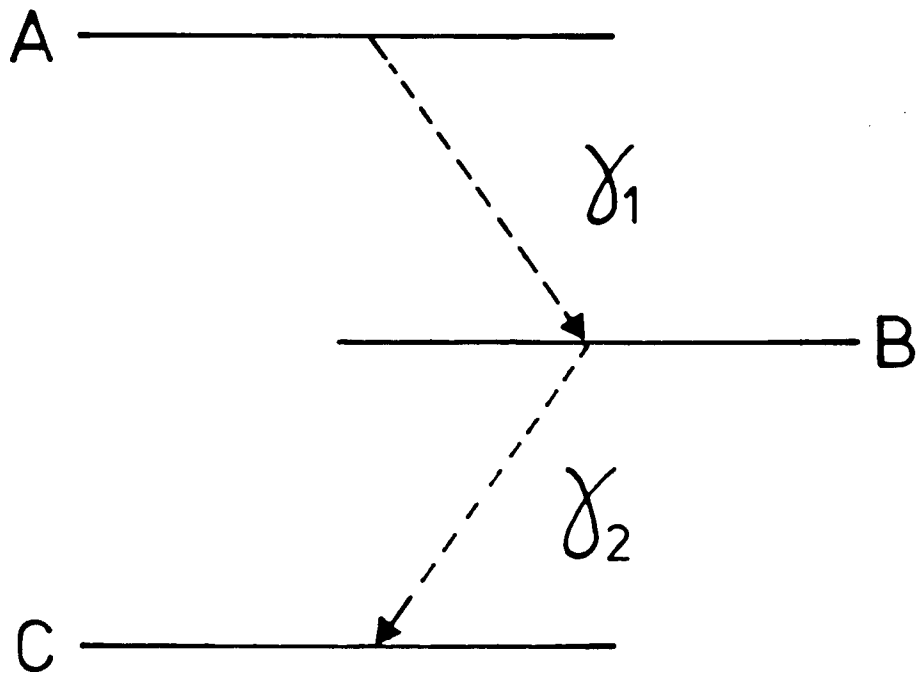

Figure 6.1. Nuclear decay scheme of a level A which decays by the emission of a radiation γ_1 into a level B and then by the emission of a radiation γ_2 into a level C.

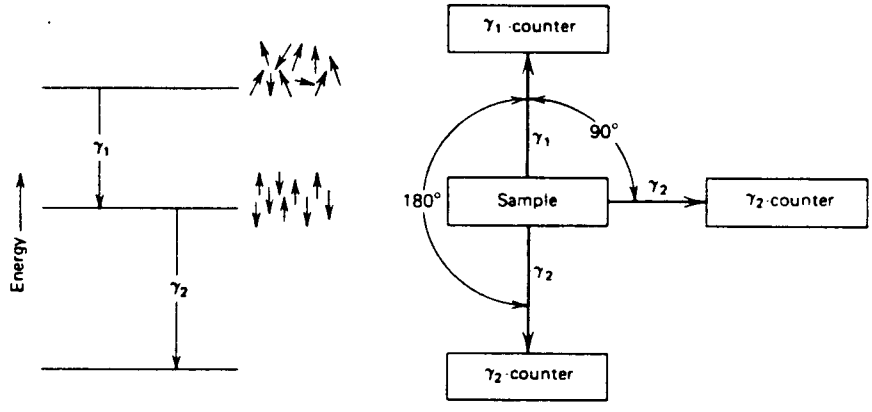

Figure 6.2. The arrangement for the directional correlation experiment, and the origin of anisotropy in direction of gamma-ray emission from initially unaligned nuclear magnetic dipoles. Although initial magnetic dipole directions are random (upper left), restricting the detection of those rays to a single direction selects nuclei that must have been aligned according to that emission direction (middle left). Gamma rays subsequently emitted (i.e., γ_1) from those aligned nuclei will be observed preferentially at 180° rather than 90° to the direction between the sample and the γ_2-counter (right).For most cases, the energies of γ_1 and γ_2 are sufficiently different that they are readily distinguisable by the detectors.

per unit time. By this arrangement, an anisotropy between γ_1 arriving at detector 1 and γ_2 arriving at detectors 2 and 3 is detected. If the molecules are able to rotate during the time between the emission of γ_1 and the observed γ_2, then the anisotropy will be partially lost due to the changing nuclear orientation of the nucleus in the intermediate state. For slow rotational motion, the anisotropy, A(t) will decrease exponentially with time. Experimentally, A(t) is obtained from the expression below

$$A(t) = \frac{[(\#\gamma_2\text{-counts at } 180°)-(\#\gamma_1\text{-counts at } 90°)]}{[\#\gamma_2 \text{ counts at } 90°]} \qquad (6.1)$$

In gamma-gamma studies, faster molecular rotation usually leads to slower exponential decay of anisotropy.

Indium-111 decays by electron capture to cadmium-111 followed by the successive emission of two gamma rays in the 173-247keV cascade as shown in Figure 6.3. For this sort of energy cascade, Steffen (131) showed that the coincidence counting rate, $W(\theta,t)$ is given by

$$W(\theta,t) = \frac{1}{\tau_N} e^{-t/\tau_N}[1+A_{22}P_2(\cos\theta)] \qquad (6.2)$$

where θ is the angle between the two gamma rays, $P_2(\cos\theta)$ is the Legendre polynomial $1/2(3\cos^2\theta-1)$, $\tau_N(1.22\text{x}10^{-7}\text{sec})$ is the mean lifetime of the intermediate nuclear state for the 247keV state of ^{111}Cd (132), t is the time interval between the emission of the two gamma rays, and A_{22} is a parameter that depends on the spins and multipolarities associated with the cascade. The theoretical value for the 173-24kKeV cascade, A_{22}=-0.18 (131).

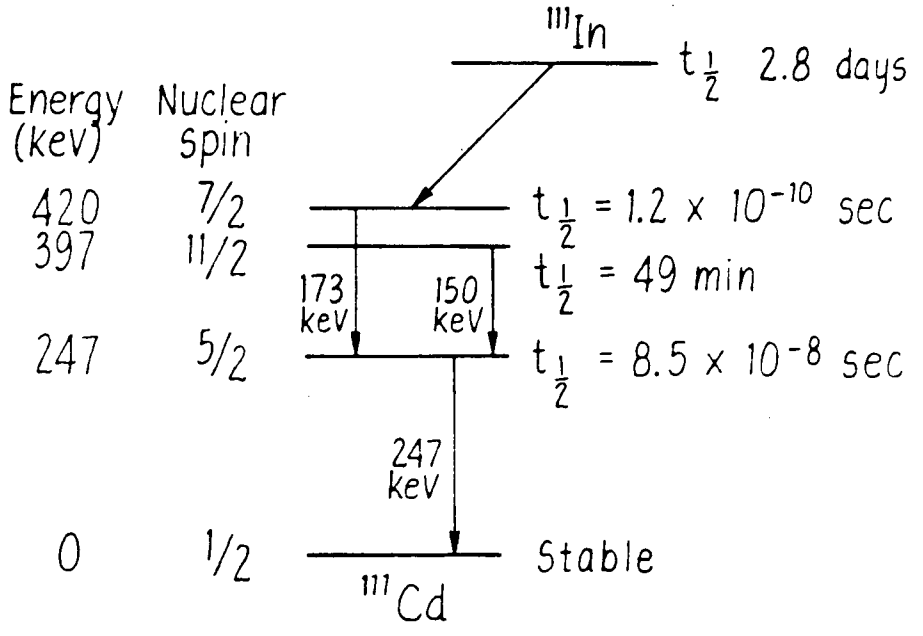

Figure 6.3. The 173-247 keV gamma-ray cascade of ^{111}Cd after the electron-capture decay of ^{111}In.

Following the emission of the first gamma, the angular correlation can be strongly perturbed by interaction of the nuclear quadrupole moment of ^{111}Cd in the metastable 247keV state with the fluctuating electric field gradient at the ^{111}Cd nucleus. The perturbation on the angular correlation can only be observed if τ_N is long enough and the nuclear moments of the intermediate state are large enough. In this case, the coefficient of $P_2(\cos\theta)$ in Eq. 6.2 can be written as $A_{22}G_{22}(t)$ where $G_{22}(t)$ is an attentuation coefficient (133). Eq. 6.2 can then be rewritten as

$$W(\theta,t) = \frac{1}{\tau_N} e^{-t/\tau_N}[1+A_{22}G_{22}(t,I,\omega_o,\eta,\tau_c)P_2(\cos\theta)] \qquad (6.3)$$

$G_{22}(t,I,\omega_o,\eta,\tau_c)$ is the perturbation factor which represents the interaction with surroundings determined by the parameters

$$\omega_o = \frac{6eQV_{zz}}{h4I(2I-1)} \quad , \quad \eta = \frac{V_{xx}-V_{yy}}{V_{zz}} \quad \text{(the asymmetry parameter)}$$

and τ_c, where Q is the quadrupole moment of the intermediate state ^{111}Cd, V_{xx}, V_{yy}, and V_{zz} are components of the field gradient in the principal axis system, and τ_c is the relaxation time. It is obvious that the information of physical interest is contained in the time-dependent perturbation factor, $G_{22}(t)$. In the unperturbed case, $G_{22}(t)=1$.

In the present studies where ^{111}In-porphyrin complex is bound to a macromolecule (myoglobin) in aqueous solution, the angular correlation is expected to be perturbed by the interaction of the nuclear quadrupole moment, Q of ^{111}Cd in the intermediate state with the fluctuating electric field gradients at the nucleus. The form of $G_{22}(t)$ then depends on the dynamical details of the molecular motion.

The approximate form of $G_{22}(t)$ may be displayed by a plot of the anisotropy

$$A(t) = \frac{W(\pi,t)-W(\pi/2,t)}{W(\pi/2,t)} - 1 \qquad (6.4)$$

$$\approx \frac{3}{2}A_{22}G_{22}(t)$$

against the delay time, t between the emissions. In practice t is the delay time between the two channels of the coincidence circuit. Experimentally $G_{22}(t)$ can be determined from the formula below

$$G_{22}(t) = \frac{2}{A(t)} \quad \frac{W(\pi,t)-W(\pi/2,t)}{W(\pi,t)+2W(\pi/2,t)} \qquad (6.5)$$

The detailed shape of the plot of $G_{22}(t)$ versus delay time depends on the relative magnitude of the molecular rotational correlation time, τ_c of the radioactive probe, and upon the nuclear quadrupole interaction (e^2qQ) between the nuclear quadrupole moment (eQ) and the electric field (eq) at the nucleus in the intermediate state.

6.2a Time-Dependent Quadrupole Interaction - The Limit of Rapid Motion

Time-dependent quadrupole interactions represent the major perturbation factor on angular correlations for the case in liquids. This arises from the Brownian motion of the molecules in a liquid which give rise to rapidly fluctuating electric field gradients that interact with the nuclear electric quadrupole moment, eQ in the intermediate state.

Using time-perturbation theory, Abragam and Pound (133) have calculated the effect of rapid molecular motion on the angular correlation (130,134). This is the case where molecular rotational correlation time, τ_c is short compared to a period of the quadrupole frequency. As an example is the situation of a small molecule in a non-viscous liquid. For the rapid motion, $G_{22}(t)$ takes the form of a simple exponential for the case of a nuclear spin, I = 5/2, and an axially symmetric electric field gradient (133)

$$G_{22}(t) = \exp(-\lambda_2 t) \tag{6.6}$$

where

$$\lambda_2 = \frac{63}{1000}\overline{\overline{(e^2qQ)^2}}\tau_c/\hbar \tag{6.7}$$

where double bar denotes an ensemble average, and τ_c is the molecular correlation time. λ_2 is known as the relaxation constant. The above equations assume that the rotational diffusion is isotropic.

The differential $G_{22}(t)$ in Eq. 6.6 can be expressed in the integral form

$$\overline{G_{22}(\infty)} = 1/\tau_N \int_o^\infty e^{-t/\tau_N} G_{22}(t)dt \tag{6.8}$$

Combining Eqs. 6.6 and 6.8 gives

$$\overline{G_{22}(\infty)} = 1/(1+\lambda_2\tau_N) \tag{6.9}$$

The differential correlation Eq. 6.6 shows that $G_{22}(t)$ decreases monotonically with time. In other words, after sufficiently long time, the original orientation of the assembly of nuclei is completely lost. This is also reflected in the integral correlation Eq. 6.9, which can become zero for large field strengths or long lifetime.

The integral correlation is easy to perform experimentally and in much less time than a measurement of differential $G_{22}(t)$. However, some information and details concerning the interaction mechanism is usually lost in the averaging process. In the present studies on ^{111}In-labelled myoglobin, time-differential technique was used, which means the angular correlation is measured as a function of t, the delay time.

From Eqs. 6.6 and 6.9, it is clear that for large values of λ_2, the attentuation factor vanishes and there is no finite lower limit. In other words, the angular correlation can be isotropic for slow motion in liquids.

The relaxation constant, λ_2 is directly proportional to the correlation time, τ_c (Eq. 6.7) which is usually small for small molecules in dilute solutions: $\tau_c \approx 10^{-11}$ sec. Consequently, as evident from Eqs. 6.6 and 6.7 that even for large quadrupole interaction, the attentuation of the angular correlation for small molecules in liquids is small. This explains why the anisotropy of angular correlations remains largely unperturbed for small molecules or free ions in dilute solutions. The present study shows that similar anisotropy pattern is observed for ^{111}InMPPIX and ^{111}InTPP in organic solvents.

Based on the Debye model (135) for polar liquids, τ_c is given by

$$\tau_c = (\frac{4\pi R^3}{3kT})\xi \qquad (6.10)$$

where R is the effective molecular radius, ξ is the viscosity, T is the absolute temperature, and k is the Boltzman's constant.

Eq. 6.10 clearly shows that τ_c is directly proportional to the viscosity of the liquid (135,136). Consequently, changing the viscosity will affect the anisotropy of the angular correlations. Measurements of time-differential angular correlations (TDAC) on aqueous solutions of $^{111}In\text{-}Cl_3$ for various viscosities have been performed by Steffen (131). The results are shown in Figure 6.4. As the molecular rotation decreases due to increase in solution viscosity, the anisotropy decreases very rapidly as expected from Eq. 6.9.

The dependence of the anisotropy on the viscosity is clearly illustrated by a plot of $\overline{G_{22}(\infty)}$ versus viscosity (137) in Figure 6.5. The solid line represents the theoretical curve calculated on the assumption that τ_c is directly proportional to the viscosity of the liquid.

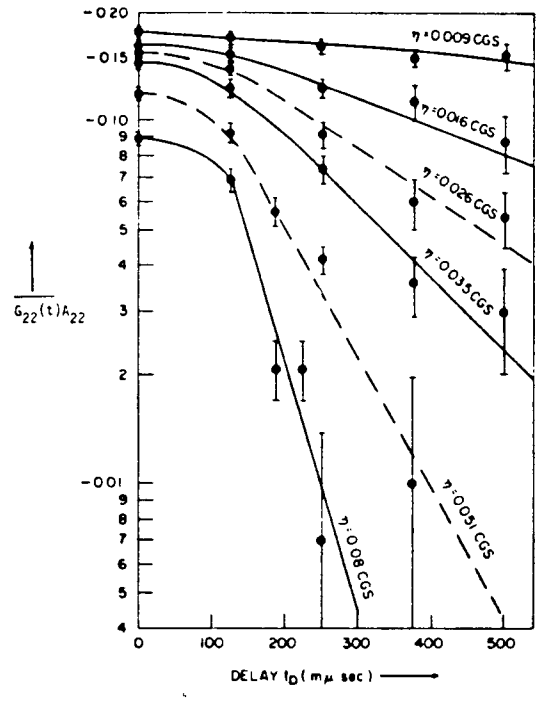

Figure 6.4. Anisotropy factor $\overline{G_{22}(t)}A_{22}$ of the ^{111}Cd γ-γ directional correlation as function of the delay time t for ^{111}In sources of various viscosities η. The source is a dilute aqueous solution in $InCl_3$ whose viscosity was varied by adding glycerine.
From Steffen (ref. 131).

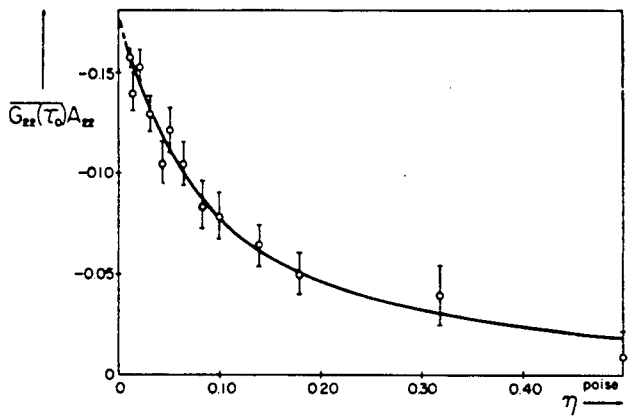

Figure 6.5. The integral anisotropy factor $\overline{G_{22}(\tau_0)}A_{22}$ of the ^{111}Cd γ-γ directional correlation as function of the viscosity η of the ^{111}In source.

From Hemmig and Steffen (ref. 137).

6.2b Static Electric Field Quadrupole Interactions - Polycrystalline Samples

Although time-dependent quadrupole interactions may occur in crystalline samples because of lattice vibrations and crystal distortions, static electric field quadrupole interaction is the principal perturbation factor. Blume (134) considered the case of a polycrystalline sample where there is no molecular rotational motion at all ($\tau_c \to \infty$). He showed that $G_{22}(t)$ takes the form

$$G_{22}(t) = (1/5)[1+(13/7)\cos\omega_o t+(10/7)\cos 2\omega_o t + (5/7)\cos 3\omega_o t] \qquad (6.11)$$

where $\omega_o = [3/2I(2I-1)](e^2qQ/\hbar)$

is the quadrupole frequency.

The differential correlation in Eq. 6.11 is a periodic function (a summation of cosines) in contrast to the case of time-dependent quadrupole interaction (rapid motion) where $G_{22}(t)$ decreases exponentially. In other words, the static quadrupole interaction does not destroy the angular correlations. Figure 6.6 shows the measurement made with a metallic ^{111}In source (138). The fact that the experimental points lie closely on the theoretical curve (solid line calculated according to the Eq. 6.11) provides evidence that, to a good approximation, only static electric quadrupole interaction is present in this polycrystalline indium metal source.

In a polycrystalline sample, the angular correlation is never wiped out completely because the static ensemble average over all emitting nuclear orientations gives a non-zero result. However, in the case of the time-dependent interactions, the angular correlation can be completely wiped out because the direction of the field at each nucleus changes

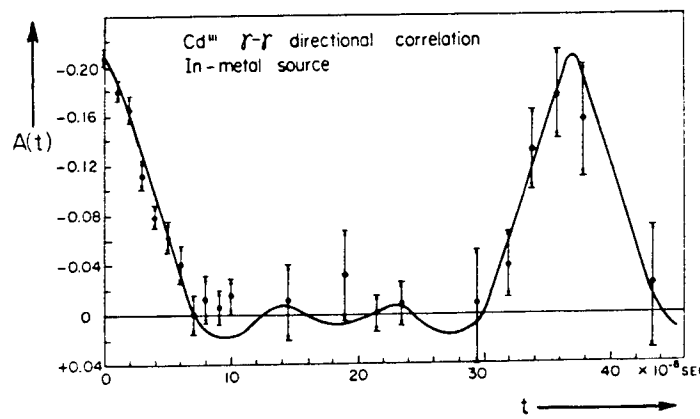

Figure 6.6 Differential anisotropy A(t) of the ^{111}Cd γ-γ directional correlation measured with a polycrstalline In-metal source.
From Lehmann and Miller (ref. 138).

continuously in a random manner during the interval between emission of γ_1 and γ_2.

Figures 6.7a and 6.7b show the anisotropy of ^{111}Cd gamma-gamma correlation displayed by polycrystalline non-metallic In_2O_3 and $In(OH)_3$ (138). The solid lines represent the theoretical curves for an axially symmetric static quadrupole interaction. The experimental curves do not show the usual characteristic periodic behavior of the differential anisotropy A(t) for static quadrupole interactions (Figures 6.7a and 6.7b) as opposed to Figure 6.6. The non-metallic sources show first a rapid decay of the correlation within about 10^{-8} sec, and then possibly fluctuate around the low values. The discrepancy is due to the effects arising from the excited electron shell after the K capture (See Appendix C).

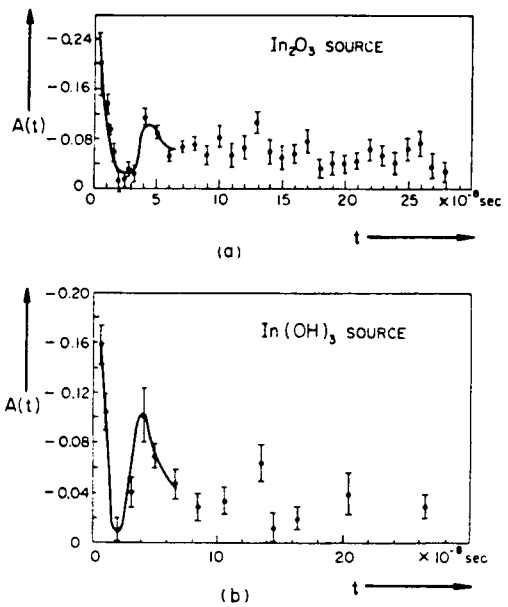

Figure 6.7. Differential anisotropy A(t) of the ^{111}Cd γ-γ directional correlation observed with sources of (a) In_2O_3 and (b) $In(OH)_3$.
From Lehmann and Miller (ref. 138).

6.2c Time-Dependent Quadrupole Interaction - The Limit of Slow Motion

In the limit of slow molecular motion, with the assumption of axially symmetric electric field, Marshall and Meares (13) show that the expression for $G_{22}(t)$ is obtained by multiplying Eq. 6.11 by the diffusion damping factor, $\exp(-t/\tau_c)$,

$$G_{22}(t) = \exp(-t/\tau_c) \sum_{n=o}^{3} a_n \mathrm{Cos}(\omega_o t) \tag{6.12}$$

where a_n are the coefficients in Eq. 6.11, and

$$\tau_c = (1/6D_{rot}) \tag{6.13}$$

where D_{rot} is the rotational diffusion constant for a spherical molecule.

The integral attentuation factor $G_{22}(t)$ is expressed as

$$\overline{G_{22}(\infty)} = (1/5\tau_N)[1/C + (13/7)(\frac{C}{C^2+\omega_o^2}) + (10/7)(\frac{C}{C^2+4\omega_o^2}) + (5/7)(\frac{C}{C^2+9\omega_o^2})] \tag{6.14}$$

in which $C = [(1/\tau_N + 1/\tau_c)]$ and

$$\omega_o = (3/20)\frac{e^2qQ}{\hbar}$$

The theoretical dependence of integral perturbation or attentuation factor $\overline{G_{22}(\infty)}$ on rotational correlation time, τ_c for the limiting cases (slow and fast motion) is clearly illustrated by a plot of $\overline{G_{22}(\infty)}$ versus log τ_c as shown in Figure 6.8. For small molecules in non-viscous solutions, τ_c can be as small as 10^{-11}sec or less, while for many proteins, τ_c is in the range of 10^{-8}sec (13).

Experiments by Barrett et al., (139) and theoretical calculations by Lynden-Bell (140) demonstrate that the value of $\overline{G_{22}(\infty)}$ varies smoothly and continuously between those two limiting cases (rapid and slow motions), as shown by the broken line in Figure 6.8.

For a correlation time, τ_c much larger than the lifetime, τ_N of the intermediate nuclear state, the perturbation mechanism can no longer be considered as time-dependent. In fact the environment of the nucleus will then be stationary during the nuclear lifetime and the resulting interaction is a static one, for which a minimum correlation anisotropy exists as shown in Figure 6.8. In the region where τ_c is of the order of magnitude of τ_N, the interaction is described appropriately neither by time-dependent nor by static interaction mechanism.

Marshall et al., (14) used parameters associated with the decay of ^{111m}Cd to generate theoretically several plots that illustrate the dependence of $\overline{G_{22}(\infty)}$ on angle of attachment of the label, molecular geometry or internal rotation rate (Figures 6.9-6.11).

As can be seen from Figure 6.9, the shape of the plot of $\overline{G_{22}(\infty)}$ versus τ_c can depend strongly on the angle at which the label is attached with respect to the symmetry axes of the overall moelcular shape.

Figure 6.10 shows how $\overline{G_{22}(\infty)}$ varies according to the rate of internal rotation and angle of attachment of the label. It is clear from Figure 6.10 that very rapid internal rotation increases the attentuation factor, $\overline{G_{22}(\infty)}$ because it effectively reduces the magnitude of the quadrupolar interaction for a fixed angle of attachment. However, it is interesting to note that in the situation where both the internal rotation of the label and re-orientation of the molecule as a whole are slow, internal rotation decreases

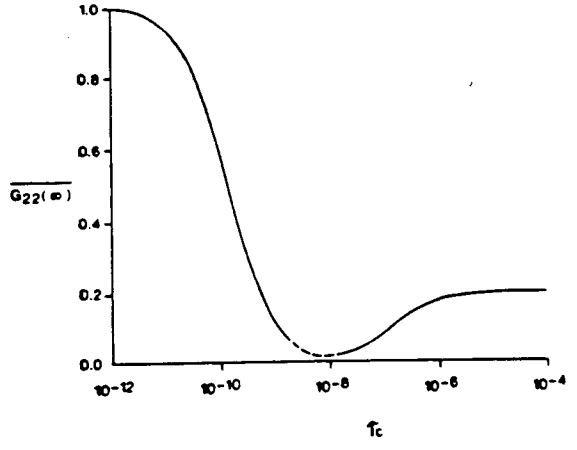

Figure 6.8. Theoretical relationship between the integral perturbation factor $\overline{G_{22}(\infty)}$ and the rotational correlation time τ_c.

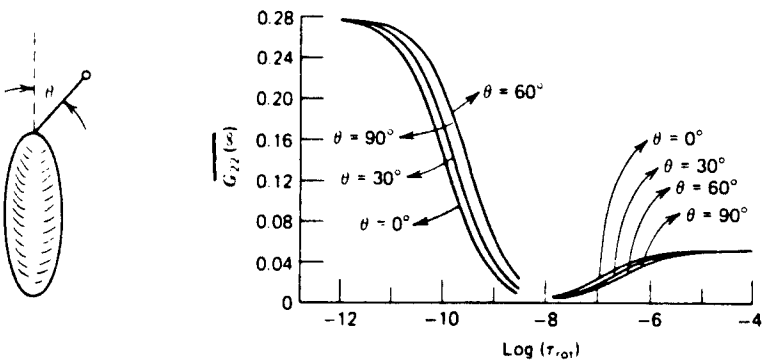

Figure 6.9. Plots of integral anisotropy, $\overline{G_{22}(\infty)}$ versus rotational correlation time, τ_{rot} (log scale) for a ^{111}Cd nucleus attached at an angle, θ, with respect to the main symmetry axis of a prolate molecular ellipsoid. In the fast-motion limit (left-hand set of curves), the integral anisotropy varies with the angle of attachment, θ, in the order $60^{\circ}>90^{\circ}>30^{\circ}>0^{\circ}$. In the slow-motion limit (right-hand set of curves), the integral anisotropy varies with θ in the order $0^{\circ}>30^{\circ}>60^{\circ}>90^{\circ}$.

From Marshall et al., (ref. 14).

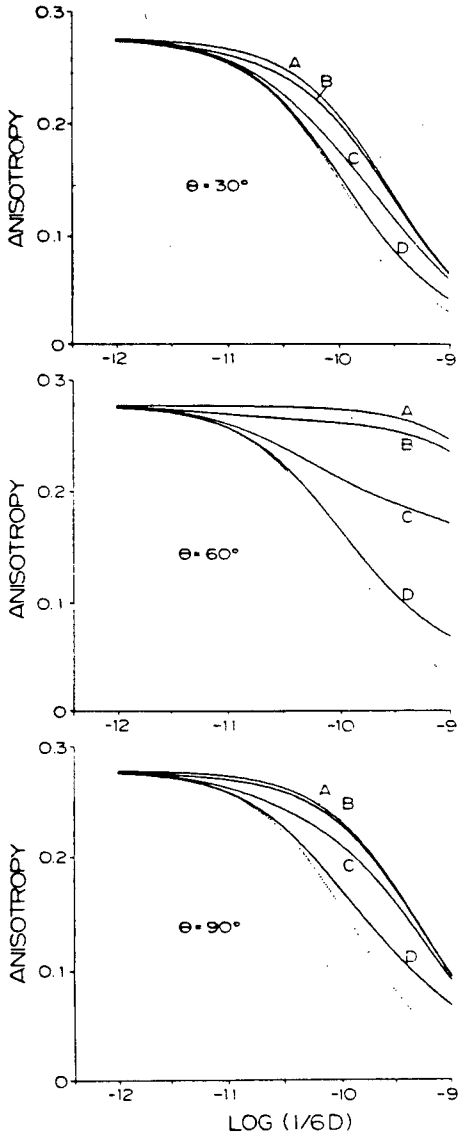

Figure 6.10. Plots of the integral anisotropy in the fast-motion limit versus log(6D), where D is the rotational diffusion constant for a spherical molecule and D_i is the diffusion constant for internal rotation. Each family of curves corresponds to a fixed choice of "attachment angle" as listed on the figure. For individual curves (A) through (D), the internal rotation diffusion constant $D_i = 10^{12}$, 10^{11}, 10^{10}, and 10^{9} sec^{-1}, respectively. The lowest curve in each set (dashed line) is the integral anisotropy in the absence of internal rotation, or equivalent for zero "attachment angle". From Marshall et al., (ref. 14).

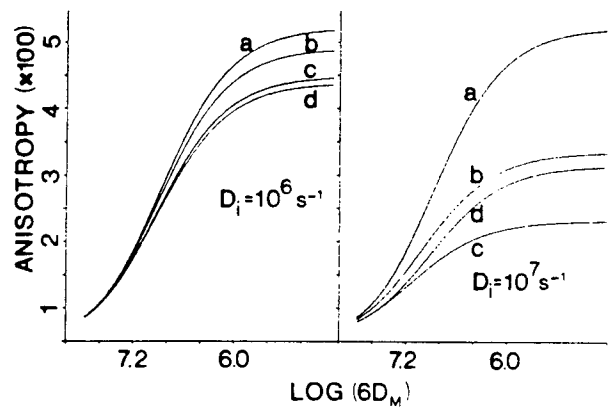

Figure 6.11. Plots of integral anisotropy versus $\log(6D_M)$, where D_M is the rotational diffusion constant for a spherical macromolecule (in the slow-motion limit). The two set curves correspond to the two choices for the integral rotational diffusion constant D_i shown on the figure. The integral anisotropy varies with the different angles of attachment in the order, $0^\circ>30^\circ>60^\circ>90^\circ$, for curves a-d, respectively. The result for $\theta=0^\circ$ is the same as for no internal rotation at all. From Marshall et al., (ref. 14).

the $\overline{G_{22}(\infty)}$ values as illustrated in Figure 6.11. It can be inferred from Figure 6.11 that when the molecular rotation is slow, internal rotation does not affect the observed $\overline{G_{22}(\infty)}$ appreciably unless the rate of internal rotation is significantly faster than the rate of rotation of the molecule as a whole. It is important to note that internal rotation, whether fast or slow, has no effect on the angular correlation when the angle of attachment of the label is zero degrees.

The above discussion clearly demonstrates the potential of gamma-gamma correlation technique as a means to study specific sites on large biologically interesting macromolecules such as hemoglobin, cytochromes. Information like the degree of internal flexibility at the site of attachment of the radioactive tracer to the macromoelcule i.e. the rate of internal motion, as well as the geometry of the complex can be obtained. Although the same information is accessible by ESR technique and fluorescence depolarization, the gamma-gamma experiment offers the advantages of requiring concentrations which can be as low as 10^{-12}M and the capability of <u>in vivo</u> experimentation.

6.2d Fields Without Axial Symmetry

The preceding discussions are restricted to the cases where axially symmetric electric field gradients (EFG) are assumed. The results for axially symmetric EFG cases can be extended to the situations of non-axially symmetric electric fields by introducing an asymmetry parameter, η to account for non-axial symmetry in the quadrupole interactions.

Considers the case of slow molecular motion, Eq. 6.12 (for axially symmetric EFG) becomes

$$G_{22}(t) = \exp(-t/\tau_c) \sum_{n=o}^{3} b_n(\eta)\cos[f_n(\eta)\omega_o t] \qquad (6.15)$$

where f_o and the coefficients $b_n(\eta)$ can be evaluated (141). For $\eta \neq 0$, the quadrupole frequencies $\omega_n(\eta)=f_n(\eta)\omega_o$ are no longer harmonic. For $\eta=o$ (axially symmetric) f_1, f_2, and f_3 take on integral values.

Matthias et al., (142,143) have performed such calculations on polycrystalline sources. Figures 6.12 and 6.13 show the differential $G_{22}(t)$ and time-integrated factor, $\overline{G_{22}(\infty)}$ for spin-values I=2 and I=5/2 and for various values of the asymmetry parameter.

Figure 6.14 shows the result for that ^{181}Ta gamma-gamma cascade with polycrystalline H_f-metal source (144). The solid line is the theoretical curve calculated on the assumption of an axially symmetric static quadrupole interaction. It is clearly evident from Figure 6.14 that there is a discrepancy between the experimental and theoretical results. However, if the experimental data are interpreted on the basis of non-axially symmetric quadrupole interactions together with an inclusion of an asymmetry parameter, $\eta \approx 0.5$ into the calculation, an excellent agreement with the experimental results is obtained. As

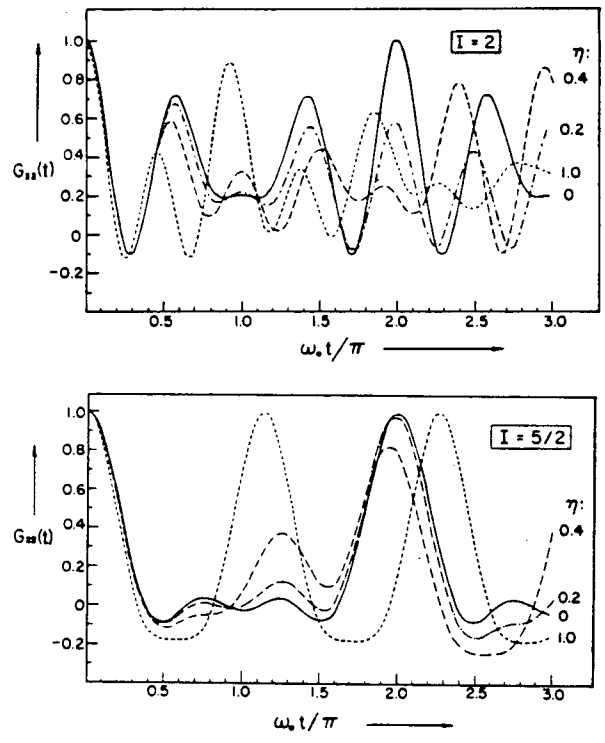

Figure 6.12. Differential attentuation coefficients $G_{22}(t)$ for rhombic quadrupole interaction in polycrystalline sources for intermediate state spins I=2 and I=5/2. The parameter η is the asymetry parameter $\eta=(V_{xx} - V_{yy})/V_{zz}$.
From Matthias et al., (ref. 142).

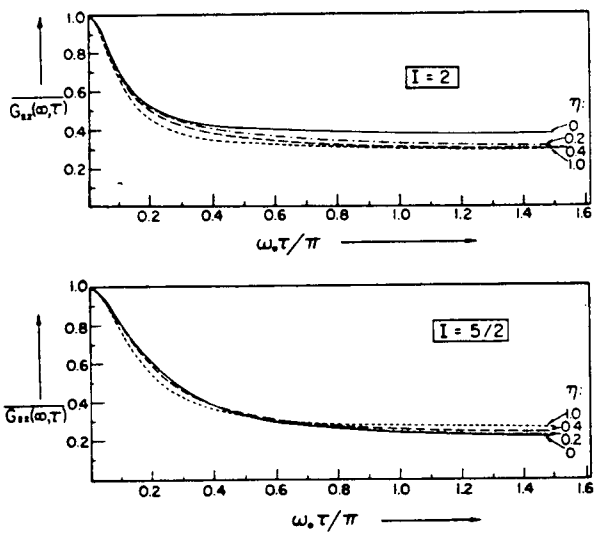

Figure 6.13. Time-integrated attentuation coefficients $\overline{G_{22}(\infty)}$ for rhombic quadrupole interaction in polycrystalline sources for spins I=2 and I=5/2.
From Matthias et al., (ref. 143).

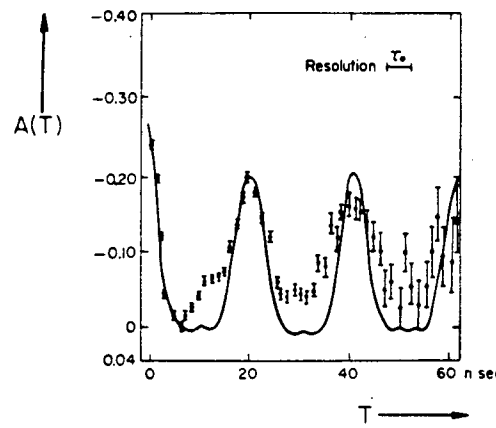

Figure 6.14. Differential anisotropy A(t) of the Ta^{181} γ-γ directional correlation measured with a polycrystalline Hf-metal source.
From Schecter and Sommerfeldt (ref. 144).

a matter of fact, this was the first indication of the presence of a non-axially symmetric static quadrupole perturbation on angular correlations.

It is clear from the two examples that the strong dependence of anisotropy on η (asymmetry parameter) can be used to give information on the geometry of the molecules under study.

CHAPTER VII

APPLICATIONS OF GAMMA-GAMMA CORRELATIONS TO BIOLOGICAL MACROMOLECULES

This chapter is intended to illustrate briefly how P.A.C. measurements can be used to obtain motional information on biological macromolecules, and for this purpose two examples will be discussed.

Meares et al., (8) applied directional gamma-gamma correlations for the study of carbonic anhydrase. The anisotropy of free $^{111m}Cd^{2+}$ in solution decreases slightly with time as illustrated in Figure 7.1a. The weakly perturbed angular correlation is as expected from Eqs. 6.6 and 6.7 since both e^2qQ and τ_c are small. Even, in the presence of native carbonic anhydrase, the anisotropy pattern is similar to that of the free $^{111m}Cd^{2+}$ except for a slightly faster decay of the gamma-ray anisotropy (Figure 7.1b). This is attributed to the increase in solution viscosity by the addition of the native enzyme. The increase in solution viscosity results in a slower rotational diffusion of ^{111m}Cd. The angular correlation is strongly perturbed when apo-carbonic anhydrase (the native enzyme with the active-site Zn^{2+} removed) was added (Figure 7.1c). In this case, $\tau_c > (e^2qQ)^{-1}$, and since the rotational diffusion of the $^{111m}Cd^{2+}$-labelled protein is now much slower, the rapid decay of the anisotropy with time is consistent with Eqs. 6.6 and 6.7.

The next example considers the application of the P.A.C. technique for <u>in vivo</u> experimentation. Goodwin et al., (145) applied P.A.C. technique to follow ^{111}In tracer metabolism in live mice. Altogether six indium-labelled complexes were injected intravenously into intact, live Swiss Webster mice, and gamma-rays were counted externally. The results of the integral

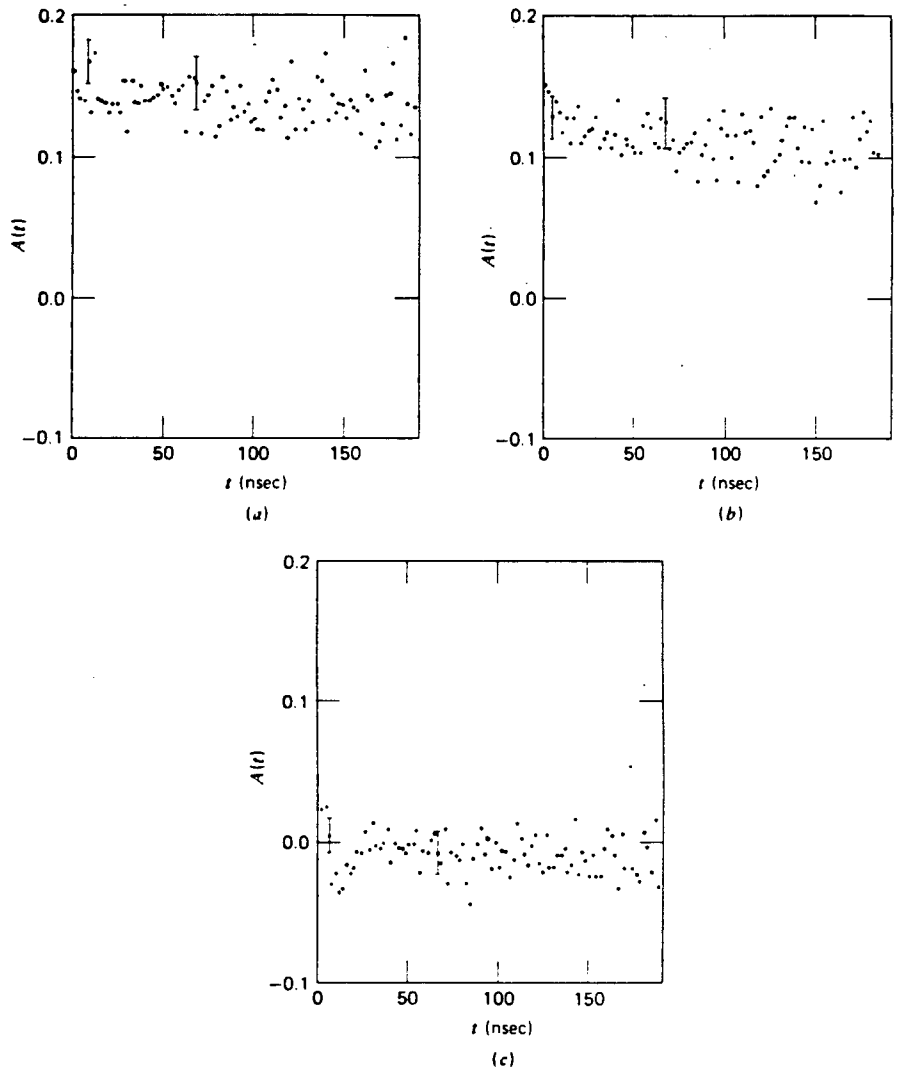

Figure 7.1. Anisotropy of correlated gamma-ray emission from $^{111m}Cd^{++}$ ion in various chemical environments. (a) free $^{111m}Cd^{++}$ in solution; (b) $^{111m}Cd^{++}$ in the presence of 3×10^{-4}M native carbonic anhydrase (i.e., enzyme with no available Cd^{++}-binding sites), and (c) $^{111m}Cd^{++}$ in the presence of 2.5×10^{-4}M apocarbonic anhydrase (i.e., enzyme with one strong Cd^{++}-binding site available).

From Meares et al., (ref. 8).

attentuation factor, $\overline{G_{22}(\infty)}$ were tabulated in Table 7.1. When $^{111}InCl_3$ was injected intravenously into a live mice, the low $\overline{G_{22}(\infty)}$ value indicates that ^{111}In binds to transferrin (Figure 7.2) which is consistent with the observation that indium binds to transferrin almost quantitatively (146,147). From Table 7.1, the low $\overline{G_{22}(\infty)}$ values for In-citrate and In-NTA after injection indicate that indium-111 dissociated from the complexes and bound to the transferrin. The low $\overline{G_{22}(\infty)}$ values reflected by the long rotational correlation times (τ_c) are characteristic values for macromolecules (8,13). In contrast, following the injection of In-EDTA, In-PhDTA, and In-CyDTA, the integral measurements give high $\overline{G_{22}(\infty)}$ values which means these compounds are essentially intact in the live mice. These studies by Goodwin et al., (145) clearly demonstrate the potential of the P.A.C. technique in determining the fate of ^{111}In-labelled tracers in humans by the external countings of the gamma-rays emitted by the radioactive tracer.

There remains a few remarks concerning the sort of information that can be extracted from the shape of the plot of anisotropy versus delay time. As mentioned in Section 6.2c, the angle of attachment of the labels can be determined by analyzing the time-differential coincidence spectrum. If the spectrum shows a series of minima, the labelled molecules are generally oriented in the same direction. The spacing between the minima will be determined by the orientation of the principal axis of an ordered array of molecules with respect to the direction of the first gamma emission. Tendon, fibers, and membranes are examples of ordered arrays of molecules that may be studied by the P.A.C. method. The study of conformational changes in polypeptide chains (especially helix-random coil transitions) has been a subject of considerable interest. A

Table 7.1. ^{111}In Compounds Studied In Vivo

Compound	*PAC		Column Chromatography (%)		RIE†
	No. of Mice	Anisotropy‡	Transferrin	Compound	Transferrin Band
In-transferrin	7	0.076±0.004	100	0	Positive
In-citrate	4	0.081±0.004	100	0	Positive
In-NTA	3	0.080±0.005	100	0	Positive
In-o-PhDTA	3	0.122±0.007	9.8	90.2	Negative
In-CyDTA	3	0.128±0.005	10.7	89.3	Negative
In-EDTA	3	0.120±0.007	10.2	89.8	Negative

* PAC = Perturbed Angular Correlation

† RIE = Radioimmunoelectrophoresis

‡ Mean of A±2 S.D.

From Goodwin et al., (ref. 145).

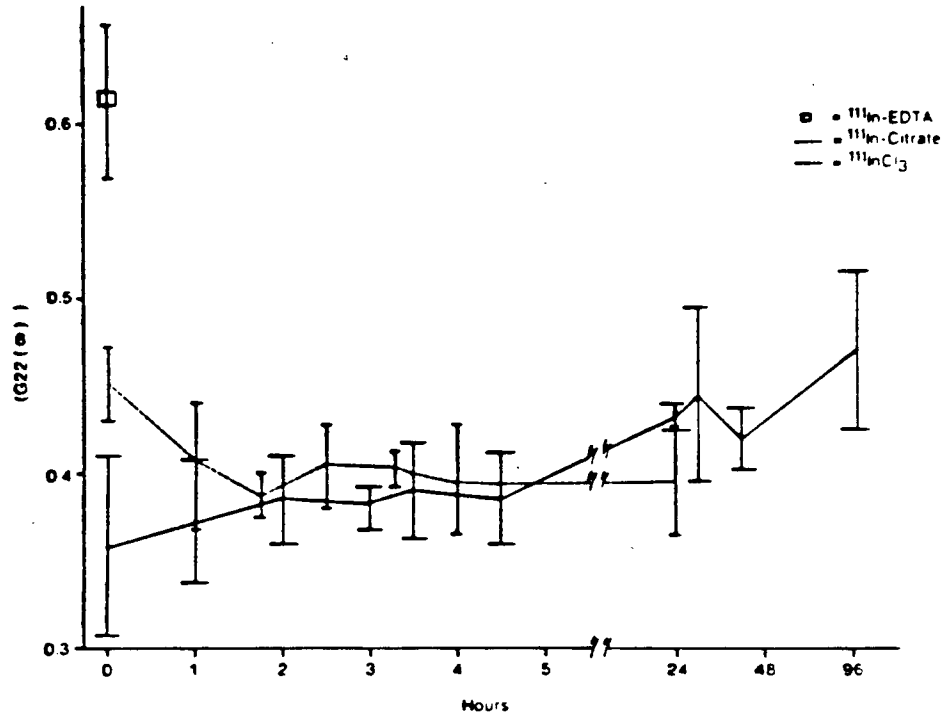

Figure 7.2. In vivo angular correlations of gamma-rays following intravenous injection of three labelled indium compounds into mice. Initial low values for citrate and chloride indicate protein-binding. In-EDTA is not protein bound.
From Goodwin et al., (ref. 145).

fairly rigid helical conformation is expected to give a coincidence spectrum with a single minimum. However, upon transition to a random coil effected by pH change, the increase in flexibility of the chain is reflected by an exponential decay curve characteristic of free molecules in solution. This is illustrated in Figure 7.3 in which Martin et al., (148) studied the helix-random coil transition in glutamic acid by P.A.C. Since P.A.C. is applicable to solids, it means surface layers, powders, composite materials etc., can also be studied.

P.A.C. can also be used to determine the size of a cleft in a macromolecule by attaching an appropriate rotational tracer of known size to the cleft. If a small rotational tracer is incorporated into the cleft, the greater movement of the tracer is reflected by an exponential decay in the time-differential coincidence spectrum. On the other hand, if a single minimum occurs, the rotational tracer is rigidly attached to the molecule and moves with a rotational correlation time that is long compared to the quadrupolar interaction.

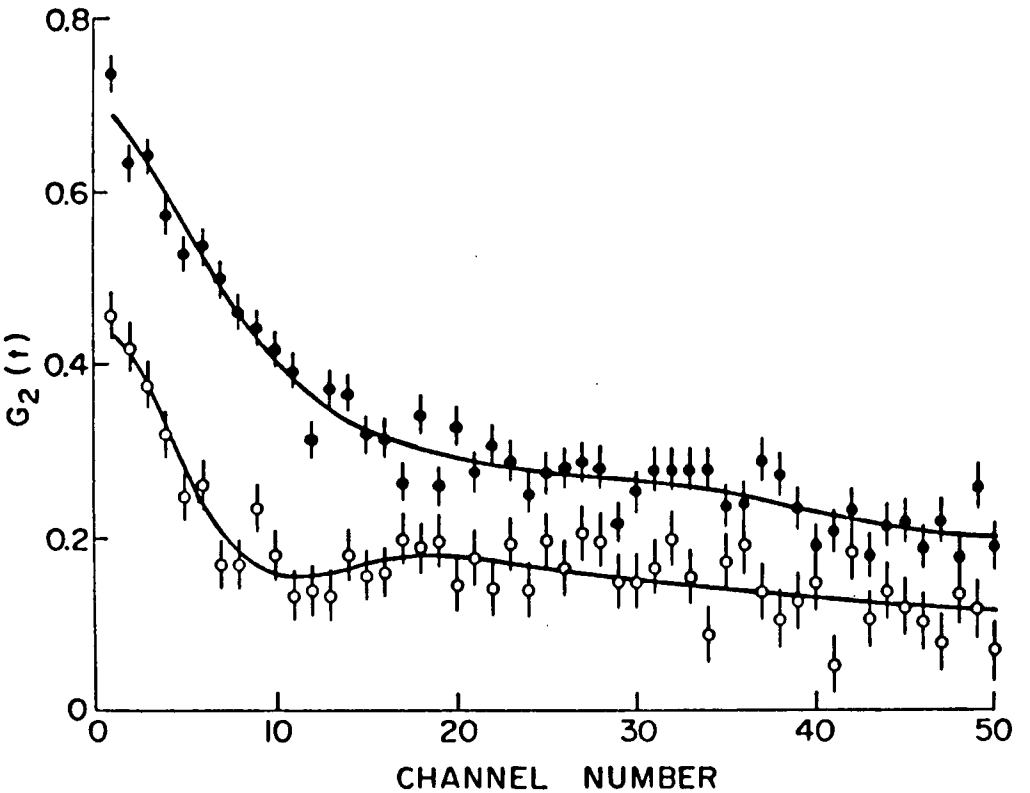

Figure 7.3. Time-differential perturbed angular correlation (TDPAC) spectra for samples of polyglutamic acid at pH=4.0 (upper curve) and pH=7.8 (lower curve). The upper curve corresponds to the tight helix conformation whereas the lower curve is for the random coil configuration.

CHAPTER VIII

EXPERIMENTAL WORK

8.1 Preparation of Meso-protoporphyrin IX

Meso-protoporphyrin IX (MPP IX) was chosen for the present study. This porphyrin is more stable than protoporphyrin IX because the vinyl groups of the protoporphyrin IX are chemically and photochemically labile. As an example, when a solution of protoporphyrin IX in benzene or pyridine is exposed to light, an oxidation product known as photo-protophyrin IX is formed (149). However, hydrogenation of the vinyl groups is accompanied by an undesirable reduction in aqueous solubility of the resulting meso-protoporphyrin IX.

Materials:

Ferri-protoporphyrin IX was obtained from Strem Chemicals, Inc.; palladium oxide (PdO. x H_2O) was from MCB; formic acid (90%) was obtained from Fisher; ammonia from Allied Chemical Canada, Ltd.; ammonium acetate from MCB; sodium tartrate AR was obtained from Mallinckrodt.

Procedure:

The procedure for the preparation of meso-protoporphyrin IX from ferri-protoporphyrin IX was essentially that of Taylor (150). The method involved the simultaneous reduction of the vinyl sidechains to ethyl groups and removal of iron through the action of formic acid. The palladium oxide was used as the reducing catalyst. Ferro-proto-porphyrin IX was initially formed by the reduction of Fe(III) to Fe(II). Since Fe(II) has a larger ionic radius, 0.74Å compared with that of Fe(III), 0.64Å, Fe(II) was more readily dissociated from the porphyrin

macrocycle, thus protoporphyrin IX was obtained. The final product meso-protoporphyrin IX was obtained by catalytic hydrogenation of the vinyl groups of protoporphyrin IX.

Ferri-protoporphyrin IX (2.0g) was suspended in formic acid (90%; 165 ml) containing palladium oxide (460 mg) in a 250 ml round-bottom flask fitted with a reflux condenser. The whole arrangement was protected from light by aluminium foil. The mixture was refluxed for 1½ hr, and the progress of the reaction was followed spectroscopically. This was achieved by withdrawing an aliquot of the reaction mixture, and then diluting with formic acid. The visible absorption spectrum was then compared with that of protoporphyrin IX (Figures 8.1 and 8.2). Completion of the reaction was determined by the disappearance of the protophyrin IX spectrum. The palladium oxide was filtered off using a sintered glass funnel of fine porosity, and was washed with formic acid The filtrate was then poured into 30% ammonium acetate solution (600 ml) with efficient stirring. After being allowed to stand for 45 min, the precipitate was collected by centrifugation and washed repeatedly with deionised water. The precipitate was taken up in 2% aqueous ammonia solution (140 ml) to give a brownish-red solution. The sodium salt of meso-protoporphyrin IX was "salted out" with 30% sodium tartrate solution (24 ml). The precipitate was collected by centrifugation, and if the supernatant remained brownish-red, the above procedure was repeated.

The sodium salt was converted into meso-protoporphyrin IX hydrochloride by the addition of boiling 25% hydrochloric acid (120 ml) to the precipitate in the centrifuge tubes. The solid dissolved instantly and crystals of the hydrochloride formed almost immediately. The

crystalline meso-protoporphyrin IX hydrochloride was collected by filtration, washed with a little 2.5% hydrochloric acid solution, and dried in air. Further drying was achieved in a desiccator containing pellets of sodium hydroxide.

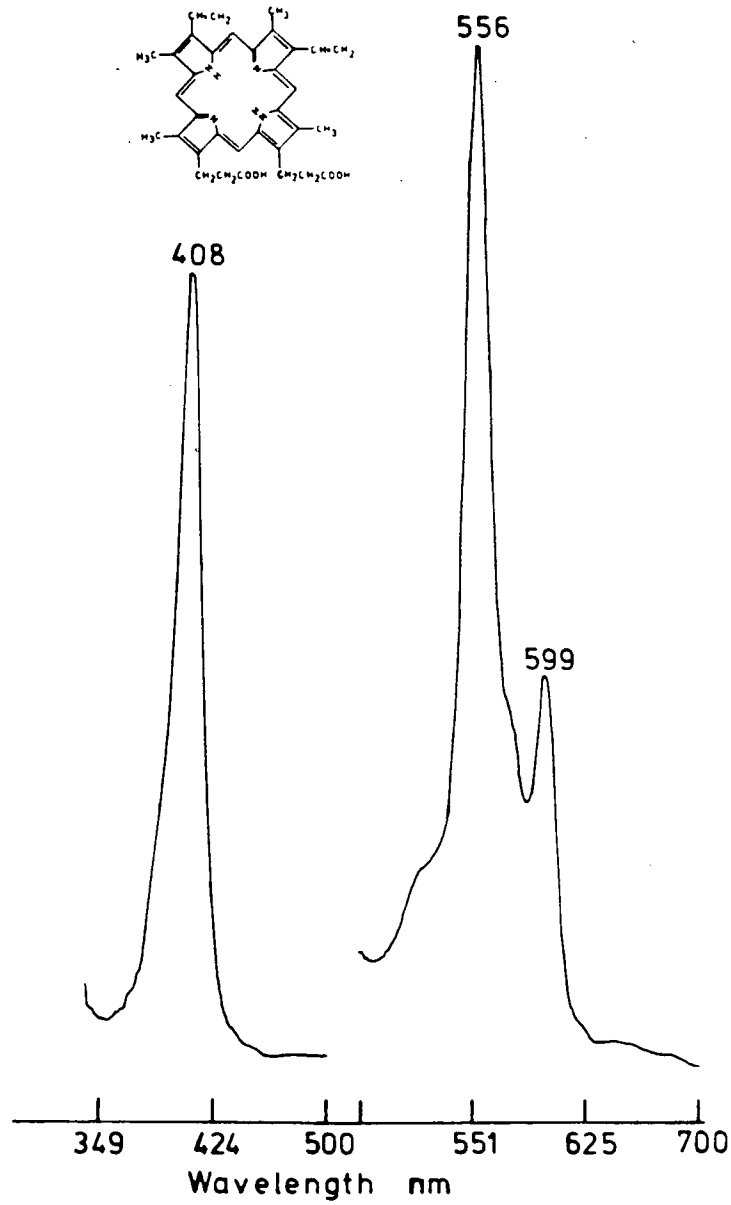

Figure 8.1. Visible absorption spectrum of protoporphyrin IX in formic acid.

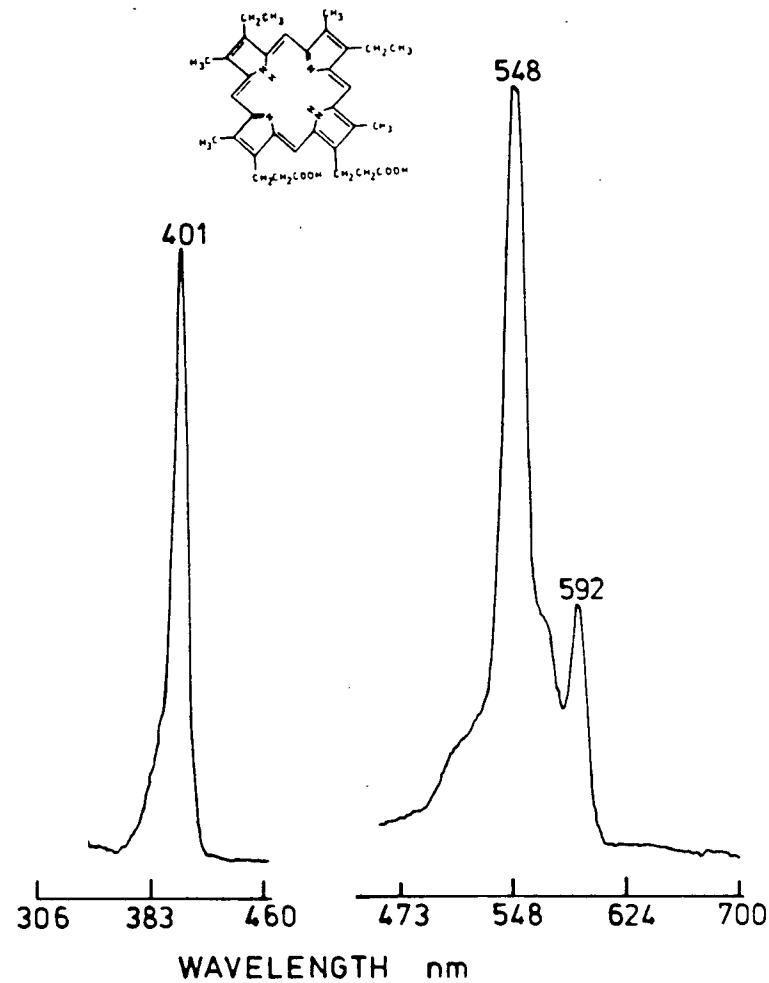

Figure 8.2. Visible absorption spectrum of meso-protoporphyrin IX in formic acid.

8.2 Preparation of Non-Radioactive Indium-Mesoprotoporphyrin IX

Materials:

Indium chloride, $InCl_3$ (anhydrous, ultra-pure) was obtained from Alfa; reagent glacial acetic acid from Allied Chemical Canada, Ltd.; silica gel (70-140 mesh) for column chromatography was obtained from Macherey, Nagel & Co., Germany; and meso-protoporphyrin IX was prepared in the laboratory according to the procedure in Section 8.1.

Procedure:

In a 250 ml one-necked round-bottom flask fitted with a reflux condenser, indium chloride (0.148g) and meso-protoporphyrin IX (0.200g) were heated to boiling in glacial acetic acid (160 ml) containing sodium acetate (0.717g). The reaction was protected from light by aluminium foil. Refluxing was continued for 4½ hr. Completion of the metallation process was determined spectroscopically by the disappearance of the visible spectrum of meso-protoporphyrin IX. The solution was concentrated on a rotary evaporator to a minimal volume. Addition of water to the warm, concentrated solution produced a copious precipitate of bright-red indium-mesoprotoporphyrin IX (InMPP IX). The solid was collected, washed with water and dried over pellets of sodium hydroxide *in vacuo*.

8.2a Thin-layer chromatography

Analytical thin-layer chromatography (tlc) was used to check the purity of InMPP IX. Eastman chromatogram sheets of silica gel with fluorescent indicator were used. After an extensive search, the best solvent system for the development of the chromatograms was a mixture of toluene/methanol (2:1). No spraying agent was required to see the spots since components of interest were intensely colored. Figure 8.3 shows the tlc results with various solvent systems.

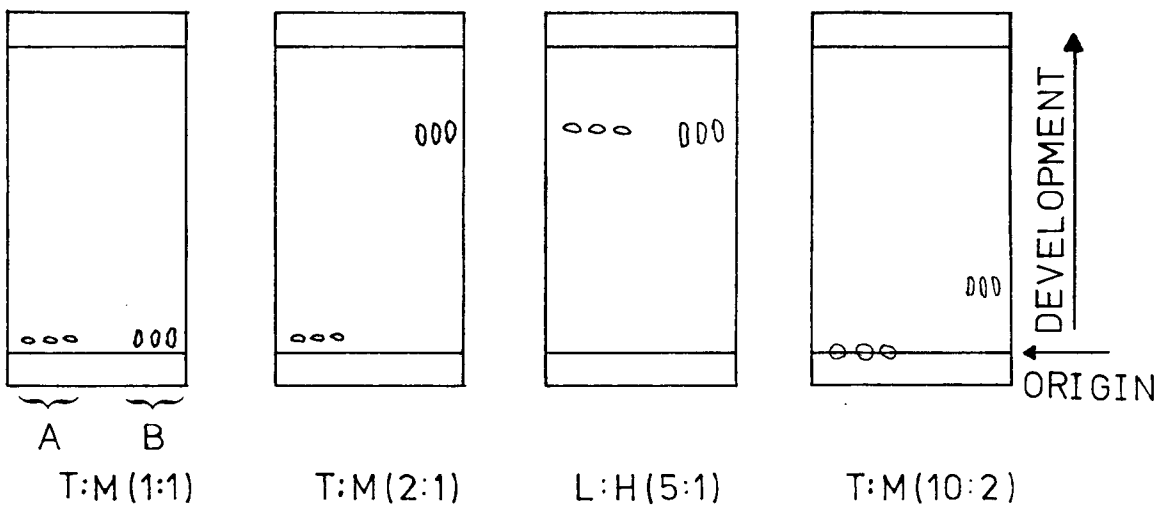

Figure 8.3. TLC of (A) meso-tetraphenylporphine IX and (B) indium meso-tetraphenylporphyrin IX
Abbreviations: solvents: T, toluene; M, methanol; H, water; L, 2,6-Lutidine.

8.2b Purification of Indium-Mesoprotoporphyrin IX

From the tlc results (Section 8.2a), the crude InMPP IX complex (100 mg) was dissolved in minimal methanol and chromatographed on a 62 cm x 1.6 cm column of silica gel packed in toluene. The column was eluted with toluene/methanol (2:1). InMPP IX was eluted first followed by unreacted MPPIX. All fractions were checked spectroscopically and by tlc. The solvent was removed in vacuo to recover the bright-red InMPPIX.

8.2c Visible Absorption Spectroscopy

The visible absorption spectra of indium-mesoprotoporphyrin IX in formic acid and benzene were recorded on a Cary Model 14 spectrophotometer. On formation of InMPP, the intensity of the α-band increased significantly to almost that of the β-band (see Figures 8.4 and 8.5). The two bands were hypochromically shifted, the α-band has λ_{max} at 573 nm and the β-band at 560 nm.

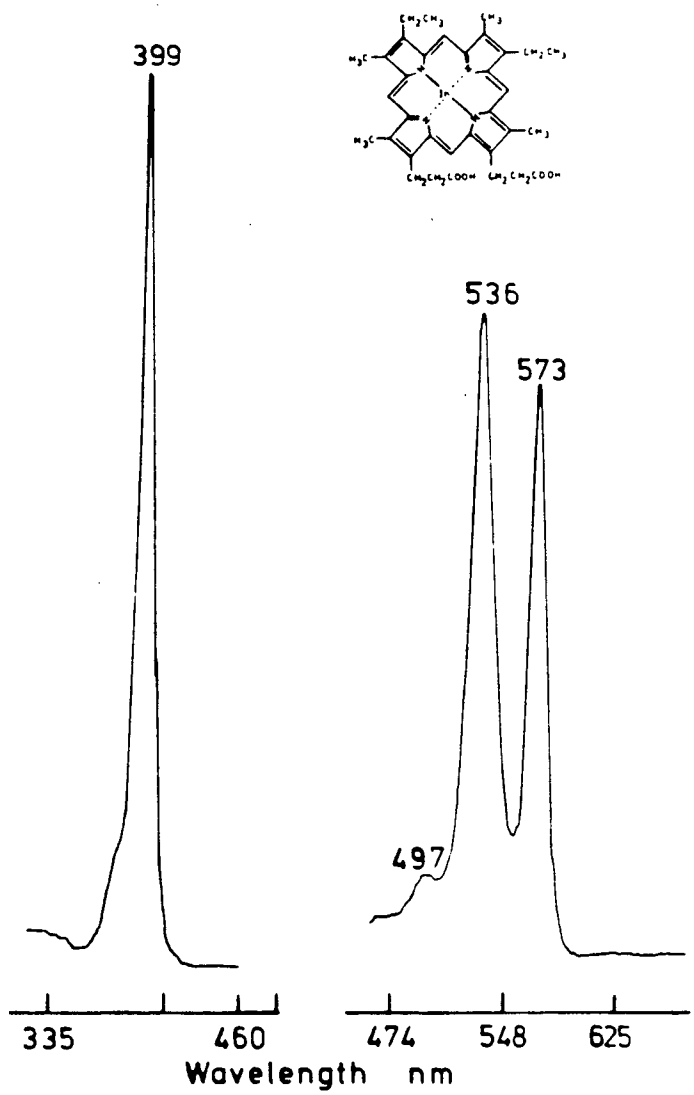

Figure 8.4. Visible absorption spectrum of indium meso-protoporphyrin IX in formic acid.

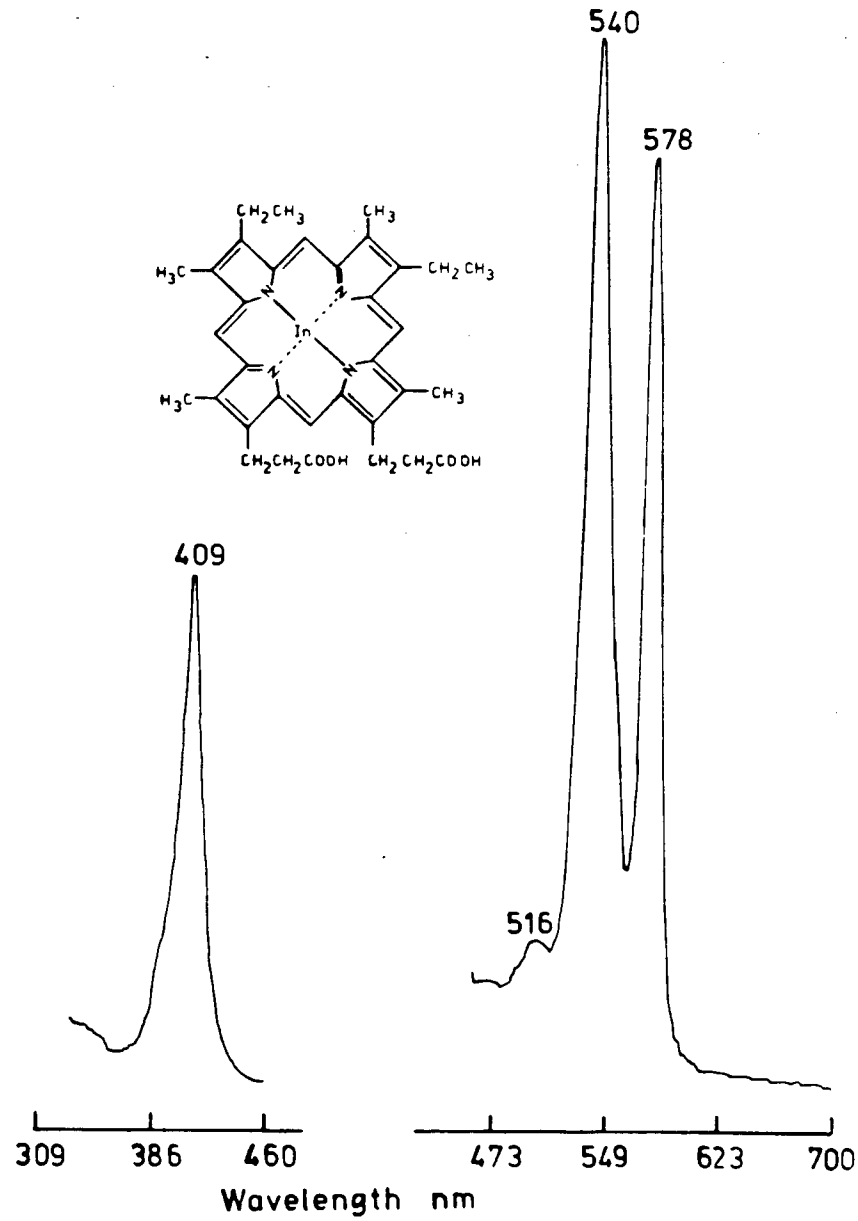

Figure 8.5. Visible absorption spectrum of indium meso-protoporphyrin IX in benzene.

8.3 Preparation of Radioactive Indium-111 Meso-protoporphyrin IX

The normal method of preparing indium-MPP is one of refluxing large excess of indium and the porphyrin as discussed in Section 8.2. This method is not applicable to the synthesis of radioactive indium-111 MPPIX since the molar ratio of radioactive indium-111 to MPPIX is extremely low. Therefore a slightly different method was developed. The search for the optimum reaction conditions was carried out with "cold" indium in view of the fact that indium-111 emits gamma rays. Several factors were considered: refluxing time, amount of "cold" indium present was critical since both "hot" and "cold" indium would compete for the porphyrin, and the amount of MPP. The method described here was obtained after an extensive search following sometimes disappointing results of low radioactivity of the reconstituted myoglobin with ^{111}InMPPIX. A high radioactivity of ^{111}InMPPIX was essential to the success of the subsequent gamma-gamma experiments on the reconstituted myoglobin.

All the experiments were carried out within an improvized lead (3 mm thick) enclosure of 50 cm x 50 cm x 40 cm in a fume-hood. This placed a severe limitation on the visibility and chemical manipulations. Since the half-life of indium-111 is short ($t_{\frac{1}{2}}$=2.8 days), all glasswares and radioactive contaminated solutions and articles were stored in the lead enclosure until the radioactivity was no longer detectable before disposal. A Picker Model 642081 Labmonitor was used for determining radiation levels, estimating sample activity, and checking contamination.

Materials:

In-111 was obtained commercially as carrier-free $^{111}InCl_3$ in

aqueous solution containing 0.45% to 0.9% sodium chloride from Medi-Physics Corp., Emeryville, California.

Procedure:

The method was essentially similar to that described in Section 8.2. In a 25 ml round-bottom flask fitted with a reflux condenser, MPP IX (6 mg), "cold" $InCl_3$ (2.3 mg), sodium acetate (9.1 mg) in glacial acetic acid (6 ml) was stirred vigorously. $^{111}InCl_3$ solution (1.1 ml; 2.2 mCi) was injected into the reaction mixture which was refluxed for 6-7 hr. The solution was then concentrated to a minimal volume by evaporation. Addition of cold deionized water to the warm, concentrated solution produced a bright-red precipitate which was washed repeatedly with cold water and air-dried. No attempt was made to purify the product. The radioactivity of the product was checked with the Labmonitor. The ^{111}InMPPIX was then immediately used for the reconstitution experiments (See Section 8.5).

8.4 Preparation of Apomyoglobin Solution

Materials:

Myoglobin from spermwhale skeletal muscle type II (salt-free lyophillised powder) was obtained from Sigma. 2-Butanone (methyl ethyl ketone) was obtained from Fisher.

Procedure:

The procedure was similar to that reported by Breslow (151). A 500 mg sample of myoglobin was dissolved in 60 ml deionized water (∿1% solution) at 0°C, and the pH carefully adjusted to 1.5 with IN HCℓ. The removal of the heme from myoglobin was insured if the pH of the initial met-Hb solution was near 1.5 which is a critical value for the cleavage of the protein-heme link. The solution was then extracted at 4°C first with an equal volume of 2-butanone, then twice more with a half-volume of 2-butanone to remove the heme. The last extraction was generally found to be superfluous. The resulting, slightly straw-colored solution was then immediately dialyzed at 4°C against 4 changes of sodium bicarbonate solution (50 mg/1 litre), and then against several changes of deionized water. The apomyoglobin solution was further dialyzed against 2 changes of 1×10^{-4} M disodium EDTA solution, and against several changes of deionized water. The apomyoglobin solution was centrifuged to remove denatured protein which had precipitated, and was concentrated to ∿10 ml by ultra-filtration using an Amicron arrangement fitted with a UM-2 membrane (>1000 M.W.). Finally, the concentrated protein solution was dialyzed against 4 changes of 250 ml sodium borate buffer (pH 9.2; ionic strength 0.16). The concentration of apomyoglobin was determined based upon its absorbance at 280 nm (ε = 15,500). The

apomyoglobin solution was immediately used for reconstitution with ^{111}InMPPIX (See Section 8.5).

8.5 Reconstitution of Apomyoglobin with Indium-111 Meso-protoporphyrin IX

All the reconstitution experiments were carried out within the lead enclosure in a fume-hood as discussed in Section 8.3. As mentioned in Section 8.3, the limited visibility (due to the lead enclosure) had been a severe handicap, hence a lead glass shielf (32 cm x 24 cm) was used during column chromatography.

Materials:

Sephadex G-25 was obtained from Pharmacia Fine Chemicals, Sweden; carboxy methyl cellulose, CM-52 (microgranular, preswollen), a cation exchanger for column chromatography was obtained from Whatman, England. ^{111}InMPPIX was obtained from the method discussed in Section 8.3. Apomyoglobin was prepared as described in Section 8.4.

Procedure:

The procedure of reconstitution was that of Srivastava (152). ^{111}InMPPIX was dissolved in a minimal volume of 0.1N NaOH and immediately diluted ten-fold with borate buffer (pH=9.2; ionic strength = 0.16). The ^{111}InMPPIX solution was immediately added to 4 ml of apomyoglobin solution [1.6×10^{-4} M/ℓ] at 0°C with stirring. The resulting solution was then stored at 0°C in a Dewar flask for about 8 hr. Normal refrigeration was impractical in view of the high gamma emissions. The solution was then chromatographed over Sephadex G-25 (48 cm x 1 cm column) which had been equilibrated with 0.005M phosphate buffer, pH6.3 and eluted with the same buffer. This step removed excess unreacted ^{111}InMPPIX. A reddish band corresponding to the reconstituted myoglobin was eluted within the void volume of the column followed by the unreacted ^{111}InMPPIX. To remove ^{111}InMPPIX that were bound to non-active sites on the proteins,

the eluted protein was absorbed on a CM-52 cellulose cation exchange column (8 cm x 2 cm) equilibrated with 0.005M phosphate, pH 6.3 (below the isoelectric point, since the pI value of myoglobin is 7.0). The CM-column was constructed from a 30 cc plastic disposable syringe as shown in Figure 8.6. The protein absorbed strongly on the cellulose while the ^{111}InMPPIX passed straight through. Elution was continued until no ^{111}InMPPIX (reddish color) was collected. The eluent was finally changed to 0.05M phosphate, pH7.0, the protein (a deep red band) immediately moved down the column and was collected. The radioactivity of the reconstituted sample was estimated with the Picker Labmonitor.

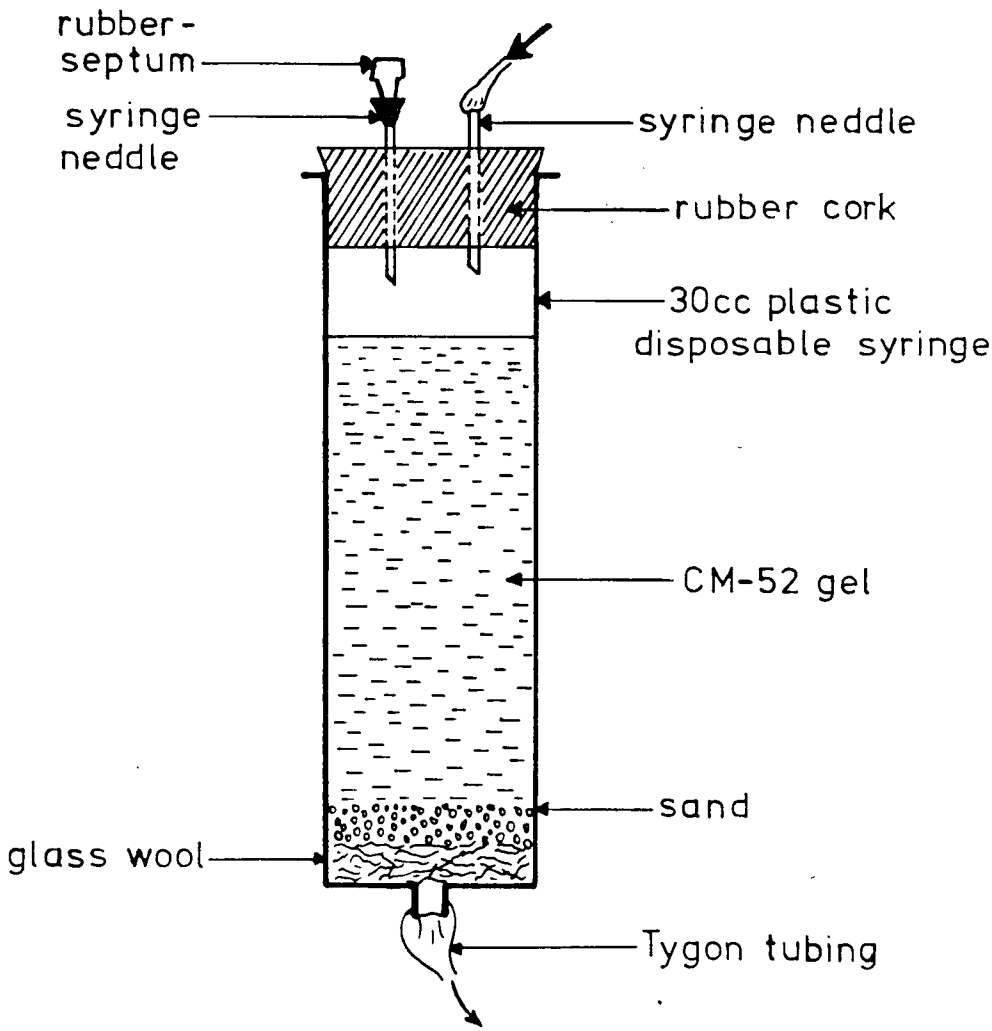

Figure 8.6. A schematic drawing of a CM-52 column constructed from a 30cc plastic disposable syringe.

8.6 Perturbed Angular Correlation Measurements

The experimental technique is concerned with the measurement of the angular distribution of the second gamma emission with respect to the direction of the first gamma emission. This requires detectors and electronic equipment which will be described briefly below.

8.6a Detectors

Scintillation detectors instead of Geiger counters were used because of their high efficiency and good energy resolution. They also provide faster pulses with much less uncertainty in time than Geiger counters which is essential in measurements requiring coincidence detection.

Thallium-activated sodium iodide detectors were used for the detection of gamma emissions. The high Z of the iodine provides a large photoelectric cross-section which allows one to choose the gamma-ray desired by pulse-height selection. The relatively long phosphor decay time of 0.25 μsec may appear to be too long for fast coincidence work; however, by operating a fast coincidence circuit on the initial part of the pulse, resolving times of one-tenth to one-hundred of the decay time could be achieved for gamma rays of 100 keV or more.

Photomultiplier tubes were used to detect pulses from the detectors, and at the same time to provide an amplification factor up to 10^8. The amplified electrical pulses were sufficiently large to operate the electronic detection system. The photomultipliers were protected from high magnetic field with magnetic shielding.

8.6b Electronics

A simplified schematic diagram of the fast-slow coincidence circuit is shown in Figure 8.7. Radiations falling within the solid angles of the detectors were counted. However, the coincidence analyzer was used to select principally only pairs of radiations γ_1 and γ_2 which are genetically related to each other (i.e. emitted in the same nuclear decay). The electrical pulses from the detectors were chanelled into two lines, "fast" and "slow" (slow was in the order of 10^{-6}sec, fast was 10^{-7} to 10^{-9}sec pulse width). A fast coincidence circuit was essential to discriminate against chance coincidences at high counting rates. Pulses on the fast lines were applied to the fast coincidence circuit.

The pulses were at the same time applied in sequence to slow linear amplifiers and to pulse-height analyzers for energy selection. The pulse height was proportional to the energy of the incident photon.

The outputs of the analyzers together with the output of the fast coincidence circuit were then applied to a slow multiple coincidence circuit that selects the event. The output pulse was then passed to a multi-channel analyzer for data storage.

In the present study, the angular distribution was studied as a function of the time between the formation of the oriented state and its decay, that is the time between the arrival of the two gamma rays. This was achieved by introducing an electronic delay in the line of the first detector.

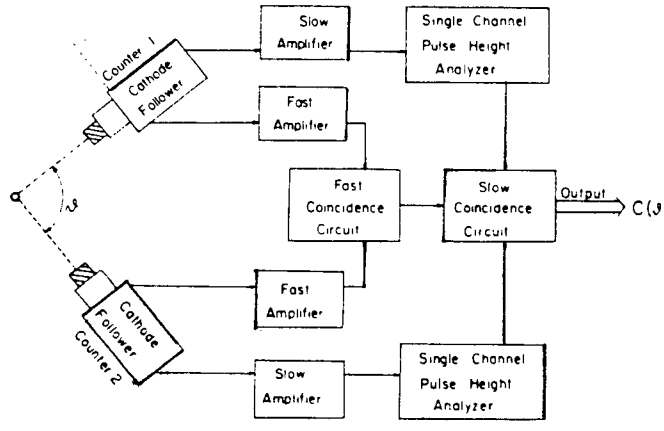

Figure 8.7. A schematic diagram for a fast-slow coincidence arrangement for P.A.C. measurements.
From Frauenfelder and Steffen (ref. 130).

8.6c Method

A three-detector fast-slow gamma ray coincidence spectrometer was used. The detectors were arranged at cardinal points around the radioactive sample. The P.A.C. measurements at 180° and 90° were performed simultaneously using three 2" x 2" dia. NaI(Tℓ) detectors. A simplified diagram of the fast-slow coincidence circuit used for the present measurements is shown in Figure 8.8, indicating how the angular correlations $W(\pi,t)$ and $W(\pi/2,t)$ are routed to separate halves of the multichannel analyzer memory. The γ-ray energies were selected in the slow side of the circuit by a timing single channel analyzer (TSCA). The time-to-amplitude converter (TAC) measured the time interval between the arrival of the start (173 keV) and stop (247 keV) pulses, while the slow coincidence logic determined between which pair of detectors the event originated. The events were then routed to separate halves of the multichannel analyzer memory. The multichannel analyzer would then provide a direct display of emission anistropy against delay time. The prompt time resolution of this system was 1.1 ns for ^{60}Co gamma rays. However, with the energy windows set appropriately for the 173 keV and 247 keV gamma rays in ^{111}Cd, this deteriorated to 2.7 ns. By measuring $W(\pi,t)$ and $W(\pi/2,t)$ simultaneously, no correction for the decay of the source was necessary, and improved counting statistics resulted. The scaler counts in the slow side-channels automatically provide the required normalizations. Gain stabilizers ensured long-term stability in the linear pulses from the amplifiers and anti-coincidence requirements were used to eliminate "cross-talk" in the counting system.

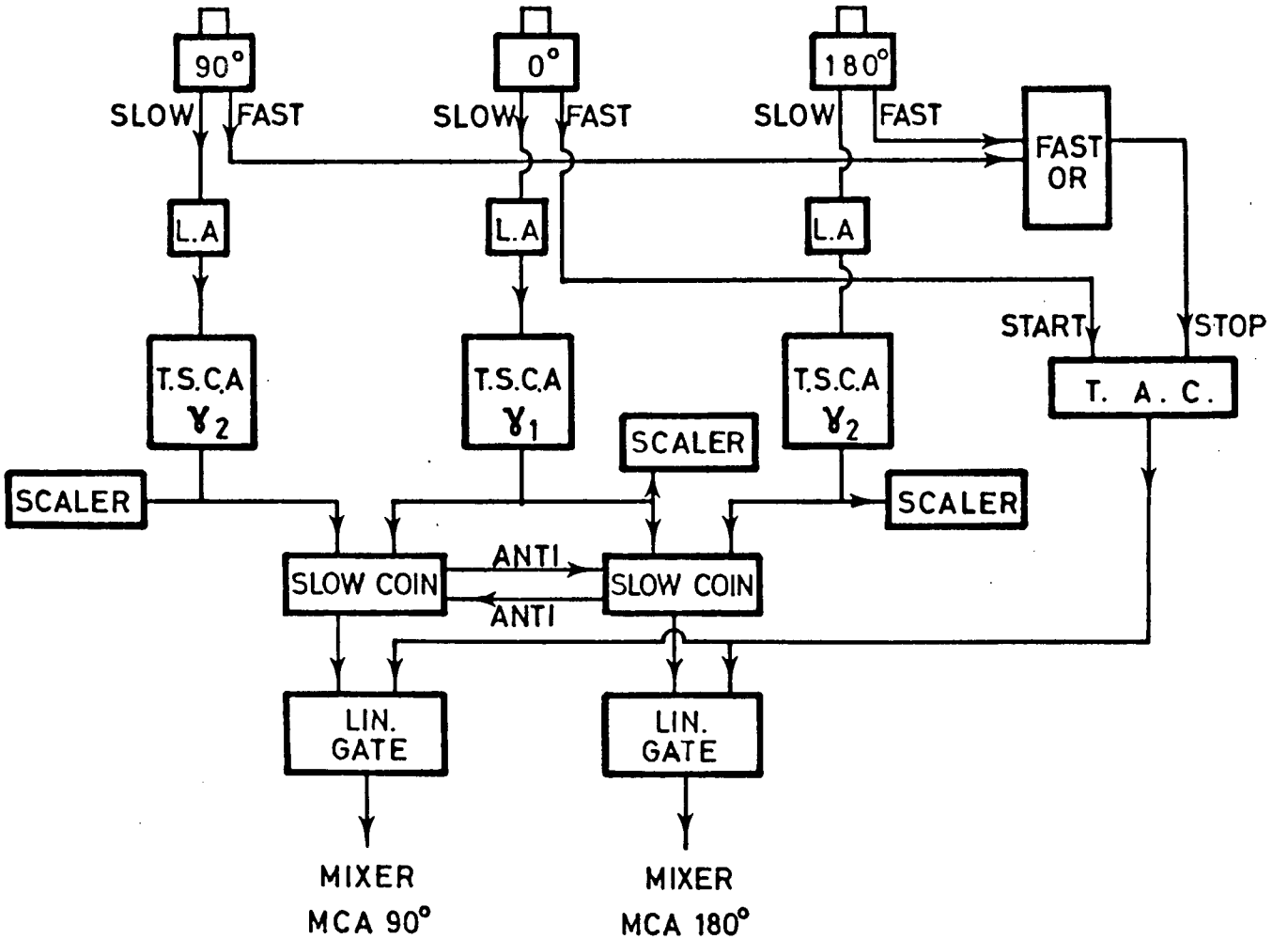

Figure 8.8. A simplified block diagram of the electronics used in the present time-differential perturbed angular correlation experiments.

The samples in solution or solid form were contained in normal glass n.m.r. tubes and kept at 10-15°C by a stream of cold air. The samples were adjusted to give a disintegration rate usually of the order of $4x10^4$ - $6x10^4$ counts per second in order to reduce the chance coincidence contribution to the true coincidence rate.

A typical time-differential perturbed angular correlation measurement takes about 2 days. The data were corrected for solid angle effects and finite time resolution. The differential non-linearity of the time spectrum was measured with random stop and start pulses in the TAC and found to be essentially over 90% of the time range.

Viscosity measurements were performed on the protein samples using a Ostwald viscometer. The change in solution viscosity was effected by adding predetermined amount of glycerine. The solid form of protein was obtained by lyophilization of the protein solution.

CHAPTER IX

RESULTS AND DISCUSSION

9.1 RESULTS-Time-Differential Perturbed Angular Correlations Data

The reconstituted ^{111}InMPP-Mb was studied in 0.05M sodium phosphate buffer, pH 7.0, and in lyophilized powder form at 12°C. The viscosity of the aqueous sample was changed by adding glycerine. In the samples for the time-differential perturbed angular correlation (TDPAC) experiments, no attempt was made to ensure complete incorporation of ^{111}InMPP IX into apomyoglobin. The excess apomyoglobin should pose no difficulty since only those myoglobin molecules containing ^{111}InMPP IX will contribute to the TDPAC signal.

The TDPAC spectra for ^{111}InMPP-Mb in aqueous buffer with and without glycerin, and in lyophilised powder form are shown in Figures 9.1-9.3. Results for the free ^{111}InMPP IX in dimethylformamide (DMF) and ^{111}InTPP:Cl in chloroform ($CHCl_3$) are illustrated in Figures 9.4-9.5. The solid curves are least-square fits to the experimental data.

The perturbation factors $G_{22}(t)$ were determined from the measured $W(\pi,t)$ and $W(\pi/2,t)$

$$G_{22}(t) = \frac{2}{A_2} \frac{W(\pi,t)-W(\pi/2,t)}{W(\pi,t)+2W(\pi/2,t)} \qquad (6.5)$$

where $A_2 = -0.18$. The data were corrected for solid angle effects with

$$A_{COR} = A_2 Q_2(\gamma_1) Q_2(\gamma_2) \qquad (9.1)$$

where Q_2 are the solid angle correction factors.

For the aqueous samples, a theoretical fit to the measured perturbation factors was made using the following function

$$G_{22}(t) = (1-A) + A\exp(^{-t}/\tau_c)G_2(t) \tag{9.2}$$

where $G_2(t)$ is the static result of polycrystalline powder. For a non-axially symmetric electric gradient, represented by the asymmetry, η and a finite spread, δ in the quadrupole interaction, $G_2(t)$ is given by

$$G_2(t,\eta,\delta) = \sum_{n=o}^{3} b_n(\eta)\exp(-\tfrac{1}{2}\omega_n{}^2\tau_c{}^2)\exp(-\tfrac{1}{2}\omega_n{}^2\delta^2t^2)\cos(\omega_n t) \tag{9.3}$$

The factor $\exp(-\frac{1}{2}\omega_n\tau_c^2)$ allows for finite time resolution and the quadrupole frequencies ω_n are given as

$$\omega_n(\eta) = f_n(\eta)\omega_o \tag{9.4}$$

The $f_n(\eta)$ values are obtained from the diagonalization of the non-symmetric field Hamiltonia (141). For η=o (axial symmetry) $f_n(\eta)$ take on the integral values 1, 2, and 3. For $\eta \neq o$, the $\omega_n(\eta)$ are no longer harmonics.

The program MINUIT (153) was used to minimize the value of χ^2 in the space of free parameters, τ_c, ω_o, and δ (the relative width parameter).

For the solid sample where there was no motion at all ($\tau_c \to \infty$), the following function was used to fit the TDPAC data

$$G_{22}(t) = G_s(t,\eta,\delta) \tag{9.5}$$

The fitted values obtained for τ_c, η, and δ for each of the case are compiled in Table 9.1

Table 9.1. Parameters derived from analysis of TDPAC spectra for ^{111}InMPP-Mb solid and in aqueous buffer solution.

	A	τ_c(ns)	ω_o(MHz)	η	δ
Lyophilized (solid)protein	1.0	∞	36±4	0.01±0.01	0.37±0.03
Aqueous protein containing 41% glycerine	0.98±0.01	22^{+4}_{-3}	30±3	0.01±0.01	0.36±0.04
Aqueous protein without glycerine	0.96±0.01	16^{+3}_{-2}	25±3	0.00±0.01	0.42±0.04

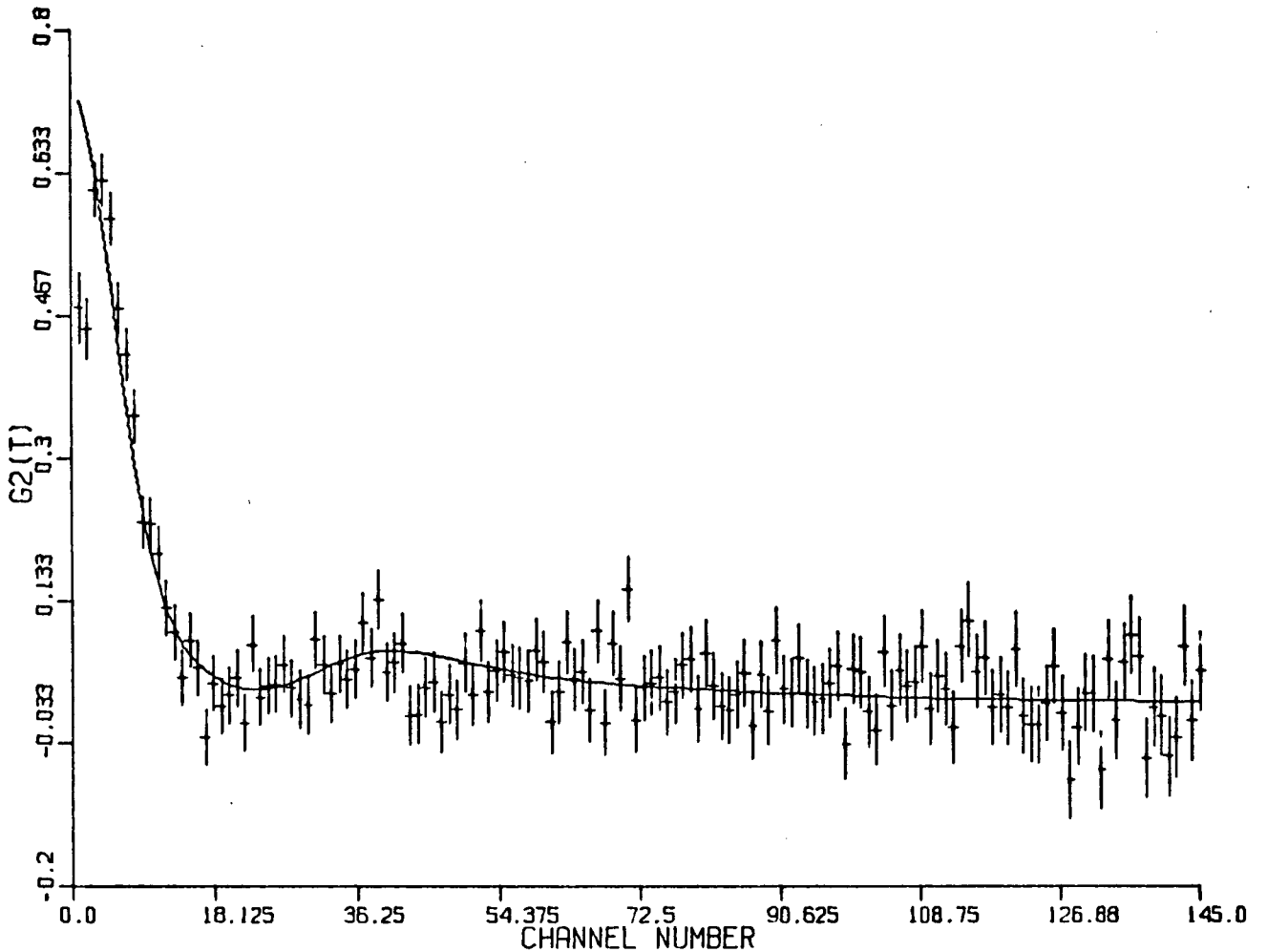

Figure 9.1. Time-differential perturbed angular correlation spectrum for ^{111}InMPP-Mb in aqueous sodium phosphate buffer (pH = 7.0) with glycerine added to give a final glycerine percentage of 41.
0.69ns per channel.

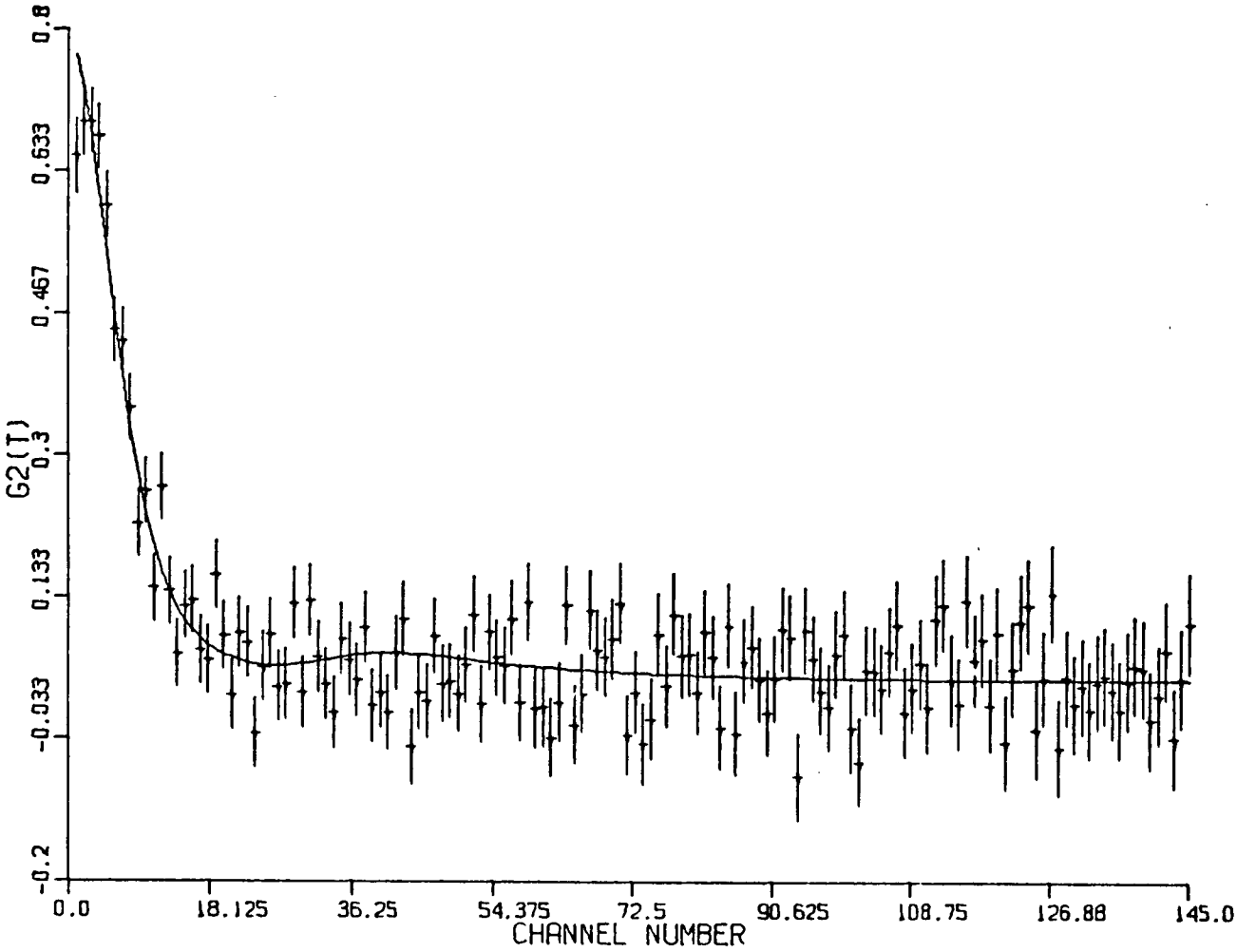

Figure 9.2. Time-differential perturbed angular correlation spectrum for ^{111}InMPP-Mb in aqueous sodium phopshate buffer (pH = 7.0) without glycerine.
0.69ns per channel.

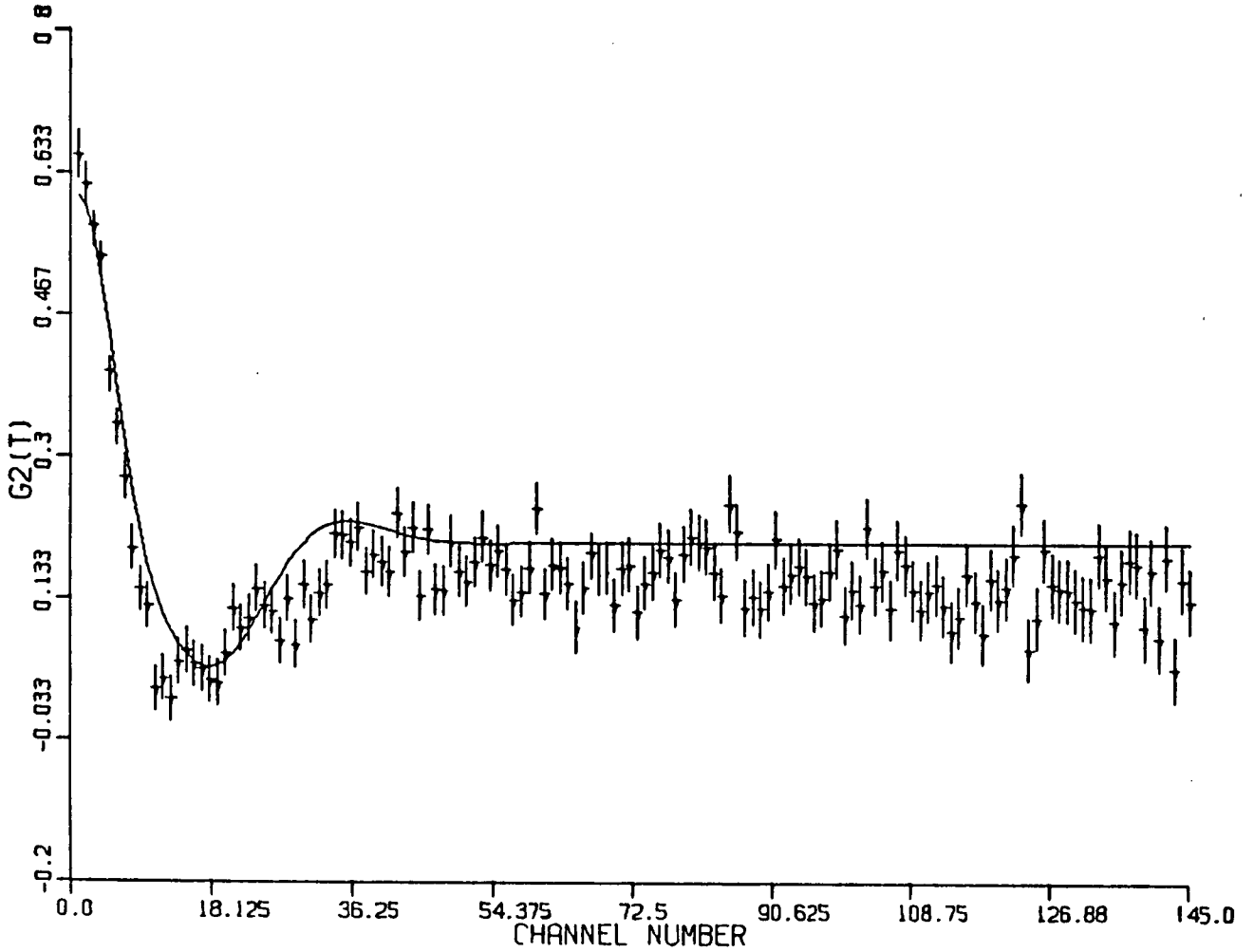

Figure 9.3. Time-differential perturbed angular correlation spectrum for ^{111}InMPP-Mb in the lyophilized powder form. 0.69ns per channel.

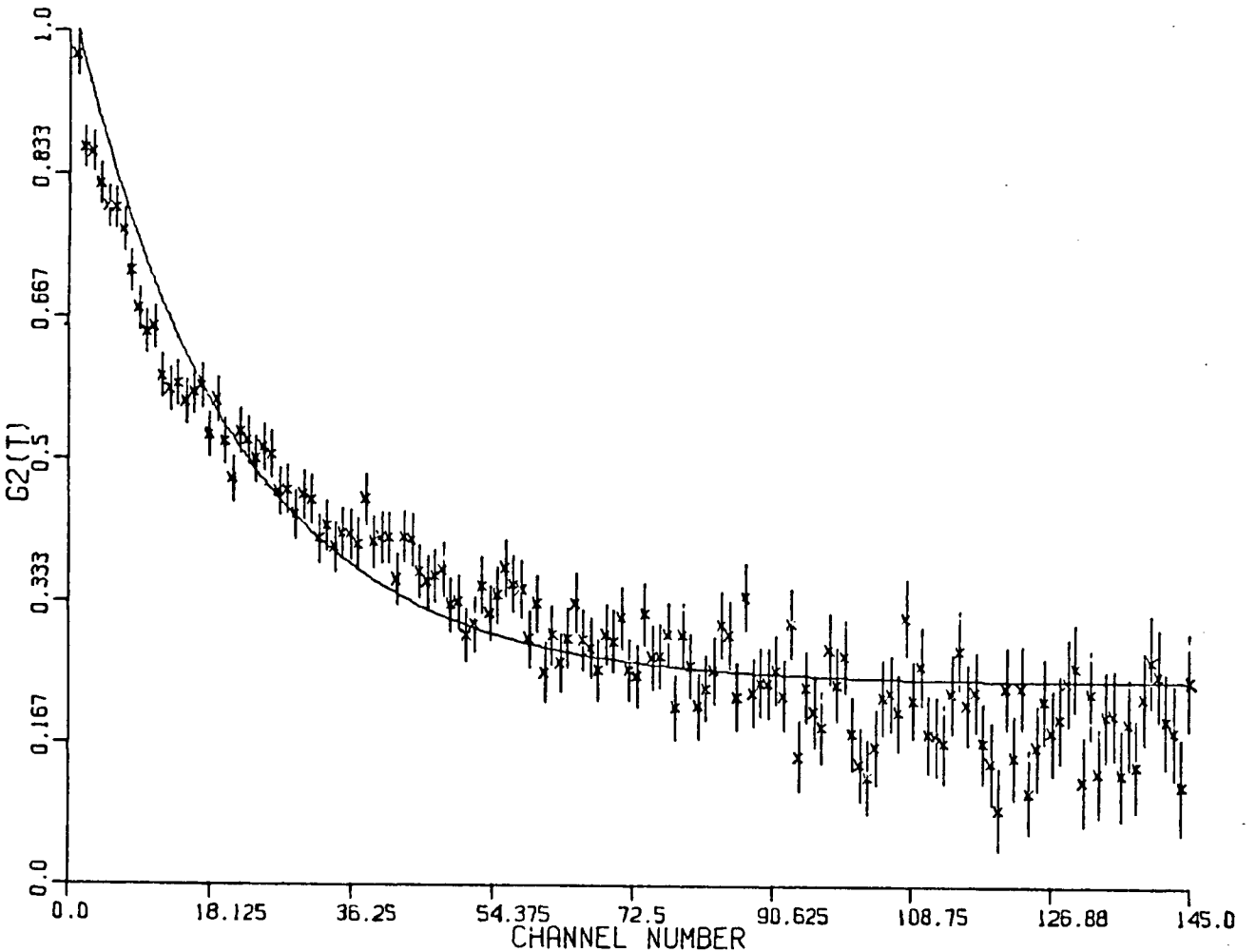

Figure 9.4. Time-differential perturbed angular correlation spectrum for ^{111}InMPP IX in dimethylformamide.

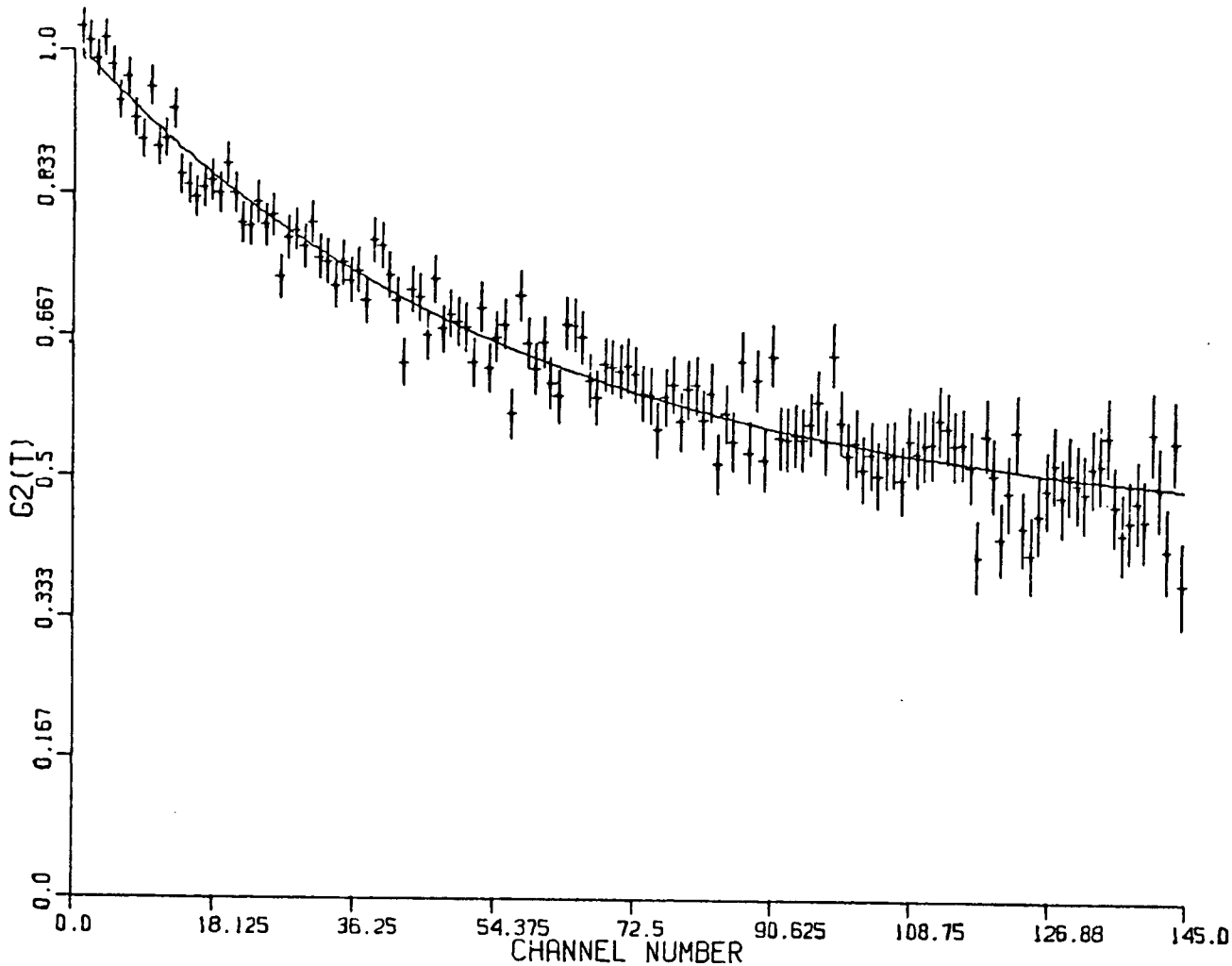

Figure 9.5. Time-differential perturbed angular correlation spectrum for ^{111}InTPP in chloroform.

9.2 DISCUSSION

9.2a Analysis of the Time-Differential Perturbed Angular Correlation Spectra

The qualitative appearance of the lyophilized ^{111}InMPP-Mb TDPAC data (Figure 9.3) confirms that ^{111}InMPP IX is tightly bound to myoglobin and is experiencing a static quadrupolar interaction. The experimental curve does not show the normal characteristic periodic behavior of the differential $G_{22}(t)$ for static interactions as occurring in polycrystalline samples (see Figure 6.6 in Section 6.2b). Instead the lyophilized protein sample shows first a rapid decay and then fluctuates around the low value. This non-periodic observation is probably due to effects arising from the excited electron shell after K-capture during the transition from ^{111}In to the excited ^{111}Cd state (see Appendix C). Lehmann and Miller also observed similar behavior for the two non-metallic sources In_2O_3 and $In(OH)_3$, as discussed in Section 6.2b.

Figure 9.2 gives the TDPAC results for ^{111}InMPP-Mb in aqueous buffer solution without glycerine at 12°C. The angular correlation is strongly perturbed. This indicates that ^{111}InMPP IX is bound and is in a relatively immobile environment (i.e., long rotational correlation time). As a control, TDPAC experiments were performed on free ^{111}InMPP IX (i.e., in the absence of protein) in DMF and ^{111}InTPP:Cl in $CHCl_3$. The results are shown in Figures 9.4 and 9.5. In contrast to the TDPAC results obtained for the ^{111}InMPP-Mb in aqueous buffer, the angular correlation is essentially unperturbed or isotropic for the free ^{111}InMPP IX and ^{111}InTPP:Cl. This observation implies much faster molecular rotation for the latter case which leads to the much slower exponential decay of anisotropy.

The attentuation factors $G_{22}(t)$ observed for the above solution samples can be explained in terms of the influence of molecular rotation in solution on anisotropy. As discussed in Section 6.2a in Chapter VI, Abragam and Pound showed that for small molecules or ions randomly oriented in dilute solutions the differential $G_{22}(t)$ takes the form of a simple exponential decay

$$G_{22}(t) = \exp(-\lambda_2/t) \tag{6.6}$$

where

$$\lambda_2 = \frac{63}{100}\overline{\overline{(e^2qQ)^2}}\tau_c/h^2 \tag{6.7}$$

It is clear from Eq. 6.7 that λ_2 is directly proportional to rotational correlation time, τ_c which is usually small for small molecules; $\tau_c \approx 10^{-11}$sec. Consequently, from Eqs. 6.6 and 6.7, a short τ_c will give rise to a small attentuation of the angular correlations in solution. This explains why the anisotropy of angular correlations remains largely unperturbed for small molecules such as ^{111}InMPP IX and ^{111}InTPP:Cl. However, for large macromolecules like myoglobin (MW = 17,000), τ_c as expected is large, which accounts for the low $G_{22}(t)$ value and the strongly perturbed angular correlation for the aqueous protein sample.

The form of $G_{22}(t)$ for the aqueous protein sample without glycerine is similar to that obtained in the lyophilized protein sample. This suggests a quasistatic interaction in which $G_{22}(t)$ is itself time-dependent. The theoretical fit to the data shows that $G_{22}(t)$ falls to a characteristic minimum followed by a secondary maximum. The latter is smeared out, presumably by inhomogeneities in the V_{zz} (component of

the electric field gradient in the z-direction) or from the after-effects of electron capture, which wipe out the angular correlations. A slightly more significant attentuation is observed in the solid case than in aqueous sample. However, the close relationship between the solid and aqueous protein samples is consistent with the idea that ^{111}InMPP IX is incorporated into the active-site on the apomyoglobin.

As discussed in Section 6.2a, the 3-dimensional molecular rotational correlation time is given by the equation below

$$\tau_c = \frac{4\ R^3}{3KT}\ \xi \qquad (6.10)$$

It can be seen from Eq. 6.10 that the direct relationship between τ_c and viscosity (ξ) suggests that changing the viscosity of the medium would cause a corresponding change in anisotropy of the angular correlations. In the aqueous protein sample containing 41% glycerine, the increase in solution viscosity leads to a longer rotational correlation time for the protein. This slower molecular motion (long τ_c) causes a rapid decrease in the anisotropy (Figure 9.1), in accordance with Eqs. 6.6 and 6.7. The more pronounced $G_{22}(t)$ minimum suggests a closer similarity between the lyophilized protein and the aqueous protein sample containing 41% glycerine than the one with no glycerine.

9.2b Lease-Squares Analyses of the Time-Differential Perturbed Angular Correlation Data

The least-squares analyses of the TDPAC data using various functions for the time-differential $G_{22}(t)$ include (a) a pure static interaction which corresponds to Eq. 9.5, and (b) a single static interaction combined

with rotational diffusion (i.e., multiplicative combination of a static and time-dependent interactions) as expressed by Eq. 9.2. It can be seen from Figures 9.1-9.3 that the theoretical fits are adequate for the early TDPAC data (<40 nsec) but are rather poor for later times (>40 nsec). Therefore, for both aqueous and solid measurements, the early TDPAC data should be more reliable and meaningful. In addition early TDPAC data has a greater statistical accuracy and intrinsically contains more significant information concerning quadrupolar interactions, whereas the later data is more prone to experimental errors.

The solid curve in Figure 9.3 represents the theoretical fit calculated using Eq. 9.5 for the lyophilized protein TDPAC data. The curve is characteristic of a single static quadrupolar interaction. Agreement with the early experimental data is good. However, the required value of δ (distribution in quadrupole frequency) in the fit was sufficiently large to wipe out all the fine structures at later times as reflected by the poor agreement with the later TDPAC data. The fitted asymmetry parameter, $\eta=0.01\pm0.01$ is consistent with the expectation that the electric field gradient around ^{111}InMPP IX should be axially symmetric in the square-pyramidal ^{111}InMPP IX complex.

The TDPAC data for both the aqueous samples (with and without glycerine) were interpreted on the basis of a combination of a static and a time-dependent interaction mechanism. The solid curves in Figures 9.1 and 9.2 represent the theoretical curves calculated using Eq. 9.2 for the two aqueous samples. The good agreement with the early TDPAC data, together with the fact that the fitted $\eta=o$, show that the ^{111}InMPP IX is indeed experiencing a static interaction due to its

surrounding electrons, as well as a time-dependent interaction arising from the rotational diffusion of the protein molecule. The situations for both the aqueous samples are similar to the results derived by Marshall and Meares (13) for slow molecular motion (see Section 6.2c). As in the case of the lyophilized protein, the fits are damped out to give an essentially flat lines at later times (>40 nsec), again due to the large required values of δ. The curves, however, are able to reproduce the early TDPAC data (<40 nsec) accurately.

The results of the least-squares analyses compiled in Table 9.1 show that the value of ω_o(30±3 MHz) for the aqueous protein containing 41% glycerine is comparable to that of the lyophilized protein (ω_o=36±4 MHz). This close relationship between these two ω_o values together with the fact that the fitted asymmetry parameter, η, is zero, confirms the correctness of the TDPAC data reduction.

9.2c Comments on the Rotational Correlation Times of myoglobin determined by the Perturbed Angular Correlation Technique

As mentioned earlier, the 3-dimensional rotational correlation time (τ_c) of a spherical molecule in a liquid medium can be obtained from the following equation

$$\tau_c = \frac{4\pi R^3}{3KT} \xi \qquad (6.10)$$

Equation 6.10 can then be used in two different ways to compute τ_c.

The first method requires the value of the Stokes (or hydrodynamic) radius (R), given by the formula below.

$$R = \frac{KT}{6\pi\eta D_{rot}} \tag{9.6}$$

where K = Boltzman constant, 1.38×10^{-16} erg K^{-1}

T = absolute temperature

η = asymmetry parameter

D_{rot} = rotational diffusion coefficient, determined by sedimentation experiments

The Stokes radius (R) for a number of biological macromolecules (apomyoglobin, chymotrypsin, hemoglobins) were calculated using published D_{rot} values according to Eq. 9.6. These Stokes radius values were then substituted into Eq. 6.10 to obtain the corresponding τ_c values. The results are listed in Table 9.2.

The second method involves the assumption that protein molecules are rigid unhydrated spheres, and each has a partial specific volume of 0.73 cm^3/g. Equation 6.10 can then be rewritten to give Eq. 9.7 as shown below

$$\tau_c = \frac{4\pi R^3}{3} \frac{\xi}{KT} \tag{6.10}$$

$$= (\text{volume/no. of molecules}) \frac{\xi}{KT}$$

$$= \frac{(\text{volume/gram})(\text{gram/mole})}{(\text{molecules/mole})} \frac{\xi}{KT}$$

$$= \frac{\bar{v}M}{N_o} \cdot \frac{\xi}{KT} \tag{9.7}$$

in which M = molecular weight of protein

$\bar{v}$ = partial sepcific volume, 0.73 cm^3/g

$\frac{4\pi R^3}{KT}$ = volume of a spherical molecule

N_o = Avogadro's number, 6.023×10^{23} molecule/mole

ξ = viscosity of water; 0.01005 g cm^{-1} sec^{-1} (c.g.s.) at 20°C; 0.012362 g cm^{-1} sec^{-1} at 12°C; 0.008937 g cm^{-1} sec^{-1} at 25°C.

The values of τ_c for the same biological macromolecules were determined using Eq. 9.7 and are also shown in Table 9.2.

A comparison of these two sets of τ_c values in Table 9.2 shows that the 3-dimensional rotational correlation times calculated using Eq. 9.7 are all smaller than the corresponding values using Eq. 6.10. This can be readily explained by reviewing the assumptions made in the derivations of those two equations. In the case of Eq. 9.7, protein molecules are assumed to be rigid unhydrated spheres with a fixed partial specific volume. This assumption is really quite a departure from the actual situation since protein molecules are known to be extensively hydrated. A much better approximation is made in Eq. 6.10, which is based on the effective molecular size of the protein from its hydrodynamic radius (R). Hence the higher τ_c values computed by the latter method should be a more accurate representation of the proteins' molecular motions.

Table 9.2 also includes some literature τ_c values obtained from ESR and fluorescence depolarization (F.D) measurements. These results are significantly different from the corresponding τ_c values computed using the hydrodynamic radius with the Debye equation 6.10. The

Table 9.2 Rotational correlation times, τ_c and Stokes radii (R), of some proteins

Protein	Molecular Weight	Temperature (°C)	$D_{20,W}$ (cm^2/s)	R(Å) from Eq.9.6	τ_c(nsec)from Eq. 9.7	τ_c(nsec)* from Eq.6.10	τ_c(nsec)from ESR	τ_c(nsec)from[a] F.D.
Myoglobin	17,000	25 20 12	11.30×10^{-7}[b]	18.9	4.5 5.1 6.5	6.1 7.0 8.9		8.3
Chymotrypsin	25,000	20			7.5		12 ± 2[f]	16.0
Hemoglobin (tertamer)	66,000	20 12	6.9×10^{-7}[c]	30.9	19.9 25.2	30.8 38.9	26 ± 2[g]	20.0
$Alpha_2$ (Hb-dimer)	33,000	20 12	8.5×10^{-7}[d]	25.1	9.9 12.6	16.5 20.8		12.3
$Beta_2$ (Hb-dimer)	33,000	20 12	8.5×10^{-7}[e]	25.1	9.9 12.6	16.5 20.8		12.3

a. Adapted from J. Yguerabide (ref. 154). Values were corrected to conform with the usual n.m.r., ESR and the P.A.C. values.

b. From Ref. 155.

c. From Refs. 156 and 157.

d,e From Ref. 158.

f From Shimshick et al., (ref. 159).

g From McCallery et al., (ref. 160)

* Assumed R is constant.

disagreement observed may be due to the added effect of internal rotational motion of the spin-label or fluorescent-label, in addition to the molecular tumbling motion of the whole labelled protein.

In common with other labelling techniques, the P.A.C. method suffers from the problem of distinguishing localised motion of probe itself from the motion of the whole molecule. However, in the present P.A.C. determination of τ_c of myoglobin, this obstacle was overcome by reconstituting the protein. The ferro-protoporphyrin IX (heme) was directly replaced with indium-111 mesoprotoporphyrin IX. In this way, the radioisotope, indium-111 was introduced into the active site of the protein. The X-ray structure of myoglobin (74, 95) shows that the heme fits tightly into the active site. Since ^{111}InMPP IX is structurally similar to ferro-protoporphyrin IX, there should be very little free rotation of the ^{111}InMPP IX at the active site of the reconstituted myoglobin. Furthermore, the indium-labelled protein is very likely to retain its native conformation, in contrast to other labelling techniques in which there is always uncertainty as to how much the label distorts the structure of the protein being studied. Consequently, since no additional flexibility is introduced at the label attachment site in the P.A.C. method, the present determination of τ_c for myoglobin is probably more accurate than fluorescence depolarization or ESR determinations.

Table 9.3 gives the rotational correlation times (τ_c) of myoglobin and ^{111}InMPP IX reconstituted myoglobin at various temperatures and viscosities. It is important to point out that the rotational correlation times calculated from Eq. 6.19 at 12°C were based on the Stokes radius (R) of the protein at 20°C. These τ_c values

Table 9.3 Rotational correlation times, τ_c of myoglobin and ^{111}InMPP reconstituted myoglobin at various temperatures and viscosities (References cited in Table 9.2)

Protein	Temperature (°C)	Viscosity (ξ) ($gcm^{-1}s^{-1}$)	τ_c(nsec)from* Eq. 6.10	τ_c(nsec)from P.A.C.	τ_c(nsec)from F.D.
Myoglobin	25	0.0089	6.1		8.3
	20	0.0100	7.0		
	12	0.0123	8.9		
^{111}InMPP-Mb in 0.05M phosphate buffer, pH7.0 without glycerine	12	0.013	9.3	16	(11.5)+
^{111}InMPP-Mb in 0.05M phosphate buffer, pH7.0 with glycerine to give a final glycerine percentage of 41%	12	0.049	35.2	22	

* Calculated with R = 18.9Å (from Table 9.2) at 20°C, and this value is assumed to remain the same at the other temperatures and viscosities.

\+ Calculated assuming linear relationship between τ_c and viscosities (from the Debye Equation, Eq. 6.10).

should be larger than indicated in Table 9.3, since myoglobin is expected to be more extensively hydrated at 12°C and thus have a larger effective molecular radius (R).

Results for ^{111}InMPP-Mb in aqueous buffer without glycerine show that the value of τ_c(P.A.C.) is greater than that calculated from the Debye equation (Eq. 6.10) by a factor of 1.7. This higher experimental τ_c(P.A.C.) can be explained by allowing for a larger effective molecular radius (R) than was used in the Debye determination. Alternately, the differences in τ_c may reflect the fact that myoglobin is <u>not</u> a spherical molecule as is assumed in the Debye calculation. The deviation from a perfect sphere causes an increase in the surface area to volume ratio for myoglobin, thus increasing rotational friction and decreasing the rate of molecular tumbling or τ_c.

It is clear from Table 9.3 that in order to compare the experimental τ_c(P.A.C.) value with τ_c(fluorescence), it is necessary to convert the only available τ_c(fluorescence) value at 25°C to 12°C. This conversion was done by assuming that τ_c varies linearly over a range of viscosities, as was demonstrated experimentally for oxyhemoglobin by McCallery et. al., (160)(Figure 9.6). The τ_c values in Figure 9.6 are plotted against the known viscosities for the sucrose concentrations used. Since the viscosity of water increases by a factor of 1.38 on lowering the temperature from 25°C to 12°C, the τ_c(fluorescence) of 9.3 nsec at 25°C should be increased by the same factor to 11.5 nsec at 12°C. The τ_c(fluorescence) at 12°C is lower than the experimental τ_c(P.A.C.) value of 16 nsec. This disagreement may again be due to the internal rotation of the fluorescent-label, in addition to the molecular motion of the whole protein. The present study does however, effectively

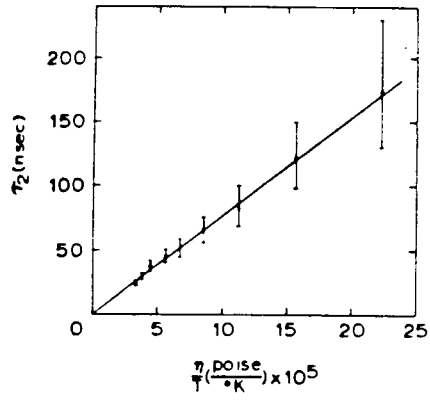

Figure 9.6. Rotational correlation time in nanoseconds for oxyhemoglobin as a function of η/T in poise/^{o}K.
Form McCallery et al., (ref. 160).

demonstrate that the P.A.C. technique can be used to yield reasonable rotational correlation times for proteins.

The Debye model for relaxation (Eq. 6.10) predicts that the rotational correlation time should be increased in the reconstituted protein solution containing 41% glycerine relative to that without glycerine. According to the direct linear relationship between τ_c and viscosity, one should expect an increase in the τ_c(P.A.C.) value of 16 nsec at 0% glycerine (ξ = 0.013 g cm^{-1} s^{-1}) to 60 nsec at 41% glycerine (ξ = 0.049 g cm^{-1} s^{-1}), assuming the Stokes radius (R) remains constant. As is evident from Table 9.3, the experimental τ_c(P.A.C.) value at 41% glycerine case is only 22 nsec. However, at high concentrations of glycerine the number of free water molecules available for solvating the protein is reduced. In other words, the hydration sphere is smaller resulting in a smaller effective molecular radius (R). Since τ_c is proportional to $R^3\xi$, any change in R will affect τ_c more significantly than an equivalent change in ξ. Hence, a decrease in the hydrated radius of the reconstituted myoglobin (in aqueous buffer containing 41% glycerine) would cause a more substantial reduction in the τ_c value than can be compensated for by the corresponding increase in the viscosity factor (ξ).

Using the Debye equation (Eq. 6.10), the decrease in the effective radius of ^{111}InMPP-Mb in 41% glycerine solution can be determined from the experimental τ_c(P.A.C.) values. This calculation suggests that, in 41% glycerine solution, the effective molecular radius for myoglobin is 72% as big as in the absence of glycerine (Table 9.4). It should be stressed, however, that Eq. 6.10 represents an oversimplification, strictly applicable only to isotropic motion of

spherical molecules. As pointed before, myoglobin is more of a flattened sphere (74,95), and this fact was not taken into account in the preceding calculations.

Table 9.4 Stokes radius of ^{111}InMPP-Mb calculated from the Debye model of relaxation using experimental τ_c(P.A.C.) values

Protein	Temp. (°C)	Viscosity(ξ) (g cm^{-1}s^{-1})	τ_c(P.A.C.) (nsec)	Stokes Radius(R)+ (Å)
^{111}InMPP-Mb in phosphate buffer without glycerine	12	0.013	16	22.6
^{111}InMPP-Mb in phosphate buffer containing 41% glycerine	12	0.049	22	16.2

+ Eq. 6.10 was rearranged to give $R = \sqrt[3]{\frac{3\tau_c kT}{4\pi\xi}}$

In conclusion, the present study effectively demonstrates that the Perturbed Angular Correlation (P.A.C.) method is an attractive, viable technique for obtaining rotational correlation times for macromolecules. Furthermore, the high sensitivity (as low as 10^{-12}M) combined with ability for *in vivo* experimentation makes the P.A.C. method a useful approach for examining other systems of physiological importance. In addition, information concerning molecular behavior of proteins in solid and liquid states can be obtained. Finally, a similar study has been extended to hemoglobin, in view of the high level of interest

and continuing debate on Perutz's stereochemical mechanism for oxygen-binding cooperativity.

APPENDIX A

CO-OPERATIVE EFFECT OF REVERSIBLE OXYGENATION IN HEMOGLOBIN

Hemoglobin (Hb) and myoglobin (Mb) are oxygen carriers in vertebrates. Hemoglobin, which is contained in red blood cells, serves as the oxygen carrier in blood. On the other hand, myoglobin facilitates the transport of oxygen in muscle and also serves as a reserve supply of oxygen in that tissue.

The shape of the oxygen dissociation curve of hemoglobin is sigmoidal whereas that of myoglobin is hyperbolic (Figure A.1). This curve is obtained by plotting the fractional saturation with oxygen versus the partial pressure of oxygen gas. However, the chemistry and structure of myoglobin is closely related to that of the individual subunits of hemoglobin. Then as Perutz (6) posed the question, "Why is it not good enough for the red cell to contain a simple oxygen carrier such as myoglobin".

The partial pressure in the lungs is ∿100 mm Hg, and as evident from Figures A.1 and A.2, both Hb and Mb are almost saturated with oxygen. In the venous blood, as in the tissues, much of the oxygen has been released from Hb whereas the myoglobin is still saturated with oxygen. For example at 20 mm Hg, the saturation of hemoglobin is about 40% while in myoglobin it is about 80% (see Figure A.1). The sigmoid shape of the curve means a greater fraction of oxygen is released more readily than the hyperbolic one. Although Hb and Mb both bind oxygen, but Hb releases it more readily in order that the tissues be adequately supplied with oxygen. Myoglobin releases oxygen at a much lower partial pressure, and if Mb were the oxygen-carrier, the tissues would be asphyxiated.

Hemoglobin can be dissociated into its constituent subunits, and

experiments have demonstrated that the individual subunits of Hb do not behave differently from myoglobin. The difference between Hb and Mb in oxygen-binding property must then be associated with the interactions between the subunits, which somehow alter the shape of the equilibrium curve. This interaction is often known as the "heme-heme interaction" (126). This expression simply states that there are functional interactions between heme groups and does not imply direct interactions or even that the interactions occur between the heme groups in the same molecule.

The sigmoid shape of the oxygen-dissociation curve of hemoglobin implies that the affinity of oxygen increases with the increase in oxygen saturation which clearly demonstrates the existence of a co-operative effect among the four subunits. In other words, the binding of oxygen to the heme group of one subunit has the effect of increasing the oxygen affinity of the neighbouring subunits of the same molecule.

Perutz (6,28,29) proposed a stereochemical interpretation of the co-operative effects in hemoglobin. For the mechanism of this effect, original papers should be consulted.

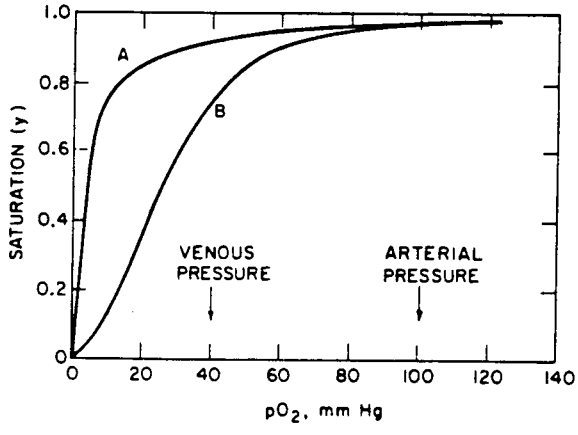

Figure A.1. Oxygen equilibrium curves of A myoglobin and B hemoglobin.

APPENDIX B

TETRAPHENYLPORPHINE DIACID

Tetraphenylporphine is violet in chloroform but green in glacial acetic acid. The former color is attributed to the porphyrin free base (Figure B.1) and the latter to the formation of diacid species (Figure B.2).

The porphinato core of tetraphenylporphine free base exhibits a marked deviation from planarity of the porphinato core (32,43). Structural studies (32,43) have shown the phenyl groups are almost perpendicular to the mean plane of the porphyrin ring because of interactions between the phenyl hydrogens and the outer pyrrole hydrogens. This arrangement of the phenyl groups prevents any π interaction between the benzene π system and the highly conjugated porphyrin system; thus the sample remains violet.

In the diacid of tetraphenylporphine, the porphinato core is even more highly distorted due to van der Waals and Columbic repulsions of the four inner hydrogen atoms. In contrast to the porphyrin free base, the tilted porphine skeleton allows the phenyl groups to rotate toward the mean porphyrin plane making a dihedral angle of 21° with it (Figure B.3). In this case, strong π interaction between the porphyrin and phenyl π electrons gives rise to the green color of the diacid species.

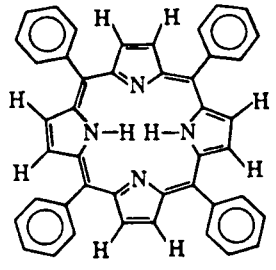

1

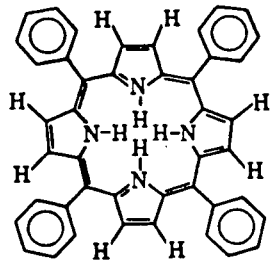

2

Figure B. 1. meso-tetraphenylporphine (free base); 2. porphyrin diacid.

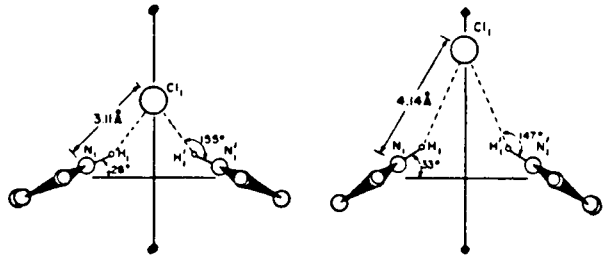

a b

Figure B.3. Geometries for porphyrin diacids.

APPENDIX C

THE EFFECT OF EXCITATION OF THE ELECTRON SHELL ON ANGULAR CORRELATION

During radioactive decay such as through a γ-γ cascade, there is a possibility that a "hole" is created in one of the inner electron (K) shells, with a resulting atomic shell in an excited state. After the formation of the K-hole, the atomic shell and nucleus tend to return to their ground states through γ-γ cascade and emission of Auger electrons and X-rays. Following the Auger process, the atom can be charged. It has been shown experimentally (161-164) that Cd can acquire an average charge 7e. The electric field originating from these excited atomic shells will perturb the angular correlation. The perturbation depends on the mean life of the exicted state (τ_N) and on the transition probabilities for X-ray and Auger emission in various shells. This lifetime is known to be very short (about 10^{-12}sec) for metals. In the case of insulators it may be as long as seconds. The interaction strength is of the order of 500 MHz which means that there will be an influence if $\tau_N \approx 10^{-9}$ sec or longer. The τ_N for the 247-KeV excited state of Cd^{111} is 1.25×10^{-7}sec, and a perturbation on angular correlation is expected. No detailed analysis of this effect has yet been developed.

After the electron capture, the K-hole created can progress rapidly towards the outermost shell and in the process generates more holes which also move outwards during such migration. This movement is the consequence of Auger effect. Once these holes have reached the outermost shell, they can decay only slowly. If their mean lifetime

is long enough, a very strong perturbation on the angular correlation often resulted. If the perturbation is of sufficient magnitude, the correlation can be attenuated below the hard core value (minimum value). The attentuation depends on the surrounding atomic environment which can be an insulator or a conductor.

In the case in which the radioactive atom is incorporated in a substance of high conductivity (i.e. the presence of conduction band), the electron shell excitation following the K-capture remains for a short period (less than 10^{-12}sec). The nucleus is thus remained unperturbed by the electric fields arising from such excited shells. The presence of the conduction band allows rapid free flow of electrons to "fill" the holes, and thus leaves the radioactive atom in its ground state. This holds true whether the conductor carrying the radionucleus is in a solid or liquid medium.

In contrast, if the radioactive atom is incorporated in a solid insulator, the absence of a conduction band in the radioisotope's environment leads to a long decay time of the holes in the outermost shell ($>>10^{-8}$sec). Consequently, the insulator source should be expected to be attentuated. However, the situation is more complex when the insulator carrier is in solution. The influence of the K-capture on the angular correlations now depends on the rotational correlation time (τ_c) and the interactions between the insulator molecules in solution. If the moelcule carrying the decaying nucleus rotates very fast (i.e., if the interaction is strong and the rotational correlation time is short), the angular correlation will be unperturbed, even if the atomic shell is not in its ground state. In the event when

the rotational correlation time is increased to a value much greater than τ_N (i.e., $\tau_c >> \tau_N$), a perturbation on the angular correlation will occur.

References

1. A. D. Adler, J. Poly. Sci., Part C, 29, 73 (1970).

2. J. P. Macquet and T. Theophanides, Can. J. Chem., 51, 219 (1972).

3. E. B. Fleischer and M. Krishamurthy, J. Am. Chem. Soc., 94, 1382 (1972).

4. J. E. Falk, "Porphyrins and Metalloporphyrins", Elsevier, New York, 1964.

5. "Structure Reports", Vol. 1-42, J. Trotter, Ed., Bohn, Scheltema & Holkema, Utrecht, 1978.

6. M. F. Perutz, Scientific American, 239, 92 (1978).

7. T. K. Lejpert, J. D. Baldeschwieler, and D. A. Shirely, Nature (London), 220, 907 (1968).

8. C. F. Meares, R. G. Bryant, J. D. Baldeschwieler, and D. A. Shirely, Proc. Natl. Acad. Sci. U.S.A., 64, 1155 (1969).

9. D. A. Shirely, J. Chem. Phys., 55, 1512 (1971)

10. C. F. Meares and D. G. Westmoreland, Proc. Cold Spring Harbor Sym. Quant. Biol., 36, 511 (1971).

11. D. A. Shirley, J. Chem. Phys., 53, 465 (1970).

12. J. C. Glass and G. Graf, Nature (London), 226, 635 (1970).

13. A. G. Marshall and C. F. Meares, J. Chem. Phys., 56, 1226 (1972).

14. A. G. Marshall, L. G. Webelow, and C. F. Meares, J. Chem. Phys., 57, 364 (1972).

15. J. L. Hoard, Science, 174, 1295 (1971).

16. M. J. Hamor, T. A. Hamor, and J. L. Hoard, J. Am. Chem. Soc., 86, 6689 (1965).

17. M. J. Hamor, T. A. Hamor, and J. L. Hoard, J. Am. Chem. Soc., 86, 1938 (1964).

18. D. M. Collins, W. R. Scheidt, and J. L. Hoard, J. Am. Chem. Soc., 94, 6689 (1972).

19. R. J. P. Williams, Fed. Proc., Fed. Amer. Soc. Exp. Biol., 20, (Suppl. 10), 5 (1961).

20. M. D. Glick, G. H. Cohen, and J. L. Hoard, J. Am. Chem. Soc., 89, 1996 (1967).

21. D. M. Collins and J. L. Hoard, J. Am. Chem. Soc., 92, 3761 (1970).

22. J. L. Hoard, in "Structural Chemistry and Molecular Biology", A. Rich and N. Dadvison, Eds., W. H. Freeman, San Franciso, California, 1968, p537.

23. J. L. Hoard, M. J. Hamor, T. A. Hamor, and W. S. Caughey, J. Am. Chem. Soc., 87, 2312 (1965).

24. W. A. Hendrickson and W. E. Love, Cold Spring Harbor Sym. Quant. Biol., 36, 1971.

25. R. Huber, O. Epp, and H. Formanek, J. Mol. Biol., 52, 349 (1970).

26. S. E. V. Phillips, Nature (London), 273, 247 (1978).

27. J. L. Hoard, in "Hemes and Hemoproteins", B. Chance, R. W. Estabrook, and T. Yonetani, Eds., Academic Press, New York, 1966, p9.

28. M. F. Perutz, Nature (London), 228, 726 (1970).
228, 734 (1970)

29. M. F. Perutz, and L. F. TenEyck, Cold Spring Harbor Symp. Quant. Biol., 36, 295 (1971).

30. D. M. Collins, R. Countryman, and J. L. Hoard, J. Am. Chem. Soc., 94, 2066 (1972).

31. R. J. Radonovich, A. Bloon, and J. L. Hoard, J. Am. Chem. Soc.,. 94, 2073 (1972).

32. M. J. Hamor, T. A. Hamor, and J. L. Hoard, J. Am. Chem. Soc., 86, 1938 (1964).

33. E. B. Fleischer, C. K. Miller, and L. E. Webb, J. Am. Chem. Soc., 86, 2343 (1964).

34. J. L. Hoard, Ann. N. Y. Acad. Sci., 206, 18 (1973).

35. D. L. Cullen and E. F. Meyer, Jr., J. Am. Chem. Soc., 96, 2095 (1974).

36. J. A. Kaduk and W. R. Scheidt, Inorganic Chem., 13, 2095 (1974).

37. E. I. Meyer, Jr., Acta. Crystallogr., Sect. B., 28, 2162 (1972).

38. E. B. Fleischer, J. Am. Chem. Soc., 85, 146 (1963).

39. T. A. Hamor, W. S. Caughey, and J. L. Hoard, J. Am. Chem. Soc., 87, 2305 (1965).

40. J. L. Hoard, G. H. Cohen, and M. D. Glick, J. Am. Chem. Soc., 89, 1992 (1967).

41. D. F. Koenig, Acta. Cryst., 18, 663 (1965).

42. L. E. Webb and E. B. Fleischer, J. Am. Chem. Soc., 87, 667 (1965).

43. S. Silvers and A. Tulinsky, J. Am. Chem. Soc., 86, 927 (1964).

44. J. C. Kendrew, R. E. Dickerson, B. E. Strandberg, R. G. Hart, D. R. Davis, D. C. Phillips, and V. C. Shore, Nature, 185, 422 (1960).

45. D. A. Buckingham, J. P. Collman, J. L. Hoard, G. Lang, L. J. Randonovich, and C. A. Reed, cited in ref. 47.

46. K. Adams, P. G. Rasmussen, K. Hatano, and W. R. Scheidt, cited in ref. 47.

47. W. R. Schedit, in "Porphyrins", D. Dolphin, Ed., Academic Press, New York, Vol. III, 1978, p463.

48. A. B. Hoffman, D. M. Collins, V. W. Day, E. B. Fleischer, T. S. Srivastava, and J. L. Hoard, J. Am. Chem. Soc., 94, 3620 (1974).

49. A. Bloon and J. L. Hoard, cited in ref. 47.

50. W. R. Scheidt and J. L. Hoard, (unpublished results), cited in ref. 47.

51. L. J. Randonovich, W. S. Caughey, and J. L. Hoard, cited in ref. 47.

52. J. E. Kenny, J. W. Buchler, and W. R. Scheidt, cited in ref. 47.

53. W. R. Scheidt, J. A. Cunningham, and J. L. Hoard, J. Am. Chem. Soc., 95, 8299 (1973).

54. W. R. Scheidt, J. Am. Chem. Soc., 96, 90 (1974).

55. R. G. Little and J. A. Ibers, J. Am. Chem. Soc., 96, 4452 (1974).

56. W. R. Scheidt and J. Ramanjua, Inorg. Chem., 14, 2643 (1975).

57. P. N. Dwyer, P. Madura, and W. R. Scheidt, J. Am. Chem. Soc., 96, 4815 (1974).

58. M. F. Perutz, Nature (London), 237, 495 (1972).

59. H. Muirhead, J. M. Cox, L. Mazzarella and M. F. Perutz, J. Mol. Biol., 28, 117 (1967).

60. M. F. Perutz, H. Muirhead, J. M. Cox, L. C. G. Godman, F. S. Mathews, E. L. McGandy, and L. E. Webb, Nature (London), 219, 29 (1968).

61. M. F. Perutz, H. Muirhead, J. M. Cox, and L. C. G. Godman, Nature (London), 217, p131 (1968).

62. W. Bolton and M. F. Perutz, Nature (London) 228, 551 (1970).

63. H. Muirhead and J. Greer, Nature (London), 228, 516 (1970).

64. J. L. Hoard and W. R. Scheidt, Proc. Natl. Acad. Sci., U.S.A., 70, 3919 (1973).

65. J. L. Hoard and W. R. Scheidt, Proc. Natl. Acad. Sci., U.S.A., 71, 1578 (1974).

66. B. Gonzales, J. Kouba, S. Yee, C. A. Reed, J. F. Kirner, and W. R. Scheidt, J. Am. Chem. Soc., 97, 3247 (1975).

67. J. J. Hopfield, J. Mol. Biol., 77, 207 (1973).

68. M. F. Perutz, J. E. Ladner, S. R. Simon, and C. H. Ho, J. Mol. Biol., cited in ref. 55.

69. M. F. Perutz, A. R. Roberts, S. R. Simon, and G. C. K. Roberts, J. Biol. Chem., cited in ref. 55.

70. M. F. Perutz, E. J. Heidner, J. E. Ladner, J. G. Bettlestone, C. Ho, and E. F. Slade, J. Biol. Chem., cited in ref. 55.

71. T. R. Lindstrom, C. Ho, and A. V. Pisciotta, Nature (London), New Biol., 237, 263 (1972).

72. S. Ogawa, R. G. Shulman, and T. Yamane, J. Mol. Biol., 70, 291 (1972).

73. S. Ogawa and R. G. Shulman, J. Mol. Biol., 70, 315 (1972).

74. G. Fermi, J. Mol. Biol., 97, 237 (1975).

75(a) F. Basolo, B. M. Hoffman, and J. A. Ibers, Acc. Chem. Res., 8, 384 (1975).

(b) B. M. Hoffman, J. Am. Chem. Soc., 97, 1688 (1975).

76. J. Leonard, T. Yonetani, and J. B. Callis, Biochemistry, 13, 1460 (1974).

77. T. L. Fabry, C. Simo, and K. Javaherian, Biochim. Biophysics. Acta., 160, 118 (1968).

78. T. Yonetani, H. R. Drott, J. S. Leigh, Jr., G. H. Reed, M. R. Waterman, and T. Asakura, J. Biol. Chem., 245, 2998 (1970).

79. K. Moffat, R. S. Loe, and B. M. Hoffman, J. Am. Chem. Soc., 96, 5259 (1974).

80(a) Q. H. Gibson, B. M. Hoffman, R. H. Crepeau, S. J. Edelstein, and C. Bull, Biochem. Biophys. Res. Commun., 59, 146 (1974).

80(b) C. Bull, R. G. Fisher, and B. M. Hoffman, Biochem. Biophys. Res. Commun., 59, 140 (1974).

81(a) B. M. Hoffman, Q. H. Gibson, C. Bull, R. H. Crepeau, S. J. Edelstein, R. G. Fisher, and M. J. McDonald, Ann. N. Y. Acad. Sci., 244, 174 (1975).

81(b) S. J. Edelstein and Q. H. Gibson, J. Biol. Chem., 250, 961 (1975).
250, 965 (1975).

82. J. E. O'Hagen, "Haematin Enzymes", Pergamon Press, Oxford, 1961, p173.

83. B. M. Hoffman, C. A. Spilburg, and D. H. Petering, Cold Spring Harbor. Symp. Quant. Biol., 36, 343 (1971).

84. B. M. Hoffman and D. H. Petering, Proc. Natl. Acad. Sci., U.S.A., 67, 637 (1970).

85. G. C. Hsu, C. A. Spilburg, C. Bull, and B. M. Hoffman, Proc. Natl. Acad. Sci., U.S.A., 69, 2122 (1972).

86. C. A. Spilburg, B. M. Hoffman, and P. H. Petering, J. Biol. Chem., 247, 4219 (1972).

87. W. H. Woodruff, T. G. Spiro, and T. Yonetani, Proc. Natl. Acad. Sci., U.S.A., 71, 1065 (1974).

88. R. G. Little, B. M. Hoffman, and J. A. Ibers, Bioinorg. Chem., 3, 207 (1974).

89. J. C. Kendrew, Science, 139, 1259 (1963).

90. J. C. Kendrew, Brookhav. Sym. Biol., 15, 216 (1962).

91. M. F. Perutz, M. G. Rossman, A. F. Cullis, H. Muirhead, G. Will, and C. T. North, Nature (London) 185, 416 (1960).

92. A. F. Cullis, H. Muirhead, M. F. Perutz, M. G. Rossman, and A. C. T. North, Proc. Roy. Soc., (Lond.), Ser. A., 263, 161 (1962).

93. J. C. Kendrew, H. C. Watson, B. E. Strandberg, R. E. Dickerson, D. C. Phillips, and V. C. Shore, Nature (London), 190, 666 (1961).

94. M. F. Perutz, "Proteins and Nuclei Acids", Holland, Elsevier Publ., 1962.

95. T. Takano, J. Mol. Biol., 110, 537 (1977).

96. L. F. Ten Eyck and Arnone, J. Mol. Biol., 100, 3 (1976).

97. R. E. Dickerson and I. Geis, "The Structure and Action of Proteins", W. A. Benjamin, Inc., California, 1969.

98. B. R. James, in "Porphyrins", D. Dolphin, Ed., Academic Press, Inc., New York, Vol. 5, 1978, p205.

99. D. Dolphin, "Porphyrins", Academic Press, Inc., New York, 1978.

100. J. P. Collman, R. R. Gagne, C. A. Reed, W. T. Robinson, and G. A. Rodley, Proc. Natl. Acad. Sci., 71, 1326 (1974).

101. H. Diekmann, C. K. Chang, and T. G. Traylor, J. Am. Chem. Soc., 93, 4068 (1971).

102. J. Almog, J. E. Baldwin, R. L. Dyer, and M. Peters, J. Am. Chem. Soc., 97, 227 (1975).

103. J. P. Collman, R. R. Gagne, T. R. Halbert, J. C. Marchon, and C. A. Reed, J. Am. Chem. Soc., 95, 7868 (1973).

104. J. P. Collman, R. R. Gagne, H. B. Gray, and J. W. Hare, J. Am. Chem. Soc., 96, 6522 (1974).

105. J. P. Collman and W. T. Robinson, Nature, 235, 438 (1972).

106(a) C. K. Chang and T. G. Taylor, Proc. Natl. Acad. Sci., U.S.A., 70, 2647 (1973).

(b) Ibid, J. Am. Chem. Soc., 95, 5810 (1973).

107. M. Bhatti, W. Bhatti, and E. Mast, Inorg. Nucl. Chem. Letters, 8, 133 (1972).

108. The computer programs used include locally written programs for data processing and locally modified versions of the following: ORFLS full matrix least squares and ORFFE, function and errors by W. R. Busing, K. O. Martin and H. A. Levy; Patterson and Fourier synthesis, FORDAP by A. Zalkin; crystal structure illustrations, ORTEP II by C. K. Johnson.

109. "International Tables for X-ray Crystallography", Vol. IV, Kynoch Press, Birmingham, England, 1972, p.99.

110. D. T. Cromer and D. Liberman, J. Chem. Phys. 53, 1891 (1970).

111. T. Mashiko, M. E. Kastner, K. Spartalian, W. R. Scheidt, and C. A. Reed, J. Am. Chem. Soc., 100, 6354 (1978).

112. W. H. Huestic and M. A. Raftery, Biochemistry, 11, 1648 (1972).

113. E. J. Heidner, R. C. Ladner, and M. F. Perutz, J. Mol. Biol., 104, 707 (1976).

114. A. Fitzgerald, private communication.

115. J. L. Hoard, N. Kim, and J. W. Buchler, Abstracts, 167th National Meeting of the American Chemical Society, Los Angeles, CA (1974), No. INOR 75.

116. D. C. Cullen, E. F. Meyer, Jr., and K. M. Smith, Inorg. Chem., 16, 1179 (1977).

117. F. Molinaro and J. A. Ibers, Inorg. Chem., 15, 2278 (1976).

118. G. B. Jameson, F. Molarino, J. A. Ibers, J. P. Collman, J. I. Brauman, E. Rose, and K. S. Suslick, J. Am. Chem. Soc., 100, 6769 (1978).

119. L. P. Spauling, E. G. Eller, J. A. Bertrand, and R. H. Felton, J. Am. Chem. Soc., 96, 982 (1974).

120. D. L. Cullen and E. F. Meyer, Jr., Acta Crystallogr., Sect. B., 32, 2259 (1976).

121. B. M. Chen, Ph.D. Thesis, Michigan State University, 1970.

122. R. Timkovich and A. Tulinsky, J. Am. Chem. Soc., 91, 4430 (1969).

123. V. W. Day, B. R. Stults, E. L. Tasset, R. S. Marianelli, and L. J. Boucher, Inorg. Nucl. Chem. Letters, 11, 509 (1975).

124. J. P. Collman, J. I. Brauman, K. M. Doxsee, T. R. Halbert, S. E. Hayes, and K. S. Suslick, J. Am. Chem. Soc., 100, 2761 (1978).

125. S. S. Eaton and G. R. Eaton, J. Am. Chem. Soc., 99, 6594 (1977).

126. R. J. Abraham, G. H. Barnett, and K. M. Smith, J. Chem. Soc., Perkin I, 2142 (1973).

127. L. Stryer, J. Mol. Biol., 13, 482 (1965).

128. T. R. Stengle and J. D. Baldeschwieler, Proc. Natl. Acad. Sci., U.S.A., 55, 1020 (1966).

129. C. L. Hamilton and H. M. McConnell, in "Structural Chemistry and Molecular Biology", A. Rich and N. Davidson, Eds., Freeman & Co., San Francisco, 1968, p115.

130. H. Frauenfelder and R. M. Steffen, in "Alpha-, Beta-, and Gamma-ray Spectroscopy", K. Siegbahn, Ed., North-Holland, Amsterdam, 1965, p997.

131. R. M. Steffen, Phys. Rev., 103, 116 (1956).

132. "Table of Isotopes", C. M. Lederer, J. M. Hollander, and J. Perlman, Eds., John Wiley & Son, New York, 1968, p252.

133. A. Abragam and R. V. Pound, Phys. Rev., 92, 943 (1953).

134. M. Blume, in "Hyperfine Structure and Nuclear Radiations", E. Matthias and D. A. Shirley, Eds., North-Holland, Amsterdam, 1968, p991.

135. P. Debye, "Polar Molecules", Dover Publications, New York, 1965.

136. N. Bloembergen, E. M. Purcell, and R. V. Pound, Phys. Rev., 73, 679 (1948).

137. P. B. Hemmig and R. M. Steffen, Phys. Rev., 92, 832 (1953).

138. P. Lehmann and J. Miller, J. Phys. Radium, 17, 526 (1956).

139. J. S. Barrett, J. A. Cameron, P. R. Gardner, L. Kezthelyi, W. V. Prestwich, and M. Kaplan, J. Chem. Phys., 53, 759 (1970).

140. R. M. Lynden-Bell, Mol. Phys., 21, 891 (1971).

141. E. Matthias, B. Olsen, and W. Schneider, Arkiv För Fysik, 24, 245 (1963).

142. E. Matthias, W. Schneider, and R. M. Steffen, Phys. Letts., 4, 41 (1963).

143. E. Matthias, W. Schneider, and R. M. Steffen, Arkiv För Fysik, 24, 97 (1963).

144. R. W. Sommerfeldt and L. Schecter, Phys. Letts., 3, 5 (1962).

145. D. A. Goodwin, C. F. Meares, and C. H. Song, Radiology, 105, 699 (1972).

146. H. S. Stern, D. A. Goodwin, and W. Scheffel, et al., Nucleonics, 25, 62 (1967).

147. F. Hosain, P. A. McIntyre, K. Poulose, et al., Clin. Chim. Acta., 24, 69 (1969).

148. P. W. Martin and C. A. Kalfas, Chem. Phys. Letts., 57, 279 (1978).

149. F. Fischer and H. Bock, Z. Physiol. Chem., 255, 1 (1938).

150. J. F. Taylor, J. Biol. Chem., 135, 569 (1940).

151. E. Breslow, J. Biol. Chem., 239, 486 (1964).

152. T. S. Srivastava, Biochim. Biophys. Acta., 491, 599 (1977).

153. F. James and M. Ross, Comput. Phys. Commun., 10, 343 (1975).

154. J. Yguerabide, in "Methods in Enzymology", C. H. W. Hirs and S. N. Timasheff, Eds., Academic Press, New York, 1972, Vol. 26, part C, p.528.

155. "Hand-Book of Biochemistry - Selected Data for Molecular Biology", H. A. Sober, Ed., The Chemical Rubber Co., Ohio, 1970, pC10.

156. D. D. Haas, R. V. Mustacich, B. A. Smith, and B. R. Ware, Biochem. Biophys. Res. Commun., 59, 174 (1974).

157. C. R. Jones and C. S. Johnson, Jr., J. Chem. Phys., 65, 2020 (1976).

158. D. D. Haas and B. R. Ware, Biochemistry, 17, 4946 (1978).

159. E. J. Shimshick and H. M. McConnell, Biochem. Biophys. Res. Commun., 46, 1 (1972).

160. R. C. McCallery, E. J. Shimshick, and H. M. McConnell, Chem. Phys. Letts., 13, 115 (1972).

161. M. L. Perlman and J. A. Miskel, Phys. Rev., 91, 899 (1953).

162. S. Wexler, Phys. Rev., 93, 182 (1954).

163. O. Kofoed-Hansen, Phys. Rev., 96, 1045 (1954).

164. P. H. Snell and F. Pleasonton, Phys. Rev., 102, 1419 (1956).